IDENTIFICATION OF THE EFFECT OF AXONAL COUPLING TO THE GLIAL MATRIX ON AXONAL KINEMATICS

BY

HAILING HAO

A Dissertation submitted to the

Graduate School – New Brunswick

Rutgers, The State University of New Jersey

and

The Graduate School of Biomedical Sciences

University of Medicine and Dentistry of New Jersey

In partial fulfillment of the requirements

for the degree of

Doctor of Philosophy

Graduate Program in Biomedical Engineering

written under the direction of

Professor David I. Shreiber

and approved by

_____

_____

_____

_____

New Brunswick, New Jersey October, 2007

ABSTRACT OF DISSERTATION

Identification of the Effect of Axonal Coupling to the Glial Matrix on Axonal Kinematics

by Hailing Hao

Dissertation Advisor: Professor David I. Shreiber

The axonal coupling to the glia matrix was hypothesized to contribute to the transition from non-affine (independent) to affine (interdependent) behavior of axonal kinematics. The effect of spinal cord growth on axonal kinematic behavior was investigated with a chick embryo spinal cord model. Chick spinal cords at different development stage (E12, E14, E16, and E18) were stretched to different levels (0, 5, 10, 15, and 20%). The tortuosity distribution of axons at each developmental stage and each stretch level was characterized. Axonal deformation showed increasing coupled behavior with development and growth. The experimental results did not follow ideal affine nor non-affine behavior. A ‘switching’ model was then employed and the values of parameters of the ‘switching’ model were determined by minimizing the difference between experimental results and predicted results. The ‘switching’ model predicted the experimental results more accurately. This percentage of axons that exhibit purely non-affine behavior decreased with development, indicating more non-affine manner at early

developmental stages. Thus axons exhibit increasing affine deformation as developing and growth progress in chick embryos.

We identified the role of axonal coupling to glia on axon kinematics by disrupting the myelination of axons. This was done by introducing GalC antibody or ethidium bromide (EB). Pure rabbit IgG and saline were used as a control respectively. Following each injection, spinal cords were incubated until E18 and two different stretch levels were applied (5, or 15%). Following EB and GalC injections, spinal cords showed predominant demyelination. Glial cells, including astrocytes and oligodendrocytes were disrupted following EB injection, but not GalC injection. Saline or pure rabbit IgG did not cause any change to the glia and myelination of axons. The transition from affine to non-affine behavior was detected from myelinated spinal cord compared to demyelianted spinal cord. The shift was very modest in spinal cord following GalC injection, though significant in spinal cord following EB injection. The results demonstrate that the role glial is important. We finally characterized the material properties of myelinated and demyelinated spinal cords. Higher ultimate stress and greater shear modulus were observed for myelinated spinal cords compared to demyelinated spinal cords. Greater strain at ultimate stress was also observed for spinal cords following GalC injection compared to EB injection. The results indicated that spinal cords were stronger when myelinated vs. demyelinated, as well as with astrocytes vs. without astrocytes. Alteration in spinal cord compositions affected the mechanical properties of the tissue, and might affect the strain transfer from tissue to microscopic cells as well.

ACKNOWLEDGEMENTS

I would like to thank my advisor, Dr. David Shreiber for his kind help with my research. Thanks also go to all my lab mates, especially Chris, Jason, and Harini. It is a big pleasure to work with all of them. I would also thank my family. Without the support from my family, I would not be able to study for my doctoral degree. They always encourage me whenever I feel depressed. At last, I would thank my friends, Wei Wu and Weimin Dian. They are my best friends and they would give me any support whenever I need them.

List of Contents

List of Figures

List of Tables

List of Equations

$$y(z) = A_o \cos\left(\frac{2\pi z}{P_o}\right) \text{ . . . . . Equation 3-1}$$

$$\lambda = \frac{Final\ Spinal\ Cord\ Length}{Initial\ Spinal\ Cord\ Length} \text{ . . . . . Equation 3-2}$$

$$y'(z) = \frac{A_o}{\sqrt{\lambda}} \cos\left(\frac{2\pi z}{\lambda P_o}\right) \text{ . . . . . Equation 3-3}$$

$$T_t = \frac{1}{L_E} \int_0^{L_E} \sqrt{1 + \left(\frac{-A_o}{\sqrt{\lambda}} \frac{2\pi}{\lambda P_o} \sin\left(\frac{2\pi z}{\lambda P_o}\right)\right)^2} \text{ . . . . . Equation 3-4}$$

$$T_t = T_o \left[\frac{1}{\lambda^3} + \frac{1}{T_0^2}\left(1 - \frac{1}{\lambda^3}\right)\right]^{\frac{1}{2}} \text{ . . . . . Equation 3-5}$$

$$T_t = \frac{1}{\lambda} T_o \quad \text{for} \quad \lambda < T_o \text{ . . . . . Equation 3-6}$$

$$T_t = 1 \quad \text{for} \quad \lambda \geq T_o \text{ . . . . . Equation 3-7}$$

$$\lambda = \frac{Final\ Spinal\ Cord\ Length}{Initial\ Spinal\ Cord\ Length} \text{ . . . . . Equation 4-1}$$

$$T = \frac{actual\ length}{end\text{ - }to\text{ - }end\ length} = \frac{L_A}{L_E} \text{ . . . . . Equation 4-2}$$

$$W = \sum_{i=1}^{N} \frac{2G_i}{\alpha_i^2}\left(\lambda_1^{\alpha_i} + \lambda_2^{\alpha_i} + \lambda_3^{\alpha_i} - 3\right) \text{ . . . . . Equation 5-1}$$

$$\sigma = \sum_{i=1}^{N} \frac{2G_i}{\alpha_i}\left(\lambda_1^{\alpha_i - 1} - \lambda_1^{-0.5\alpha_i - 1}\right) \text{ . . . . . Equation 5-2}$$

Chapter 1: Introduction

Clinical significance

Injury remains a leading public health problem in the United States (Sosin, Sacks et al. 1989; Kraus and McArthur 1996). Traumatic brain injury (TBI) and spinal cord injury (SCI) have profound, lifelong impacts on the patient, and together they account for a significant proportion in the cost (Runge 1993). TBI is the leading cause of death in children and adults under the age of 45 (Sauaia, Moore et al. 1995; Kraus and McArthur 1996), and remains the leading cause of death following motor vehicle accidents. Almost 2 million new brain injuries occur annually, and the annual cost associated with head injuries is more than 30 billion dollars (Pope 1991). Approximately 2.5 million people were reported to live with SCI in 2004, with more than 130,000 new injuries reported each year (Thuret, Moon et al. 2006). The pathophysiology of SCI and TBI involves a primary mechanical injury to both gray and white matter followed by a number of secondary insults, including ischemic and excitotoxic insults (Hovda, Becker et al. 1992; McIntosh, Smith et al. 1996; Tator and Koyanagi 1997). The severity of injury depends on the degree of mechanical load and the location of injury. While each of the entities of central nervous tissue is susceptible to primary and secondary injuries, it is the disruption of axons that primarily results in varying degrees of disability following injuries (Adams, Graham et al. 1982).

No fully restorative therapies for SCI have yet been reported, and prevention is truly the best medicine. Finite element modeling (FEM) has emerged as a potential tool for understanding injury biomechanics to ultimately develop improved prevention

techniques and safety guidelines for human head and spinal cord injuries (Lee 1987; Miller and Meaney 1998). The accuracy of the FEM hinges on the mechanical description of tissue structure and tolerance criteria for nervous tissue. In particular, the relationship between macroscopic tissue strain and subsequent axonal injury is important for the development of tolerance criteria for nervous tissue. However, little is known about the stain transfer from tissue-level to axons. Thus, determining the relationship between tissue strain and axonal strain during mechanical loadings is important to understand the biomechanics of injury and thus to identify preventive strategies for injury. In this thesis, our primary goal is to understand the quantitative relationship between spinal cord strain and axonal deformation, and to investigate the contributors to the relationship.

Axonal injury

Axonal injury is the primary contributor to SCI and TBI. Previous studies have established that the inertial and tensile forces associated with TBI and SCI invoke axonal injury scattered throughout the tissue (Graham, Adams et al. 1995; Meaney, Margulies et al. 2001). The forces are commonly induced during motor vehicle crashes, falls, and assaults. In most mechanical injuries, longitudinal stretch is assumed to be the primary cause for axonal damage in the white matter in both brain (Meaney, Margulies et al. 2001) and spinal cord injury (Blight and Decrescito 1986; Torg, Thibault et al. 1995). For instance, in non-centroidal acceleration models of brain injury, which approximate the loads experienced in a typical head on or rear motor vehicle collision, the brain experiences large shear deformation which injures axons that are oriented such that they

experience maximum tension (Meaney, Smith et al. 1995; Bain and Meaney 2000; Meaney, Margulies et al. 2001; Miller and Chinzei 2002). Similarly, in impact models of spinal cord injury, such as the weight drop model, the compression of spinal cord tissue in the dorso-ventral direction causes axial stretch, which damages axons (Young 2002).

Previous studies suggested that under even simple tension loading, the mechanical transfer of strain from the tissue to the axons is complex. It is observed that the relative injury increases proportionately with mechanical load from different axonal injury models, including in vitro (Ellis, McKinney et al. 1995; Ellis EF 1995; Cargill and Thibault 1996), in situ (Shi and Borgens 2000; Bain, Shreiber et al. 2003), and in vivo models (Gennarelli, Thibault et al. 1989; Maxwell, Kosanlavit et al. 1999; Bain and Meaney 2000). Both histological and electrophysiological impairments are characterized in these models. The plasma membrane may be immediately damaged (Ellis EF 1995) and axonal conduction block may result from stretch (Shi and Blight 1996; Shi and Pryor 2000). Those impairments may result from a change in ionic homeostasis (Choi 1994; Olney 1994; Chen, Perkins et al. 1997). Influx of sodium and calcium happen after stretch (Maxwell, McCreath et al. 1995; Maxwell, Kosanlavit et al. 1999; Shi and Pryor 2002). The axonal deficits caused by a primary mechanical event result in tissue damage associated with CNS injury (Hovda, Becker et al. 1992; McIntosh, Smith et al. 1996).

Although axonal pathology has been well characterized in humans and animal experimental models, little is known about the immediate events during and after the mechanical load. Previous research has demonstrated that neurofilaments are misaligned and membrane permeability is changed immediately in traumatic axonal injury using a cat model or in vitro model (Pettus, Christman et al. 1994; Povlishock and Pettus 1996).

Information about the immediate events may help in understanding the mechanical factors that initiate the axonal pathology. The deformation or strain of axons is proposed to be the initial event in traumatic axonal injury as a result of mechanical loadings (Morrison, Saatman et al. 1998). Defining the relationship between the mechanical load and the structure deformation is critital in understanding the induction of axonal pathology. For instance, the information of mechanical tolerance of individual axons is important to develop preventative strategies for traumatic axonal injury.

The tolerance of individual axons has been studied in vitro (Smith, Wolf et al. 1999) and ex vivo (Gray and Ritchie 1954; Galbraith, Thibault et al. 1993). However, the in vitro models do not represent the organotypic architecture of in vivo axons. In real world, strain that axons experience is transferred from tissue-level strain. Axons are tortuous in CNS tissue and the actual strain is thus not necessarily the same with tissue strain. It is difficult to measure injury tolerance for individual axons in vivo with current techniques. However, studies of tissue-level thresholds for axonal injury in vivo were possible and have been studied in guinea pigs. Thus, the development of strain transfer from macroscopic tissue to microscopic cells/cellular processes is important to understand axonal tolerance for individual axons. Due to the potential similarities of CNS axons among different species, tolerance for individual axons might be more widely applicable to the study of human CNS injury than tissue-level thresholds.

In this thesis, we focus on axonal tortuosity distribution in developing chick embryo spinal cords to different tissue-level stretch ratios. We will investigate the effects of growth and development on axonal deformation. The experimental results will be used to evaluate the mathematical models as described in the next paragraph.

Axonal microstructure kinematics

The deformation of axons as the result of mechanical loading is not simple (Adams, Doyle et al. 1984; Thibault LE 1990; Grady, McLaughlin et al. 1993). For instance, axons in the optic nerve and spinal cord are tortuous and will uncoil and straighten following stretch of the macroscopic tissue, which results in individual axons experiencing different levels of axonal strain at the same level of tissue strain (Breig 1960; Bain, Shreiber et al. 2003). Breig first demonstrated the change of axonal tracts during simple loading (Breig 1960). Bain et al. first demonstrated the quantitative relation between change of axon tortuosity and tissue strain (Bain, Shreiber et al. 2003). They isolated optic nerve from guinea pig and stretched the nerve manually. With measuring the tortuosity of axons, they found out that the tortuosity decreased dramatically following stretch. Based on axon microstructure, Bain et al. developed a mathematical model describing affine deformation or non-affine deformation. The tortuosity of axons is defined as the value of the actual pathlength divided by the end-to-end length. When axons are stretched, the axon straightens, and tortuosity will decrease in affine or non-affine manner:

Affine: In affine model, axons are completely coupled to the surrounding matrix. Axons are assumed to experience the same geometrical deformation as the macroscopic tissue.

Non-affine: In non-affine model, axons are assumed to be completely uncoupled to each other or with surrounding matrix and straighten independently. The final tortuosity is calculated directly from the original tortuosity and the applied stretch ratio.

Bain observed that axons first straighten uncoupled (i.e. in a non-affine manner), and then becomes increasingly interdependent (i.e. in an affine manner) as stretch level increases. The reason why axonal deformation switches from non-affine to affine with increasing stretch levels is not clear. It was suggested that axons are more coupled to tissue as the stretch level increases. Since glial cells surround the axons in the central nervous system, it was suggested that glial coupling contributed to the switch.

Glia

Neurons are surrounded and held in place by glial cells (Virchow 1856). Recent studies suggest that glial cells might form a soft matrix around the neurons and protect neurons from mechanical trauma (Lu, Franze et al. 2006). Astroctyes, oligodendrocytes, and microgia are the three types of CNS glial cells while the glial cells of the PNS are known as Schwann cells. Astrocytes are star shaped glial cells and provide physical support to neurons via separate contacts with blood vessels in formation of the blood brain barrier (Butt, Colquhoun et al. 1994; Kakunaga, Ikeda et al. 2005). Astrocytes also contact with axons at nodes of Ranvier through cell adhesion molecules (Kakunaga, Ikeda et al. 2005). Oligodendrocytes are one of the primary structural constituents in white matter, and are suggested to provide the tissue with mechanical integrity (Bunge 1968; Palay, Sotelo et al. 1968; Peters 1990). Oligodendrocytes closely associate with nerve cells and produce a myelin sheath, which surrounds axons and allows for the efficient conduction of action potentials down the axon. The interaction between oligodendrocytes and axons occur at paranodal junctions, where the axonal cytoskeleton is adhered to the oligodendrocytes through interactions of Caspr and contactin with

neurofascin 155 (Peles, Nativ et al. 1997; Charles, Tait et al. 2002). The formation of an axo-glial junction between the distal, uncompacted loops of myelin and the axolemma is an early event during myelination, which will separate the node from the juxtaparanode (Sherman and Brophy 2005). Oligodendendrocytes extend several processes, each of which myelinates distinct internodes, usually on different axons. Thus, CNS tissue, and white matter in particular, can be seen as a complex composite of axonal fibers connected to glia. The coupling between glia and axons might affect the axonal deformation during stretch of the tissue. Myelin can be used as a marker to demonstrate the degree of axonal coupling to glia in tissue.

There is a positive correlation between the myelin sheath thickness and the axon diameter: bigger axons have thicker myelin, and vice versa (Hildebrand and Hahn 1978; Hildebrand, Remahl et al. 1993). Myelin breakdown occurs early following injures (Waxman 1989; Bunge, Puckett et al. 1993). It is characterized by initial swelling of myelin sheath. The loss of myelin is almost always associated with axonal pathology. In most vertebrate animals, including humans, myelin will continue developing years after birth (Miller 2002). In vivo, myelination can be disrupted by many different methods such as toxin induction (Blakemore 1978; Graca and Blakemore 1986; Harry, Goodrum et al. 1989) and immunological means (Keirstead, Pataky et al. 1997).

Oligodendrocyte apoptosis has been documented in humans and experimental animals following injuries (Li, Brodin et al. 1996; Abe, Yamamoto et al. 1999). Astrocytes undergo hypertrophy as detected by an abundant amount of cytoplasm at the edge of lesion (Norenberg, Smith et al. 2004). Two or three weeks after injury, astrocytes send out longer and thicker cytoplasmic processes, which results in a glial scar. Previous

studies have demonstrated that there is an enormous amount of cell-cell interaction among glial cells, and between glial cells and neurons (Johnson-Green, Dow et al. 1992; Ness and David 1997). If the glia affect the axonal kinematics, then the primary and secondary injury to glia are critical components that contribute to the physiological and functional deficits observed post-trauma. In this thesis, we will characterize the effects of glia on axonal kinematics, as well as the effects of myelination.

The chick embryo model and the changing glial environment

The primary goal of this thesis is to understand how axonal coupling to the glia affects axon kinematics and deformation. To examine this process, we selected the developing chick embryo as our model in this thesis, partially due to the fact that myelin development has been well characterized in chick embryo spinal cords. In the four regions of the chick spinal cord (cervical, brachial, thoracic, and lumbar), myelination appears to begin at the same time (Macklin and Weill 1985; Keirstead, Dyer et al. 1995). In general, myelin basic protein (MBP), which is synthesized in the myelin growth process, appears at E13 except in the brachial spinal cord where it appears at E12. The time course of myelination in the chicken ventral funiculus (VF) is characterized using electron microscopy (Anderson, Bjartmar et al. 2000). The first axon-oligodendrocyte connections are seen at E10 with formation of compact myelin at E12. Myelination proceeds quickly after E15. Almost 60% of axons are myelinated by E18. Chicken oligodendrocytes are demonstrated showing a structural heterogeneity analogous to that described in mammalian white matter (Anderson, Bjartmar et al. 1999).

Thesis overview

Our research aims to determine the relationship between tissue-level stretch and microstructure deformation in the developing spinal cord and model the mechanical behavior of axons. In this thesis, we employed the developing chick embryo spinal cord model to identify axonal mechanical responses to controlled stretch levels. Our goal is to understand how different cellular components can influence the axon mechanical behavior and how they can affect the parameters in axon kinematics models. First, in Chapter 2, we utilize the chick embryo model to describe the change in axon tortuosity distribution at different development stages at different stretch ratios. We also characterize the myelination in the spinal cord for each development stage by myelin basic protein (MBP) immunoreactivity. In Chapter 3, we predict axon kinematics with non-affine, affine, and 'switching' models. Predictions are compared to experimental data at each development stage and at each stretch level. Parameters in the 'switching' model are identified for each development stage. In Chapter 4, examine the influence of glia on coupling of axons at the micro-scale by demyelinating the spinal cord by injection of EB or GalC antibody. We characterize and quantify the myelination as well. Axon kinematics in the demyelinated spinal cord are studied and compared to the myelinated spinal cord. In Chapter 5, we examine the effects of glial coupling at the macro-scale by determining the material properties for myelinated and demyelinated spinal cords at the same developmental stage. In the final chapter, we summarize the study and results, state our conclusions, discuss future work, and consider the implications of our work with respect to axon injury.

Reference

Abe, Y., T. Yamamoto, et al. (1999). "Apoptotic cells associated with Wallerian degeneration after experimental spinal cord injury: a possible mechanism of oligodendroglial death." J Neurotrauma 16(10): 945-52.

Adams, J. H., D. Doyle, et al. (1984). "Diffuse axonal injury in head injuries caused by a fall." Lancet 2(8417-18): 1420-2.

Adams, J. H., D. I. Graham, et al. (1982). "Diffuse axonal injury due to nonmissile head injury in humans: an analysis of 45 cases." Ann Neurol 12(6): 557-63.

Anderson, E. S., C. Bjartmar, et al. (2000). "Myelination of prospective large fibres in chicken ventral funiculus." J Neurocytol 29(10): 755-64.

Anderson, E. S., C. Bjartmar, et al. (1999). "Molecular heterogeneity of oligodendrocytes in chicken white matter." Glia 27(1): 15-21.

Bain, A. C. and D. F. Meaney (2000). "Tissue-level thresholds for axonal damage in an experimental model of central nervous system white matter injury." J Biomech Eng 122(6): 615-22.

Bain, A. C., D. I. Shreiber, et al. (2003). "Modeling of microstructural kinematics during simple elongation of central nervous system tissue." J Biomech Eng 125(6): 798-804.

Blakemore, W. F. (1978). "Observations on remyelination in the rabbit spinal cord following demyelination induced by lysolecithin." Neuropathol Appl Neurobiol 4(1): 47-59.

Blight, A. R. and V. Decrescito (1986). "Morphometric analysis of experimental spinal cord injury in the cat: the relation of injury intensity to survival of myelinated axons." Neuroscience 19(1): 321-41.

Breig, A. (1960). "Biomechanics of the Central Nervous System." Stockholm:Almqvist & Wiksell.

Bunge, R. P. (1968). "Glial cells and the central myelin sheath." Physiol Rev 48(1): 197-251.

Bunge, R. P., W. R. Puckett, et al. (1993). "Observations on the pathology of human spinal cord injury. A review and classification of 22 new cases with details from a case of chronic cord compression with extensive focal demyelination." Adv Neurol 59: 75-89.

Butt, A. M., K. Colquhoun, et al. (1994). "Three-dimensional morphology of astrocytes and oligodendrocytes in the intact mouse optic nerve." J Neurocytol 23(8): 469-85.

Cargill, R. S., 2nd and L. E. Thibault (1996). "Acute alterations in [Ca2+]i in NG108-15 cells subjected to high strain rate deformation and chemical hypoxia: an in vitro model for neural trauma." J Neurotrauma 13(7): 395-407.

Charles, P., S. Tait, et al. (2002). "Neurofascin is a glial receptor for the paranodin/Caspr-contactin axonal complex at the axoglial junction." Curr Biol 12(3): 217-20.

Chen, Q. X., K. L. Perkins, et al. (1997). "Secondary activation of a cation conductance is responsible for NMDA toxicity in acutely isolated hippocampal neurons." J Neurosci 17(11): 4032-6.

Choi, D. W. (1994). "Calcium and excitotoxic neuronal injury." Ann N Y Acad Sci 747: 162-71.

Ellis, E. F., J. S. McKinney, et al. (1995). "A new model for rapid stretch-induced injury of cells in culture: characterization of the model using astrocytes." J Neurotrauma 12(3): 325-39.

Ellis EF, M. J., Willoughby KA, Liang S, Povlishock JT (1995). "a new model for rapid stretch-induced injury of cells in culture:charaterization of the model using astrocytes." J Neurotrauma 12(3): 325-39.

Galbraith, J. A., L. E. Thibault, et al. (1993). "Mechanical and electrical responses of the squid giant axon to simple elongation." J Biomech Eng 115(1): 13-22.

Gennarelli, T. A., L. E. Thibault, et al. (1989). "Axonal injury in the optic nerve: a model simulating diffuse axonal injury in the brain." J Neurosurg 71(2): 244-53.

Graca, D. L. and W. F. Blakemore (1986). "Delayed remyelination in rat spinal cord following ethidium bromide injection." Neuropathol Appl Neurobiol 12(6): 593-605.

Grady, M. S., M. R. McLaughlin, et al. (1993). "The use of antibodies targeted against the neurofilament subunits for the detection of diffuse axonal injury in humans." J Neuropathol Exp Neurol 52(2): 143-52.

Graham, D. I., J. H. Adams, et al. (1995). "The nature, distribution and causes of traumatic brain injury." Brain Pathol 5(4): 397-406.

Gray, J. A. and J. M. Ritchie (1954). "Effects of stretch on single myelinated nerve fibres." J Physiol 124(1): 84-99.

Harry, G. J., J. F. Goodrum, et al. (1989). "Tellurium-induced neuropathy: metabolic alterations associated with demyelination and remyelination in rat sciatic nerve." J Neurochem 52(3): 938-45.

Hildebrand, C. and R. Hahn (1978). "Relation between myelin sheath thickness and axon size in spinal cord white matter of some vertebrate species." J Neurol Sci 38(3): 421-34.

Hildebrand, C., S. Remahl, et al. (1993). "Myelinated nerve fibres in the CNS." Prog Neurobiol 40(3): 319-84.

Hovda, D. A., D. P. Becker, et al. (1992). "Secondary injury and acidosis." J Neurotrauma 9 Suppl 1: S47-60.

Johnson-Green, P. C., K. E. Dow, et al. (1992). "Neurite growth modulation associated with astrocyte proteoglycans: influence of activators of inflammation." Glia 5(1): 33-42.

Kakulas, B. A. (1999). "A review of the neuropathology of human spinal cord injury with emphasis on special features." J Spinal Cord Med 22(2): 119-24.

Kakunaga, S., W. Ikeda, et al. (2005). "Nectin-like molecule-1/TSLL1/SynCAM3: a neural tissue-specific immunoglobulin-like cell-cell adhesion molecule localizing at non-junctional contact sites of presynaptic nerve terminals, axons and glia cell processes." J Cell Sci 118(Pt 6): 1267-77.

Keirstead, H. S., J. K. Dyer, et al. (1995). "Axonal regeneration and physiological activity following transection and immunological disruption of myelin within the hatchling chick spinal cord." J Neurosci 15(10): 6963-74.

Keirstead, H. S., D. M. Pataky, et al. (1997). "In vivo immunological suppression of spinal cord myelin development." Brain Res Bull 44(6): 727-34.

Kraus, J. F. and D. L. McArthur (1996). "Epidemiologic aspects of brain injury." Neurol Clin 14(2): 435-50.

Lee, M., Melvin, J., and Ueno, K., (1987). Finite Element Analysis of Traumatic Subdural Hematoma. Proc of 31st Stapp Car Crash Conference.

Li, G. L., G. Brodin, et al. (1996). "Apoptosis and expression of Bcl-2 after compression trauma to rat spinal cord." J Neuropathol Exp Neurol 55(3): 280-9.

Lu, Y. B., K. Franze, et al. (2006). "Viscoelastic properties of individual glial cells and neurons in the CNS." Proc Natl Acad Sci U S A 103(47): 17759-64.

Macklin, W. B. and C. L. Weill (1985). "Appearance of myelin proteins during development in the chick central nervous system." Dev Neurosci 7(3): 170-8.

Maxwell, W. L., R. Kosanlavit, et al. (1999). "Freeze-fracture and cytochemical evidence for structural and functional alteration in the axolemma and myelin sheath of adult guinea pig optic nerve fibers after stretch injury." J Neurotrauma 16(4): 273-84.

Maxwell, W. L., B. J. McCreath, et al. (1995). "Cytochemical evidence for redistribution of membrane pump calcium-ATPase and ecto-Ca-ATPase activity, and calcium influx in myelinated nerve fibres of the optic nerve after stretch injury." J Neurocytol 24(12): 925-42.

McIntosh, T. K., D. H. Smith, et al. (1996). "Neuropathological sequelae of traumatic brain injury: relationship to neurochemical and biomechanical mechanisms." Lab Invest 74(2): 315-42.

Meaney, D. F., S. S. Margulies, et al. (2001). "Diffuse axonal injury." J Neurosurg 95(6): 1108-10.

Meaney, D. F., D. H. Smith, et al. (1995). "Biomechanical analysis of experimental diffuse axonal injury." J Neurotrauma 12(4): 689-94.

Miller, K. and K. Chinzei (2002). "Mechanical properties of brain tissue in tension." J Biomech 35(4): 483-90.

Miller, R., Margulies, S., Leoni, M., Nonaka, M., Chen, X., Smith, D., and and D. Meaney (1998). Finite Element Modeling Approaches for Predicting Injuryin an Experimental Model of Severe Diffuse Axonal Injury. Proc. of 42ndStapp Car Crash Conference.

Miller, R. H. (2002). "Regulation of oligodendrocyte development in the vertebrate CNS." Prog Neurobiol 67(6): 451-67.

Morrison, B., 3rd, K. E. Saatman, et al. (1998). "In vitro central nervous system models of mechanically induced trauma: a review." J Neurotrauma 15(11): 911-28.

Ness, R. and S. David (1997). "Leptomeningeal cells modulate the neurite growth promoting properties of astrocytes in vitro." Glia 19(1): 47-57.

Norenberg, M. D., J. Smith, et al. (2004). "The pathology of human spinal cord injury: defining the problems." J Neurotrauma 21(4): 429-40.

Olney, J. W. (1994). "New mechanisms of excitatory transmitter neurotoxicity." J Neural Transm Suppl 43: 47-51.

Palay, S. L., C. Sotelo, et al. (1968). "The axon hillock and the initial segment." J Cell Biol 38(1): 193-201.

Peles, E., M. Nativ, et al. (1997). "Identification of a novel contactin-associated transmembrane receptor with multiple domains implicated in protein-protein interactions." Embo J 16(5): 978-88.

Peters, a., Palay, S.L., Webster, D. (1990). the fine structures of the nervous system. Saunders, Philadephia.

Pettus, E. H., C. W. Christman, et al. (1994). "Traumatically induced altered membrane permeability: its relationship to traumatically induced reactive axonal change." J Neurotrauma 11(5): 507-22.

Pope, A. M. a. T., A.R. (1991). Disabilities in America: Toward a national agenda for prevention. National Academy Press, Washington, D.C.

Povlishock, J. T. and E. H. Pettus (1996). "Traumatically induced axonal damage: evidence for enduring changes in axolemmal permeability with associated cytoskeletal change." Acta Neurochir Suppl 66: 81-6.

Runge, J. W. (1993). "The cost of injury." Emerg Med Clin North Am 11(1): 241-53.

Sauaia, A., F. A. Moore, et al. (1995). "Epidemiology of trauma deaths: a reassessment." J Trauma 38(2): 185-93.

Sherman, D. L. and P. J. Brophy (2005). "Mechanisms of axon ensheathment and myelin growth." Nat Rev Neurosci 6(9): 683-90.

Shi, R. and A. R. Blight (1996). "Compression injury of mammalian spinal cord in vitro and the dynamics of action potential conduction failure." J Neurophysiol 76(3): 1572-80.

Shi, R. and R. B. Borgens (2000). "Anatomical repair of nerve membranes in crushed mammalian spinal cord with polyethylene glycol." J Neurocytol 29(9): 633-43.

Shi, R. and J. D. Pryor (2000). "Temperature dependence of membrane sealing following transection in mammalian spinal cord axons." Neuroscience 98(1): 157-66.

Shi, R. and J. D. Pryor (2002). "Pathological changes of isolated spinal cord axons in response to mechanical stretch." Neuroscience 110(4): 765-77.

Smith, D. H., J. A. Wolf, et al. (1999). "High tolerance and delayed elastic response of cultured axons to dynamic stretch injury." J Neurosci 19(11): 4263-9.

Sosin, D. M., J. J. Sacks, et al. (1989). "Head injury-associated deaths in the United States from 1979 to 1986." Jama 262(16): 2251-5.

Tator, C. H. and I. Koyanagi (1997). "Vascular mechanisms in the pathophysiology of human spinal cord injury." J Neurosurg 86(3): 483-92.

Thibault LE, G. T., Margulies SS, Marcus J, Eppinger R (1990). The strain dependent pathophysiological consequences of inertial loading on central nervous system tissue. Lyon.

Thuret, S., L. D. Moon, et al. (2006). "Therapeutic interventions after spinal cord injury." Nat Rev Neurosci 7(8): 628-43.

Torg, J. S., L. Thibault, et al. (1995). "The Nicolas Andry Award. The pathomechanics and pathophysiology of cervical spinal cord injury." Clin Orthop Relat Res(321): 259-69.

Virchow (1856). Gesammelte Abhandlungen zur Wissenschafilichen medicin. von Meidinger Sohn, Frankfurt, Germany.

Waxman, S. G. (1989). "Demyelination in spinal cord injury." J Neurol Sci 91(1-2): 1-14.

Young, W. (2002). "Spinal cord contusion models." Prog Brain Res 137: 231-55.

Chapter 2: Axonal kinematics during development in chick embryo spinal cord

Abstract

The axonal kinematic response to different level of strain was examined in developing chick embryo spinal cords. Spinal cords were dissected from chick embryos at different days of development (E12, E14, E16, and E18), and the myelination of chick embryo spinal cord was characterized by immunohistochemical labeling of myelin basic protein (MBP), which is synthesized in the myelination process. Spinal cords at each developmental stage were dissected, exposed to different stretch ratios (1.05, 1.1, 1.15, 1.20), and fixed with paraformaldehyde at the stretched length. Spinal cords were then sectioned, stained immunohistochemically for neurofilament proteins, and imaged with epifluorescence microscopy. The tortuosities of hundreds of axons were traced by measuring the actual pathlength and the end-to-end length of randomly selected individual axons. The tortuosity distribution of axons before and after stretch was examined. During development, the length of the spinal cord increased 55% from E12-E18 and white matter tracts were significantly myelinated. Axons in the unstretched spinal cord at each development stage were undulated. After stretching the spinal cord, axons straightened, with the decrease in tortuousity dependent on the development stage. The results indicated that in unstretched embryonic chick spinal cords, the average tortuosity of axons decreases naturally during development. Also, the percentage of

axons remaining tortuous at higher stretch ratios increased with growth and development. The increase correlated positively to increases in myelination of the white matter.

Introduction

Axonal injury in the white matter is the largest contributor to physiological and functional deficits following brain and spinal cord injury (Gentleman, Roberts et al. 1995; Kakulas 1999). Mechanical strain is demonstrated as the proximal cause of traumatic axonal injury in numerous studies (Graham, Adams et al. 1995; Meaney, Margulies et al. 2001). The initial event in traumatic axonal injury is the strain of axons as the result of inertial loading for brain injury (Adams, Doyle et al. 1984; Thibault LE 1990; Grady, McLaughlin et al. 1993). In most mechanical trauma, longitudinal stretch is assumed to be the primary cause for axonal damage in the white matter (Blight and Decrescito 1986; Torg, Thibault et al. 1995; Meaney, Margulies et al. 2001). As tension increases, the relative number of injured axons and glial cells increases concomitantly (Crowe, Bresnahan et al. 1997; Grossman, Rosenberg et al. 2001). These observations suggest that under even simple tensile loading, the mechanical transfer of strain from tissue to the axons or glial cells is complex. However, since the mechanism of strain transfer from tissue to axons is unclear, the mechanical parameters necessary to injure axons *in vivo* are currently not known.

Strain thresholds for morphological injury were reported by *in vitro* studies of the squid giant axon and frog sciatic nerve axons (Thibault 1981; Galbraith, Thibault et al. 1993; Saatman 1993). However, the tolerance of individual axons in these studies was based on complete structural failure of the axon. Secondary axotomy is delayed, and can

take several hours to several days to occur (Povlishock, Becker et al. 1983; Povlishock 1992; Povlishock and Christman 1995). Thus, thresholds predicted from these in vitro tests for primary axotomy are likely to overestimate the strain required to produce axonal injury as seen in TBI and SCI.

Axons in white matter, such as in the spinal cord and optic nerves, have a tortuous, undulated morphology (Breig 1960; Bain, Shreiber et al. 2003). When axons are stretched, they will straighten and become less tortuous. How the tortuosity of axons changes following tissue strain is unclear. Breig first demonstrated the change of axonal tracts during simple load (Breig 1960). Bain et al. first studied how axon tortuosity will change during stretch and presented a quantitative description relating tissue level strain with the subsequent geometry change of axons in the guinea pig optic nerve (Bain, Shreiber et al. 2003). Their studies demonstrated that uncoiling of axons did not follow idealized descriptions of either affine (fully coupled) nor non-affine (completely uncoupled) mechanical behavior. Instead, axons first deform independently, then gradually transition to coupled behavior as the tissue strain increased.

Bain et al. proposed that axon-level threshold predictions relies on the accuracy of the experimental axonal tortuosity distribution (Bain, Shreiber et al. 2003). A tortuous axon that deforms in a purely non-affine manner will not experience stretch until it has completely straightened; it is free to unfold as the nerve is elongated. Due to the tortuous nature of axons, this behavior would significantly decrease the actual axon threshold from the tissue-level threshold. However, at larger tissue strain level, axons tend to exhibit affine behavior. Thus, for a particular tissue-level strain, the strain experienced by an individual axon depends on its initial tortuosity and connectivity to the surrounding

tissue. This variability in axonal strain provides a potential explanation for the non-uniform pattern of axonal pathology with increasing injury severity. This non-uniform threshold for axon injury may also elucidate why certain areas of the white mater are more prone to injury than others. Therefore, it may be more appropriate to define unique parameters for different areas depending on their microstructure. Therefore, both the tortuosity and the dynamics of axon coupling must be known in order to understand the relationship between strain in the microstructure of the CNS and the deformation in the tissue. Understanding this relationship is critical for predicting what forces will cause injury in CNS axons.

The dynamics responsible for the switch from non-affine to affine behavior may be due to connections between axons as well as an interaction between axons and other components, such as glial cells within the nerve. An understanding of the effects of other cell components on axon kinematics is important for predicting the axon injury threshold. We hypothesize that axons behave in more affine manner as development proceeds because of the increasing cell connectivity. Axons in the CNS are myelinated by specialized glial cells known as oligodendrocytes. Oligodendrocytes are one of the primary structural constituents in white matter, providing the tissue with mechanical integrity (Bunge 1968; Palay, Sotelo et al. 1968; Peters 1990). Axon coupling via the glial matrix has clear importance for axonal injury mechanics, and also has strong implications for glial injury. For example, just as axonal pathology increases progressively with higher levels of applied stretch, so does glial injury. Only recently has the primary injury response of these cells to mechanical trauma been investigated.

In this chapter, we examined the influence of spinal cord growth and development on axon kinematics. We selected the developing chick embryo model to study the effect, since myelination during development in chick embryos has been extensively studied and characterized. Functional axons in the chick embryo are present at 7 days post-fertilization (E7) (O'Donovan, Sernagor et al. 1992). However, maturation of oliogodendrocytes does not begin until a few days later. While the myelination process begins at E10 in some parts of the CNS, such as the ventral funiculus of the spinal cord, the first compact myelin sheath isn't observed until E12 (Anderson, Bjartmar et al. 2000). Myelination develops rapidly from E12 until hatching, the progress of which can be detected with immunohistochemical staining of the myelin basic protein (MBP) (Anderson, Bjartmar et al. 2000), which is synthesized during the myelination process. During this time, the spinal cord is increasingly vascularized, which may also increase mechanical coupling via astrocytes. Thus, we expect axons to demonstrate increasingly affine behavior as development and myelination progress.

Methods

Chick embryo spinal cord measurements and isolation

Fresh fertile eggs were incubated at 38°C until the appropriate day (E12, E14, E16, or E18). The embryo was transferred from the egg and the spinal column was dissected in PBS. The ventral/dorsal vertebrae (C2/3 – T4/5) were removed to expose the spinal cord surface while the other vertebrae were left intact. Two measurements were collected using a digital caliper: 1) the *in ovo* gauge length between the two opened vertebrae, and 2) the length between ganglion 3 and ganglion 13 (G3-G13) where ganglion 11 was

always at the widest site of the spinal cord. The second measurement was collected to identify the elongation of the spinal cord due to growth. Every measurement was repeated three times and the average value was calculated. The *in situ* lengths among developmental stages were statistically compared using ANOVA with repeated measures, followed by Scheffe's post hoc test ($P<0.05$). After the two measurements, the other half of the vertebrae (C2/3 – T4/5) was taken off to expose the entire surface of spinal cord. The gauge length between C2/3 and T4/5 was measured again in triplicate to obtain the average value. This measurement was defined as the *in vitro* length after full dissection. To examine the shrinkage due to dissection, the *in vitro* length was compared with *in ovo* length.

Fully dissected spinal cords were then immediately transferred to a stretching device built in our lab as shown in Fig 2-1. The device consists of a chamber filled with PBS buffer and two manipulators that can provide precise stretch ratios. The two ends of the spinal cord were clamped with the cord submerged in (buffer). The gauge length was measured to restore the cord to its in situ length. The spinal cord was then stretched manually at a slow rate to one of the four stretch ratios (1.05, 1.1, 1.15, or 1.2) (Table 2-1).

Embryonic Day	Stretch Levels	Cords Tested at Each Situation
12	1, 1.05, 1.1, 1.15, 1.2	3
14	1, 1.05, 1.1, 1.15, 1.2	3
16	1, 1.05, 1.1, 1.15, 1.2	3
18	1, 1.05, 1.1, 1.15, 1.2	3

Table 2-1. Spinal cords at E12, E14, E16, or E16 are stretched to one of the stretch levels (1, 1.05, 1.1, 1.15, 1.2). Three cords are tested at each situation.

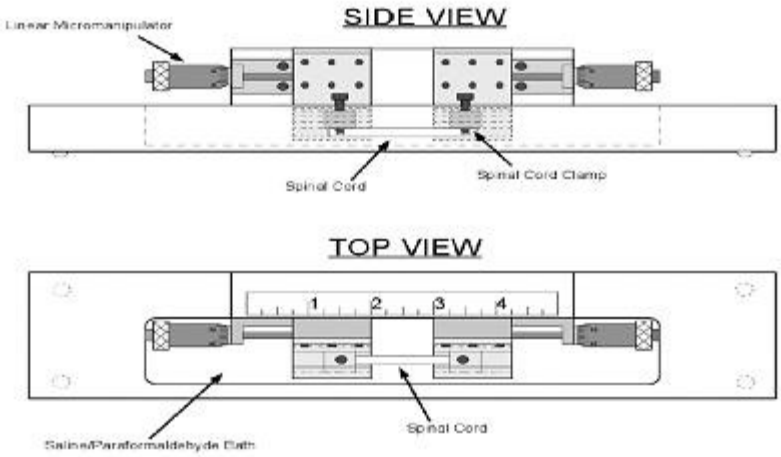

Figure 2-1: Schematic of device to impact cocntrolled stretch to spinal cord excised from chick embryos.

Immediately after stretching each cord to the desired stretch ratio, the buffer solution was replaced with 4% paraformaldehyde for at least 30 minutes to fix the spinal cords in the stretched state. The ends of the spinal cords were then unclamped and the length was measured again to ensure the cords remain elongated without shrinking. A previous study has demonstrated that fixing with paraformaldehyde will not damage the morphology of tortuous axons (Bain, 2003). After storage in paraformaldehyde overnight at 4°C, the cords were then transferred to a 20% sucrose-saline solution overnight. The sucrose was used as a cryoprotectant in preparation for immunohistochemical labeling of axons and MBP.

Immunohistochemical labeling

Spinal cords were cut to 10 μm coronal sections and 5 μm transverse sections were also cut with a cryostat (Thermo Electron, Pittsburgh, PA). Sections were then collected on pre-treated glass microslides (Fisher Scientific, Hampton, NH). The sections were

used for immunohistochemical labeling of axons and MBP using an immunostaining workstation (ThermoShando, Pittsburgh, PA). To trace the axons, sections were rinsed in a buffer solution (1% bovine serum albumin (BSA – Sigma), 0.5% TritonX-100 (Sigma) in phosphate buffered saline (PBS - Sigma)) for 5 minutes at room temperature, and then incubated in a 10% solution in immuno buffer of goat serum (Atlanta Biologicals, Lawrenceville, GA) for 1 hour for to block non-specific binding. Sections were then incubated overnight at 4 degree in a 1:1000 dilution of mouse α-neurofilament-200 (Sigma, N-0142). The next day, sections were washed with buffer for 5 minutes, and then incubated in a 1:400 dilution of Alexa 546 goat anti-mouse secondary antibody (Molecular Probes, A11018) for 1 hour. Sections were again rinsed for 5 minutes, and slides were coverslipped (Vectashield mounting medium for fluorescence, Vector Labs, Burlingame, CA).

To characterize the myelin, slides were double-labeled with a 1:1000 dilution of mouse anti-neurofilament-200 (Sigma, #N-0142) and 1:400 rabbit anti-human MBP antibody (Accurate chemical scientific corp., #AXL746). The secondary antibodies used were a 1:400 dilution of Alexa 546 goat anti-mouse secondary antibody (Molecular Probes, Eugene, OR, #A11018) and goat anti-rabbit FITC conjugated immunoglobulin (Caltag Laboraties, # L42001).

Microscopy and image analysis

Composite images of spinal cord sections from C4/5 – T2/T3 were generated with Olympus Microsuite software controlling an Olympus IX81 inverted epifluorescent microscope (Olympus, Melville, NY) and a Hamamatsu ORCA 285 digital camera

(Hamamatsu City, Japan). Each spinal cord section was divided into two segments, cervical and thoracic. Each image was divided to three columns, and 20-30 axons were randomly picked from each column for measurements. Two measurements were made for each axonal segments with the Microsuite software. The actual path length was found by tracing the segment with the cursor. The end-to-end length was then identified from the coordinates of the beginning and end of the traced line. These two measurements were made for several hundred randomly located axons for each spinal cord, and the results were recorded.

Additionally, to evaluate potential differences along the length of the spinal cord, tortuosity values were grouped according to position as either "cervical" or "thoracic" for statistical comparisons. Axonal tortuosity distribution graphs were created using KaleidaGraph software.

To characterize myelination in spinal cords at different stages of development, composite images were generated from double stained slides. MBP staining and NF staining were imaged at the same location and then overlaid.

Statistics

Tortuosity distributions were compared statistically using a Kruski-Wallis (K-W) non-parametric test for comparison among development days and stretch levels, followed by pairwise Kolmogorov-Smirnov (K-S) non-parametric test (SPSS, Chicago, IL). K-S tests alone were used for comparisons of tortuosity between cervical and thoracic locations. Significance values are set $P < 0.05$.

Results

Growth of chick embryo spinal cord

Spinal cords grew significantly from E12 to E18 (Figure 2-2) (ANOVA with repeated measures, followed by Scheffe's post hoc test, max $P < 0.001$). During this time, the length of the spinal cord between the 11 nerve roots increased almost 8mm. Spinal cords did not shrink following excision of the whole spinal column from the chick, but did consistently decrease in length ~5% following removal of the vertebrae excision from the spinal column, indicating a level of *in vivo* tension. No trends relating the percentage of tissue shrinkage to development stage were observed.

Immunohistochemistry

Digital imaging following immunolabeling of neurofilaments with α-NF200 revealed many continuously-labeled axons that were easily viewed with epifluorescence microscopy at all stretch levels (Fig 2-4, 2-5, 2-6, 2-7). The progression of myelination differentiation was confirmed with immunolabeling of myelin basic protein (α-MBP) (Fig 2-3).

Myelin characterization

MBP is synthesized in the myelination process, and thus it can represent the degree of myelination in axons during development. Both coronal and transverse spinal cord showed a significant increase in myelination proportional with developmental stage. As shown in Fig 2-3, myelin was virtually absent at E12 and was ubiquitous at E18. Myelin represents the connection between oligodendrocytes and axons. One oligodendrocyte can

myelinate multiple axons. The increase in the myelination showed an increase in the interconnectivity between axon and oligodendrocyte with growth in chick embryo spinal cords.

Tortuosity characterization

Digital imaging following immunolabeling of neurofilaments with α-NF200 revealed many continuously labeled axons. They were easily viewed with epifluorescence microscopy at all stretch levels. Axons in unstretched, controlled spinal cords were visibly undulated, and became noticeably straighter with increasing stretch ratios. Representative images and associated tortuosity distributions are presented for E12 (Figure 2-4), E14 (Figure 2-5), E16 (Figure 2-6), and E18 (Figure 2-7) spinal cords.

Summary statistics of the tortuosity characterization are presented in Table 2-2 and normalized distributions for all embryonic stages and stretch levels are shown in Fig 2-8. Tortuosity distributions in unstretched spinal cords generally followed a Gamma distribution, which was consistent with axons in the guinea pig optic nerve (Bain, Shreiber et al. 2003). With stretch, the distribution changed markedly, but the nature of the changes depended upon the developmental stage. Statistical analysis of axonal tortuosity in control, unstretched spinal cords revealed significant changes in tortuosity distributions with development among all stages (K-W test, $p<0.001$), and from E12 to E14 ($p=0.001$) and E14 to E16 ($p=0.001$, K-S test). Tortuosity distributions from unstretched E16 and E18 spinal cords were not significantly different (K-S test, $p=0.177$). Tortuosity generally decreased with increasing development. Among all stages and within each stage, stretch significantly decreased tortuosity ($p<0.001$, K-W test followed

by K-S tests for pairwise testing of stretch levels). The following pairwise comparisons were not significant (K-S test) :E12 versus E14, 10% stretch (p=0.519); E12 versus E18, 5% stretch (p=0.139); and E14 versus E16, 5% stretch (p=0.055). All other pairwise comparisons were significant. (max p=0.042). Tortuosity distribution for stretched spinal cord depended not only on the initial tortuosity, but also the developmental stage. Following stretch, axons from spinal cords harvested later in development were more tortuous than those from spinal cords harvested earlier in development, which was consistent with a switch to affine behavior with axon coupling following growth. Additionally, control axonal tortuosity in cervical spinal cord white matter was compared to thoracic spinal cord white matter for each spinal cord at each developmental stage. No significant differences were observed for any of the four developmental stages (K-S test, $P > 0.25$).

Discussion

In this investigation, we studied how deformation of the underlying axonal microstructure of spinal cord white matter changes during the period of rapid growth in chick embryos from E12-E18. Axons in the optic nerve and spinal cord have been characterized as tortuous, but straighten as a result of stretching (Breig 1960; Bain, Shreiber et al. 2003). To characterize the mechanical behavior, we took advantage of the tortuous, undulated nature of axons in normal white matter. A previous study by Bain *et al.* described general methods to quantify axonal tortuosity in the guinea pig optic nerve, where tortuosity was defined as actual length divided by end-to-end length (Bain, Shreiber et al. 2003). The tortuosity decreases with stretch and never goes below one.

That study also compared the changes in axonal tortuosity that resulted from straightening during stretch to mathematical predictions of ideal affine and non-affine behavior. It was concluded that neither model described the experimental data perfectly. Axon mechanics in the guinea pig optic nerve appeared to transition from non-affine behavior at low stretch levels to affine behavior at high stretch levels. It was proposed that interaxonal connections, as well as connections between axons and other tissue components such as the glial matrix, were responsible for this transition. Based on these assumptions, we believed that the degree of interconnectivity of axons via the glial matrix would increase with chick embryo growth and would be demonstrated as a transition from predominantly non-affine to affine behavior during development. We also wanted to examine the response of other white matter that is more often injured during trauma. Therefore, we characterized the tortuosity distribution of axons in response to controlled stretch levels in the developing chick embryo spinal cord during a period of rapid myelination. We chose four different stretch levels between 5% and 20% for two reasons: first, the morphological injury threshold for the optic nerve has been shown between 25-40%; and second, the spinal cord started to break at strains higher than 20%.

Based on a normal distribution of tortuosity, Bain et al. reported that axons in the optic nerve exhibit tortuosity between 1.0 and 1.5, with a mean value of 1.13. In our study, axons in chick embryo spinal cord exhibited tortuosity between 1.0 and 1.3, with mean values of 1.083-1.096 for the different development stages (Bain, Shreiber et al. 2003). Our results for the tortuosity of spinal cord axons fall within the range estimated for collagen fibrils and axons in optic nerves. Tortuosity in embryonic chick spinal cord axons followed a Gamma distribution at all stages of development and showed a modest

but significant decrease from E12-E18 (Fig 2-4A, 2-5A, 2-6A, 2-7A), as well as an increase in the number of "perfectly straight" axons. This observation represents a shift in the tortuosity distribution towards straighter axons (a 'left-censored' distribution). However, the degree to which the axon population straightened as a result of growth-induced tissue stretch was far less than that predicted by any of the kinematics models examined. The decrease in tortuosity from E12-E14, E14-E16, and E16-E18 was 0.0036, 0.006, and 0.001 respectively. Assuming that the decrease was caused by a non-affine stretch, the stretch ratio then results in 3.6%, 0.6%, and 0.1% respectively. The estimated values of the applied stretch ratio are minimal compared to the percent increase in growth (20%, 17%, and 10%, respectively). Thus, we conclude that tissue stretch during growth contributes minimally to the kinematic behavior of axons. However, the increase in spinal cord length results from mechanical forces imparted by the growing skeleton. These mechanical forces may be transferred to the axons and induce axonal elongation during growth. Our observation implies that there is an inherent mechanism to preserve axon tortuosity as the axon grows during development. New axoplasm, and axolemma are either generated in a tortuous geometry or are contracted to that geometry by other cells, such as oligodendrocytes or astrocytes, or by active contraction of axonal cytoskeleton elements.

For each developmental stage, axons' tortuosity progressively decreased with increasing stretch level. Axon tortuosity distribution for chick embryo spinal cord at controlled stretch levels shift towards straighter axons (a "left-censored" distribution) (Lindsey, Byrom et al. 2000). The trend of shift depends on the development stage. Following stretch of spinal cord, axons maintained higher degree of undulation for spinal

cords at later phases compared to spinal cords at earlier phases, especially at higher stretch levels. For example, the mean tortuosity decreased to 1.004 for E12 at 20% stretch but only to 1.014 for E18, even though E12 axons were initially more tortuous than E18 axons (1.096 at 0% stretch for E12 vs. 1.083 for E18). The percentage of "perfectly straight" axons at 20% stretch decreased from E12-E18, indicating an increase in affine, coupled kinematic behavior with growth and development. Axons exposed to controlled stretch generally followed the same trends as adult guinea pig optic nerve axons, demonstrating a transition from non- affine mechanics at low stretch levels to affine mechanics at high stretch levels. As expected, non-affine, uncoupled behavior was more prevalent earlier in development and affine, coupled behavior increasingly prevailed later in development, though at no stage was behavior purely non-affine or affine.

In addition to lengthening of the spinal cord, many other changes occur in chick embryo spinal cord white matter during development period studied, such as the formation of new axon tracts, maturation of existing tracts, maturation of oligodendrocytes and subsequent myelination of axons, and vasculogenesis. Though different cytoskeletal changes have been observed in small- vs. large-caliber axons exposed to dynamic stretch, no correlation has been observed between "injury" and axon diameter in these models (Jafari, Maxwell et al. 1997; Jafari, Nielson et al. 1998; Shi and Pryor 2002). Thus, axon diameter is not considered as a contributor to the change of axon kinematics with development. Taking the advantage of MBP which was only processed and expressed in myelinating oligodendrocytes, we evaluated the myelination degree at each development stage based on MBP immunoreactivity. Myelination increased with growth, especially between E14 and E16. Axons are coupled to oligodendrocytes via

myelin formation. Thus, we can conclude that the observed change in axonal mechanics during development correlates positively with increased coupling. We are examining more directly the role of the axonal coupling to glia in axon kinematics in Chapter 4.

In our study, we used neurofilament antibody immunohistochemistry labeling to visualize axon projections. First, we isolated the spinal cord from chick embryos and stretched in situ. Nerves will not lose their antigenicity. Second, the neurofilament is a structure unit of the cytoskeleton and predominately throughout the axon. We believe that the method we use to visualize axon represents the actual axon tortuosity.

Tissue is shrunk whenever it is fixed or dissected from the embryo (Boonstra, Oosterhuis et al. 1983; Grace and Llinas 1985; Lum and Mitzner 1985; Collan, Torkkeli et al. 1987). We tried to measure the tissue length before taking it out and restored the original length such that it was the same as *in vivo*. The shrinking was minimized by stabilizing the ends of the spinal cord during fixing. We measured three spinal cords at each stretch ratio and at each developmental stage. Characterization of axon tortuosity was reproducible, and the tortuosity decreased dramatically with increasing stretch levels. Thus, we believe that the patterns we visualized were due to the tortuosity of the axons. We sectioned the spinal cord along the whole stretched length to 50-60 slices and randomly measured 10-15 slices. We measured 30-50 axons for each slice and axons were picked randomly with at least 4-5 consistent waves. In summary, we believe that our results represent the overall kinematic behavior of stretched spinal cord.

The tortuosity of an axon is also affected by the assumption of a two-dimensional axonal path. In both the study by Bain *et al.* (Bain, Shreiber et al. 2003) and our study, axon tortuosity is measured within the 2-dimensional plane that is imaged, and it is

modeled as a 2D sinusoidal wave. All measurements were performed on a 2D plane sectioned with ventral side and dorsal side top and down; indicating slices were sectioned from ventral side to dorsal side. We also took a few images that sectioned with the ventral side flipped ninety degrees, indicating ventral side and dorsal side were sectioned in same slices, and observed tortuous morphology of axons as well. There is one possibility that axons traversed through the thickness of the plane. If the axon is helical, we would see inconsistent staining in one plane. However, all images showed continuous, consistent, and tortuous axons. It is not clear how the axon maintains a tortuous morphology in both planes. In any case, approximating the 3D tortuous path of the axon with its 2D projection underestimates the actual path length of the axon, but maintains the end-to-end length, thereby underestimating the actual tortuosity of the axon. With an increase in the initial tortuosity of axons, the threshold for axon morphological injury and functional injury may increase as well. This error increases as the axons become wavier (or more coiled). We would expect this to be systematic error and not to change with growth/development, although we are investigating methods to extract and measure the 3D pathway in an efficient manner for 3D tortuosity characterizations.

We selected the developing chick embryo spinal cord as our model tissue in our research. There are several advantages of this model for this study. Chick embryo tissue is readily available through procurement of fresh, fertilized eggs and is cost effective when compared to small mammals. Maintaining eggs during development is relatively simple, and development period for eggs is relatively short. It only takes 21 days for eggs to hatch. Chick embryos grow very quickly within a short period. Therefore, harvesting tissue at a desired developmental stage is relatively simple and the time period is

relatively short. The kinetics of spinal cord myelination in the chick has been well characterized. Myelination proceeds quickly, so it is easy to isolate spinal cords with different levels of myelination. Axons in the spinal cord have a tortuous morphology and are longitudinally aligned parallel to the direction of stretch, thus allowing a direct interpretation of the relationship between macroscopic tissue stretch and microscopic axonal deformation. Unlike optic nerves, spinal cord consists of both white matter and gray matter. However, axons are only aligned in white matter and we are largely interested in the mechanical strain transfer from white matter to microstructure in white matter. Therefore, the kinematic behavior of axons based on pure strain of white matter should be relatively independent of the gray matter. We did not expect gray matter to influence initial tortuosity during development or white matter mechanics. However, material properties of spinal cord and optic nerve are markedly distinct since gray matter will significantly contribute to the mechanostructural, material response (i.e. stress-strain response) of the spinal cord. Axonal mechanics may follow the same functional form in chick embryo spinal cord and guinea optic nerve, but require separate characterizations to capture the individual tortuosity and kinematics.

Regardless of what happened during spinal cord growth in axons and connective tissue, the observed differences in chick embryo spinal cord at different development stages have clear implications for defining tolerance for brain and spinal cord injury. The strain transfer from macroscopic, tissue-level to microscopic, axonal-level is decided primarily by the degree of tortuosity and the axon kinematics, which combine to dictate the threshold for morphological and functional injury. Our results demonstrated that any spatial and or/temporal changes in tortuosity and kinematics during development would

affect the injury response. Thus, axons in the human spinal cord could change in tortuosity and kinematics during development as well. Unlike chick spinal cord, in which myelination may be nearly complete at hatching, myelination of the human spinal cord is incomplete at birth and continues to at least 3 years of age, and maturation of white matter fiber tracts (thickening of axons and myelin sheaths) can continue well into adolescence, especially in tracts involved in motor pathways. Hence, the tolerance of human white matter to stretch could very well vary significantly during development. It is known that the mechanical properties of brain tissue change with development, which would, in turn, affect the injury response of the brain. The changes in microstructure kinematics could contribute to the observed changes in macroscopic tissue mechanical behavior, and any microstructure model of white matter mechanics would require careful consideration of both the axon's tortuosity and the dynamics of kinematics coupling.

Figures and Tables of Results

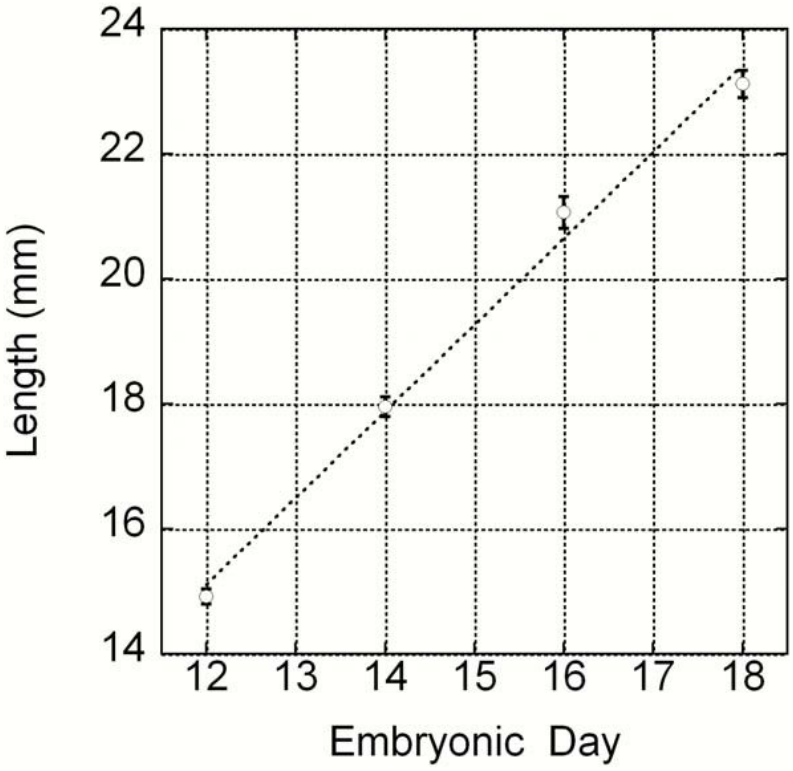

Figure 2-2: Chick embryo spinal cord growth in ovo from E12 to E18. During this period of development, the length between the 11 nerve roots increased almost 55%. Significant increases in length were observed from stage-to-stage (ANOVA with repeated measures, followed by Scheffe's post hoc tests, max P<0.001). Growth during this period was linear (R2 = 0.99), with a slope (+/- std err) of 1.38 +/- 0.02 mm/day.

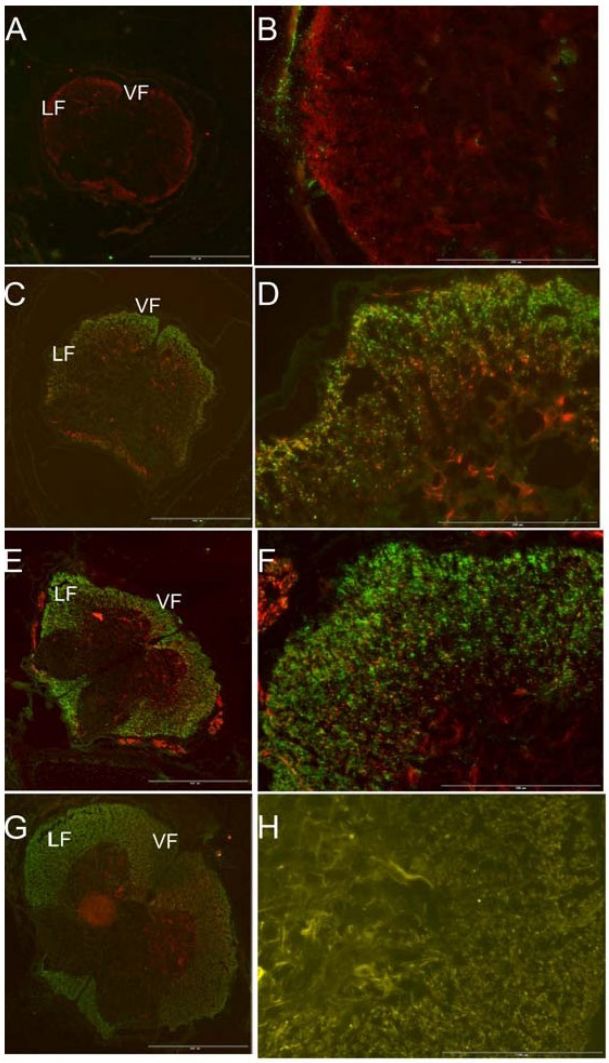

Figure 2-3: Progression of myelination in the chick embryo spinal cord. Low magnification images (A,C,E,G) of whole cross-sections and higher magnification images(B, D, F, H) of the lateral funiculus were taken following immunohistochemical double-labeling of the chick embryo spinal cord were double-labeled immunohistochemically for neurofilament proteins (NF-200 - red) and myelin basic protein (MBP-green). Little myelin was observed in E12 spinal cords (A,B). At E14 (C,D), myelination is pronounced in the ventral funiculus (VF), but less so in the lateral funiculus (LF). By E16 (E,F), myelination has begun in nearly all white matter tracts, and by E18 (G,H) myelin is pronounced throughout the white matter, including the lateral funiculus. (I) The degree of myelination (average +/- standard deviation) increased significantly from E12 to E18 (ANOVA, followed by Scheffe's post hoc test, max P = 0.008). (Scale bars = 200µm for A, C, E, and G, 500µm for B, D, F, and H.)

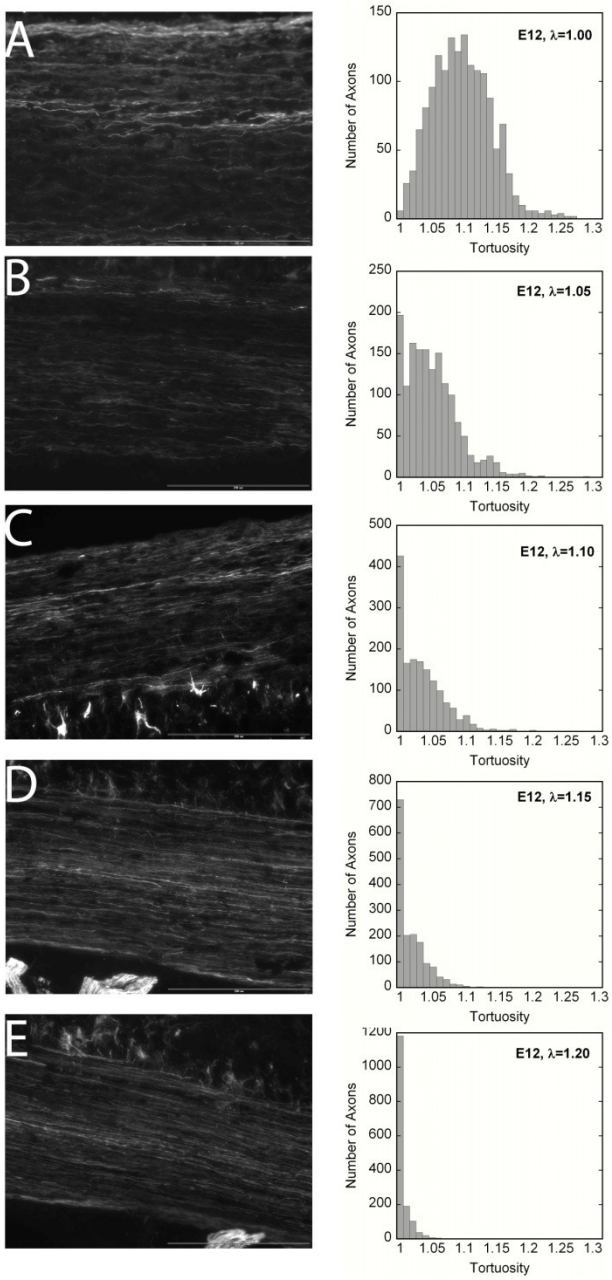

Figure 2-4: Immunohistochemistry and tortuosity characterization for E12 spinal cords. Fixed spinal cords were sectioned coronally and immunhistochemically stained for neurofilament proteins. The tortuosity distribution for axons in the sections was determined by tracing several hundred axons from each spinal cord. (A) Many axially- oriented, wavy axons were observed in unstretched spinal cords. The distribution of axonal tortuosity followed a normal distribution. As stretch increased (B = 5%, C = 10%, D = 15%) axons became progressively straighter, and a significant number of axons had tortuosity equal or near one. At the highest stretch ratio (E = 20%), almost all axons appeared to be straight or nearly straight. (Scale bars = 200μm.)

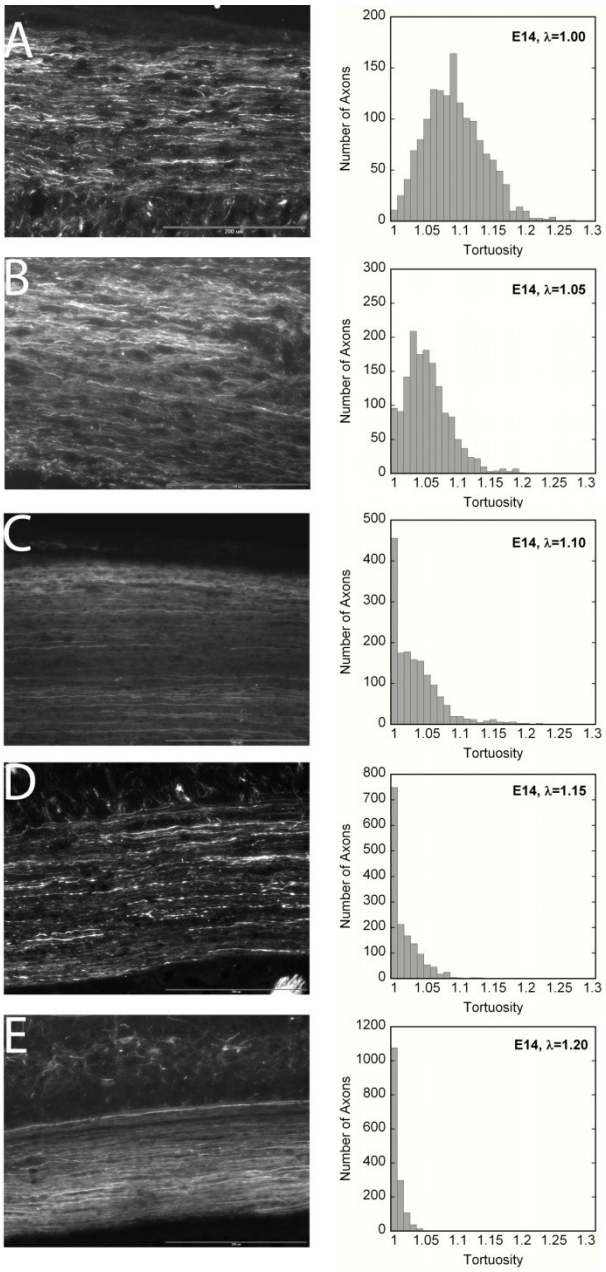

Figure 2-5: Immunohistochemistry and tortuosity characterization for E14 spinal cords. The tortuosity distribution for axons was similar to axons in E12 spinal cords. (A) Many axially- oriented, wavy axons were observed in unstretched spinal cords. The distribution of axonal tortuosity followed a normal distribution. As stretch increased (B = 5%, C = 10%, D = 15%) axons became progressively straighter, and a significant number of axons had tortuosity equal or near one. At the highest stretch ratio (E = 20%), almost all axons appeared to be straight or nearly straight. (Scale bars = 200μm.)

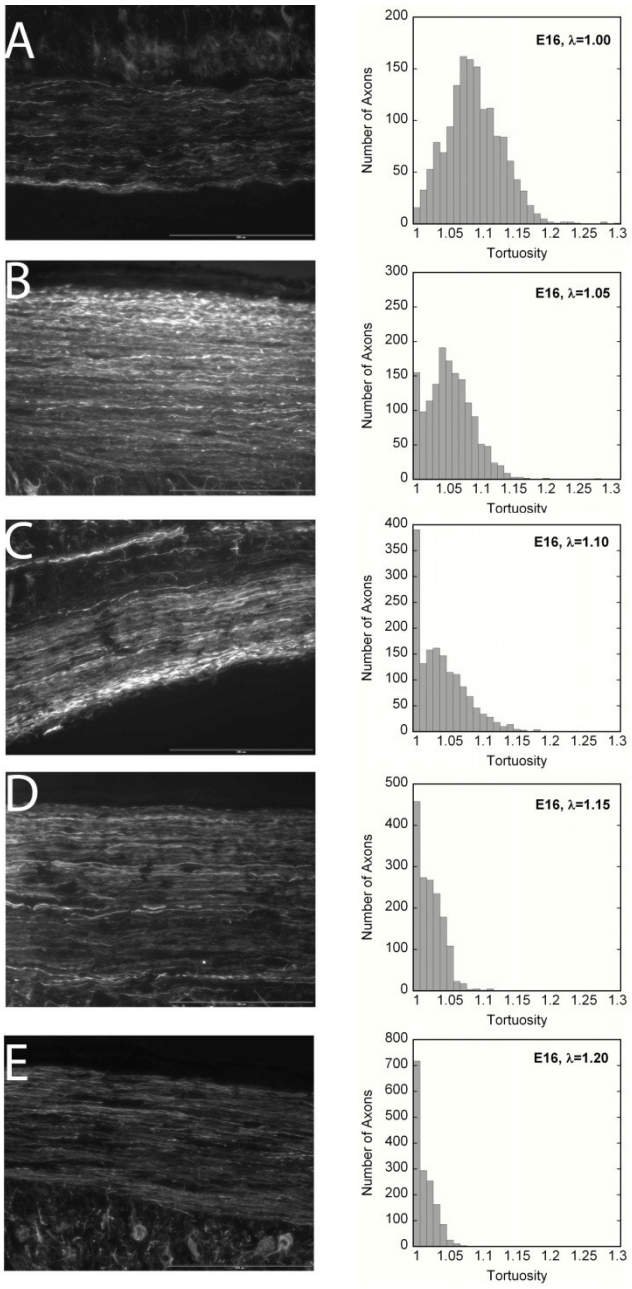

Figure 2-6: Immunohistochemistry and tortuosity characterization for E16 spinal cords. The tortuosity distribution for axons in the sections was different at higher stretch levels compared to E12 and E14 spinal cords. (A) Many axially- oriented, wavy axons were observed in unstretched spinal cords. The distribution of axonal tortuosity followed a normal distribution. As stretch increased (B = 5%, C = 10%, D = 15%, E = 20%) axons became progressively straighter, and a significant number of axons had tortuosity equal or near one. At the highest stretch ratio (D,E), higher percentage of axons maintained tortuous morphology compared to E12 and E14 spinal cords. (Scale bars = 200μm.)

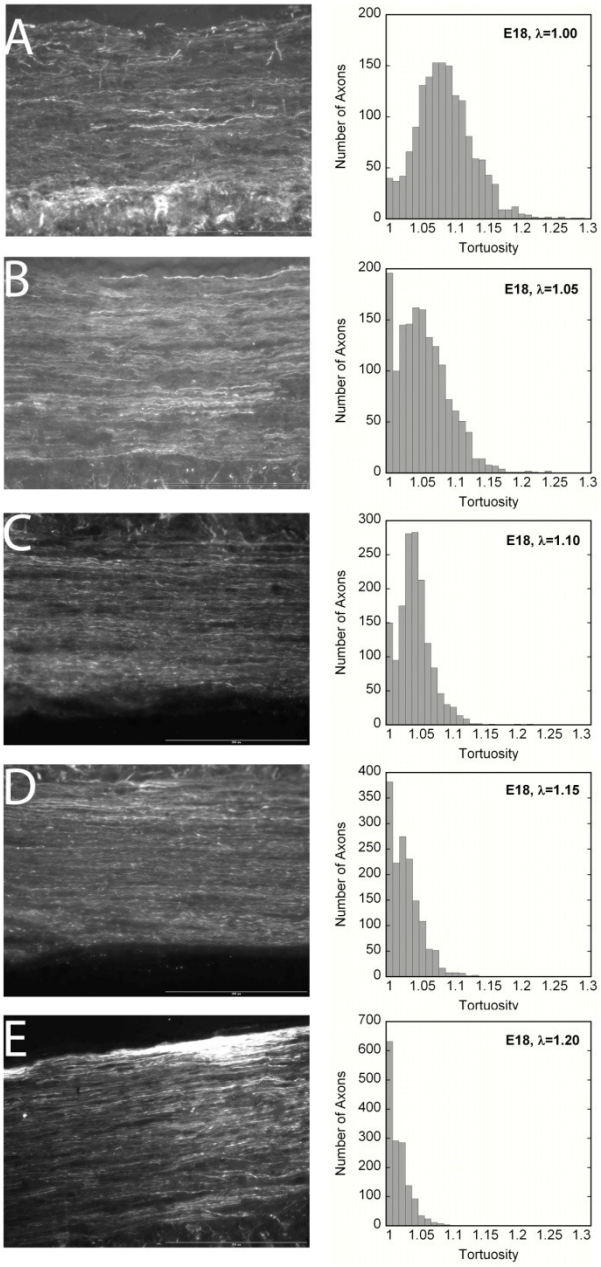

Figure 2-7: Immunohistochemistry and tortuosity characterization for E18 spinal cords. The tortuosity distribution for axons in the sections was similar to E16 spinal cords. (A) Many axially-oriented, wavy axons were observed in unstretched spinal cords. The distribution of axonal tortuosity followed a normal distribution. As stretch increased (B = 5%, C = 10%, D = 15%, E = 20%) axons became progressively straighter, and a significant number of axons had tortuosity equal or near one. At the highest stretch ratio (D,E), higher percentage of axons maintained tortuous morphology compared to E12 and E14 spinal cords. (Scale bars = 200μm.)

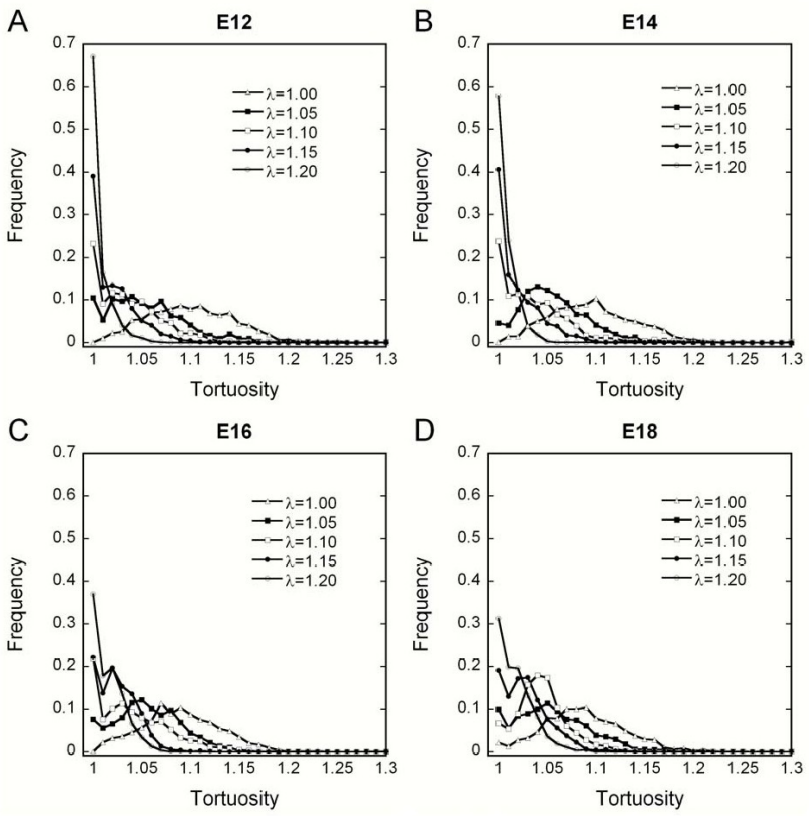

Figure 2-8: Normalized axonal tortuosity distributions following controlled stretch for (A) E12, (B) E14, (C) E16, and (D) E18 chick embryo spinal cords. Each embryonic stage demonstrated similar distributions in unstretched spinal cords and as stretch was increased. The peak of the distributions for unstretched cords (open triangles, λ= 1) shifted left from E12-E18, indicating a progressive straightening of axons with growth and development. With increasing stretch, E12 axons tortuosity demonstrated a pronounced shift to the left (in a left-censored fashion), such that at 20% stretch, over 60% of the axons had a tortuosity ~1, and a sharp drop-off in the distribution followed (open diamonds, λ= 1.20). With growth and development, distributions shifted to the left to lesser degrees, such that at E18, just over 30% of the axons had a tortuosity ~1, and the subsequent fall-off was less steep.

Development Stage	Stretch Level	Mean Tortuosity	Standard Deviation	Total Number of Axons
E12	0%	1.096	0.046	1553
	5%	1.051	0.042	1531
	10%	1.033	0.034	1556
	15%	1.012	0.021	1599
	20%	1.004	0.010	1552
E14	0%	1.092	0.044	1523
	5%	1.052	0.035	1524
	10%	1.034	0.042	1580
	15%	1.017	0.028	1530
	20%	1.005	0.009	1544
E16	0%	1.085	0.041	1523
	5%	1.052	0.035	1532
	10%	1.038	0.037	1536
	15%	1.021	0.021	1582
	20%	1.012	0.014	1558
E18	0%	1.083	0.043	1561
	5%	1.051	0.039	1552
	10%	1.040	0.026	1533
	15%	1.025	0.023	1522
	20%	1.014	0.017	1527

Table 2-2: Summary statistics for tortuosity measurements.

Reference

Adams, J. H., D. Doyle, et al. (1984). "Diffuse axonal injury in head injuries caused by a fall." Lancet **2**(8417-18): 1420-2.

Anderson, E. S., C. Bjartmar, et al. (2000). "Myelination of prospective large fibres in chicken ventral funiculus." J Neurocytol **29**(10): 755-64.

Bain, A. C., D. I. Shreiber, et al. (2003). "Modeling of microstructural kinematics during simple elongation of central nervous system tissue." J Biomech Eng **125**(6): 798-804.

Blight, A. R. and V. Decrescito (1986). "Morphometric analysis of experimental spinal cord injury in the cat: the relation of injury intensity to survival of myelinated axons." Neuroscience **19**(1): 321-41.

Boonstra, H., J. W. Oosterhuis, et al. (1983). "Cervical tissue shrinkage by formaldehyde fixation, paraffin wax embedding, section cutting and mounting." Virchows Arch A Pathol Anat Histopathol **402**(2): 195-201.

Breig, A. (1960). "Biomechanics of the Central Nervous System." Stockholm:Almqvist & Wiksell.

Bunge, R. P. (1968). "Glial cells and the central myelin sheath." Physiol Rev **48**(1): 197-251.

Collan, Y., T. Torkkeli, et al. (1987). "Application of morphometry in tumor pathology." Anal Quant Cytol Histol **9**(2): 79-88.

Crowe, M. J., J. C. Bresnahan, et al. (1997). "Apoptosis and delayed degeneration after spinal cord injury in rats and monkeys." Nat Med **3**(1): 73-6.

Decraemer, W. F., M. A. Maes, et al. (1980). "An elastic stress-strain relation for soft biological tissues based on a structural model." J Biomech **13**(6): 463-8.

Decraemer, W. F., M. A. Maes, et al. (1980). "A non-linear viscoelastic constitutive equation for soft biological tissues, based upon a structural model." J Biomech **13**(7): 559-64.

Diamant, J., A. Keller, et al. (1972). "Collagen; ultrastructure and its relation to mechanical properties as a function of ageing." Proc R Soc Lond B Biol Sci **180**(60): 293-315.

Galbraith, J. A., L. E. Thibault, et al. (1993). "Mechanical and electrical responses of the squid giant axon to simple elongation." J Biomech Eng **115**(1): 13-22.

Gentleman, S. M., G. W. Roberts, et al. (1995). "Axonal injury: a universal consequence of fatal closed head injury?" Acta Neuropathol (Berl) **89**(6): 537-43.

Grace, A. A. and R. Llinas (1985). "Morphological artifacts induced in intracellularly stained neurons by dehydration: circumvention using rapid dimethyl sulfoxide clearing." Neuroscience **16**(2): 461-75.

Grady, M. S., M. R. McLaughlin, et al. (1993). "The use of antibodies targeted against the neurofilament subunits for the detection of diffuse axonal injury in humans." J Neuropathol Exp Neurol **52**(2): 143-52.

Graham, D. I., J. H. Adams, et al. (1995). "The nature, distribution and causes of traumatic brain injury." Brain Pathol **5**(4): 397-406.

Grossman, S. D., L. J. Rosenberg, et al. (2001). "Temporal-spatial pattern of acute neuronal and glial loss after spinal cord contusion." Exp Neurol **168**(2): 273-82.

Hunter, J. A. and B. Finlay (1973). "Scanning electron microscopy of connective tissues in health and disease." Int Rev Connect Tissue Res **6**: 217-55.

Jafari, S. S., W. L. Maxwell, et al. (1997). "Axonal cytoskeletal changes after non-disruptive axonal injury." J Neurocytol **26**(4): 207-21.

Jafari, S. S., M. Nielson, et al. (1998). "Axonal cytoskeletal changes after nondisruptive axonal injury. II. Intermediate sized axons." J Neurotrauma **15**(11): 955-66.

Kakulas, B. A. (1999). "A review of the neuropathology of human spinal cord injury with emphasis on special features." J Spinal Cord Med **22**(2): 119-24.

Lindsey, J. K., W. D. Byrom, et al. (2000). "Generalized nonlinear models for pharmacokinetic data." Biometrics **56**(1): 81-8.

Lum, H. and W. Mitzner (1985). "Effects of 10% formalin fixation on fixed lung volume and lung tissue shrinkage. A comparison of eleven laboratory species." Am Rev Respir Dis **132**(5): 1078-83.

MacKenna, D. A., S. M. Vaplon, et al. (1997). "Microstructural model of perimysial collagen fibers for resting myocardial mechanics during ventricular filling." Am J Physiol **273**(3 Pt 2): H1576-86.

Meaney, D. F., S. S. Margulies, et al. (2001). "Diffuse axonal injury." J Neurosurg **95**(6): 1108-10.

O'Donovan, M., E. Sernagor, et al. (1992). "Development of spinal motor networks in the chick embryo." J Exp Zool **261**(3): 261-73.

Palay, S. L., C. Sotelo, et al. (1968). "The axon hillock and the initial segment." J Cell Biol **38**(1): 193-201.

Peters, a., Palay, S.L., Webster, D. (1990). the fine structures of the nervous system. Saunders, Philadephia.

Povlishock, J. T. (1992). "Traumatically induced axonal injury: pathogenesis and pathobiological implications." Brain Pathol **2**(1): 1-12.

Povlishock, J. T., D. P. Becker, et al. (1983). "Axonal change in minor head injury." J Neuropathol Exp Neurol **42**(3): 225-42.

Povlishock, J. T. and C. W. Christman (1995). "The pathobiology of traumatically induced axonal injury in animals and humans: a review of current thoughts." J Neurotrauma **12**(4): 555-64.

Rigby, B., Hirai, Nishio, Spikes, John and Eyring, Henry (1959). "The mechanical properties of rat tail tendon." The Journal of General Physiology **43**: 265-283.

Saatman, K. E. (1993). An isolated single myelinated nerve fiber model for the biomechanics of axonal injury. Ph.D. Dissertation, University of Pennesylvania.

Shi, R. and J. D. Pryor (2002). "Pathological changes of isolated spinal cord axons in response to mechanical stretch." Neuroscience **110**(4): 765-77.

Thibault LE, G. T., Margulies SS, Marcus J, Eppinger R (1990). The strain dependent pathophysiological consequences of inertial loading on central nervous system tissue. Lyon.

Thibault, L. E. a. G. J. S. (1981). The effects of high strain rate uniaxial extension on the electrophysiology of isolated nerual tissue. in Advances in Bioengineering, ASME. New York

Torg, J. S., L. Thibault, et al. (1995). "The Nicolas Andry Award. The pathomechanics and pathophysiology of cervical spinal cord injury." Clin Orthop Relat Res(321): 259-69.

Chapter 3: Modeling axon kinematics in developing chick embryo spinal cord

Abstract

The experimental data of axon tortuosity distribution at each stretch ratio for each development stage (E12, E14, E16, and E18) was compared to predicted results from affine and non-affine models, as well as a model that transitions from non-affine to affine behavior as stretch increases, to discern the trend of axon kinematics. Axon tortuosity data from unstretched spinal cords were pooled by development stage and used as input data into MATLAB scripts. The tortuosity distributions following stretch were predicted from different mathematical model at each stretch level and compared to experimental results. The axon kinematics did not follow idealized affine nor non-affine behavior. The 'switching' model predicted the axon mechanical behavior more accurate. Parameters in the 'switching' model were decided by minimizing the net difference between predicted results and experimental results. The values of parameters were significantly different for each development stage and demonstrated different percentage of axons that perform solely non-affine behavior. This percentage decreased dramatically with development and indicated a transition from non-affine to affine mechanical behavior following stretch from E12-E18 spinal cord.

Introduction

In Chapter 2, we studied changes in axon kinematics in situ in the developing chick embryo spinal cord, and found that the kinematic behavior changes significantly during a period of rapid growth and white matter myelination. Modeling the relationship between the microstructure changes and the strain applied to the tissue is important to understand the specific mechanical behaviors in developing spinal cord and can help us to predict the mechanical behavior in CNS. Three mechanical models of tissue deformation have been studied in previous studies: non-affine, affine, and 'switching' model (Lanir 1979; MacKenna, Vaplon et al. 1997; Bain, Shreiber et al. 2003). We employed all of these models to our experimental data and predicted axon tortuosity distribution at each stretch ratio for each development stage. Predicted results were compared to experimental results to discern axon kinematics trend for each development stage.

Non-affine and affine models have been studied for other tissues such as fibrils and skin in previous studies. Some studies have examined the changes in fibril orientation in stretched tissue and many structural models based on non-affine deformation have been designed successfully to replicate these changes mathematically (Rigby 1959; Markenscoff and Yannas 1979; Decraemer, Maes et al. 1980; Kastelic, Palley et al. 1980; Kwan and Woo 1989; Belkoff and Haut 1992; Billiar and Sacks 1997; Hurschler, Loitz-Ramage et al. 1997; MacKenna, Vaplon et al. 1997). In non-affine models, final tortuosity is decided directly from the original tortuosity and the applied stretch ratio. However, these models rarely predict the experimental data. Lanir first developed an affine model for certain soft tissue (e.g., skin) by assuming that tissue response is due to the additive contributions of a fluid matrix, elastin fibers, and collagen fibers (Lanir

1979). This approach was employed later for other tissues such as lung tissue and passive myocardium.

Bain et al. first demonstrated the quantitative relation between change of axon tortuosity and tissue strain (Bain, Shreiber et al. 2003). Based on axon microstructure, Bain et al. developed a mathematical model describing the deformation of affine, in which axons deform fully coupled to macroscopic tissue, or non-affine, in which axons are completely uncoupled and straighten independently. They observed that axons first straighten completely uncoupled (i.e. in a non-affine manner), and then axonal deformation becomes increasingly interdependent (i.e. in an affine manner) as stretch level increases. Depending on the behavior, they also developed a 'switching' model that describes gradual coupling, and proposed that the coupling was due to the effects of the glial matrix on axonal elements. They defined two tortuosity values (T_1 and T_2), which divide axons into three regions. Axons that fall in the region of tortuosity less than T_1 will perform as an affine deformation while axons that fall in the region of tortuosity larger than T_2 will perform as a non-affine deformation. Axons that have tortuosity between T_1 and T_2 will switch from non-affine to affine. Compared to the affine or non-affine model, the switching model can match the measured results more accurately. By minimizing the difference between predicted results and measured results, they defined T_1 as 0.98 and T_2 as 1.08 for axons in the optic nerve of the adult guinea pig.

We employed the models developed by Bain et al. to our experimental results and observed a transition from non-affine behavior to affine-behavior with development. The trends were confirmed by employing the 'switching' model as well. We determined the values of lower bound (T_1) and upper bound (T_2), which demonstrate the transition

behavior of axons from non-affine to affine, for chick embryo spinal cord at each development stage. A dramatic increase was observed in T_1 values, whereas T_2 was insensitive to development stage. We compared our results to those in adult guinea optic nerves. T_1 value in optic nerve stayed close to those in chick spinal cord while T_2 was slightly greater than E18 spinal cord.

Methods

Kinematic Models

The tortuosity data from Chapter 2 was pooled by developmental stage and stretch level. Pooled control data (unstretched) for each developmental stage was used as input data into MATLAB scripts (Mathworks, Inc, Natick, MA) based on the affine and non-affine models (Bain, Shreiber et al. 2003) to predict tortuosity distributions at various stretch levels at each idealized extreme case. The predicted results were then compared to the experimental distributions to discern affine and/or non-affine trends in the experimental data. These models have been briefly reviewed in the background.

Affine Model: Axons are completely coupled to the surrounding matrix in this model. Axons are assumed to experience the same geometrical deformation as the macroscopic tissue. The tortuosity of axons is defined as the value of actual pathlength divided by end-to-end straight length (Figure3-1).

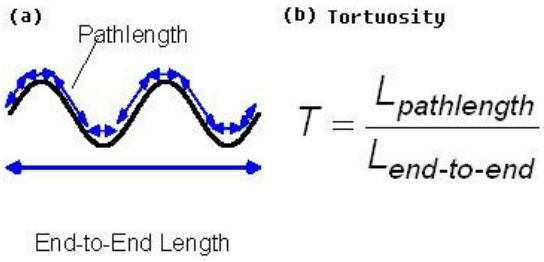

Figure 3-1: Definition of axonal tortuosity. (a) Geometry of an undulated axon, showing the actual length and end-to-end straight length. (b) Tortuosity of axon is defined as the value of pathlength divided by end-to-end length.

The geometry of a tortuous axon is modeled as a periodic wave with amplitude, A_o and period, P_o:

$$y(z) = A_o \cos\left(\frac{2\pi z}{P_o}\right) \quad \text{.....Equation 3-1}$$

Under the stretch ratio of λ, which is defined as:

$$\lambda = \frac{Final\ Spinal\ Cord\ Length}{Initial\ Spinal\ Cord\ Length} \quad \text{.....Equation 3-2}$$

the amplitude and period of an axon become $A_o(\lambda)^{-1/2}$ and $P_o\,\lambda$. The equation of the stretched axon's geometry becomes:

$$y'(z) = \frac{A_o}{\sqrt{\lambda}} \cos\left(\frac{2\pi z}{\lambda P_o}\right) \quad \text{.....Equation 3-3}$$

The transformed tortuosity, T_t of the axon is then determined as:

$$T_t = \frac{1}{L_E} \int_0^{L_E} \sqrt{1 + \left(\frac{-A_o}{\sqrt{\lambda}} \frac{2\pi}{\lambda P_o} \sin\left(\frac{2\pi z}{\lambda P_o}\right)\right)^2} \quad \text{..... Equation 3-4}$$

The solution is approximated with a simplification that applies for tortuosity values close to 1.0 (Bain, Shreiber et al. 2003).

$$T_t = T_o\left[\frac{1}{\lambda^3} + \frac{1}{T_0^2}\left(1 - \frac{1}{\lambda^3}\right)\right]^{\frac{1}{2}} \quad \text{. . . . . Equation 3-5}$$

Non-affine model: Axons are assumed to be completely uncoupled to each other or with surrounding matrix in this model. The final tortuosity is calculated directly from the original tortuosity and the applied stretch ratio (Bain, Shreiber et al. 2003).

$$T_t = \frac{1}{\lambda}T_o \quad \text{for} \quad \lambda < T_o \text{. . . . . .Equation 3-6}$$

When the nerve stretch ratio (λ) is equal or larger to the axon's original tortuosity (T_0), the axon will become completely straight and has tortuosity as 1:

$$T_t = 1 \quad \text{for} \quad \lambda \geq T_o \text{. . . . . .Equation 3-7}$$

Using these models, tortuosity distributions were predicted for the control populations of axons from chick embryo spinal cords at different stages of development exposed to increasing levels of controlled stretch.

'Switching' Model

The model describing gradual coupling of axons to glial network has been briefly reviewed in the background. Generally, three regimes are defined:

Regime 1: $T<T_1$ Affine behavior

Regime 2: $T>T_2$ Non-affine behavior

Regime 3: $T1 \leq T \leq T_2$ Potential transition from non-affine to affine behavior

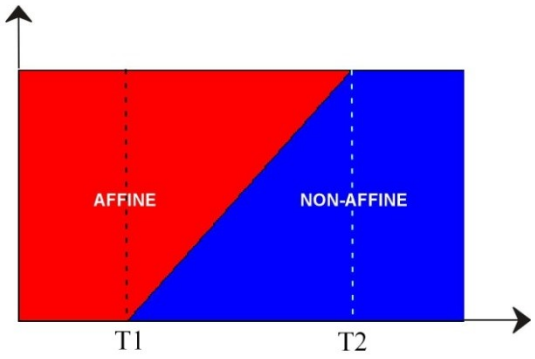

Figure 3-2: Three regimes in the switching model.

Axons in regime 1 deform in a fully uncoupled behavior, which is defined as non-affine. Axons in regime 2 deform in a fully coupled behavior, which is defined as affine. Axons in regime 3 deform in a transition from non-affine to affine behavior. For each axon, the transition point, $T_{pt,}$ is picked randomly between T_1 and T_2. Therefore, the values of T_1 and T_2 define the transition behavior for a group of axons. T_1 and T_2 are determined by minimizing the net difference between experimental results and modeled results.

To optimize the values of T_1 and T_2 for each developmental stage, pooled control data was used as the input to the MATLAB script based on the switching model. The predicted cumulative histograms were compared to the experimental histograms across all the stretch levels. The optimized values were determined by minimizing their difference using a Levenberg-Marquart scheme. The optimization was executed 50 times for each developmental stage since the transition point T_{pt} was assigned randomly for a given axon in the switching model. Then the mean transition values and standard deviations were determined.

The impact of T_1 and T_2 on the results of the model was examined with a baseline case of T_1=1, T_2=1.2. Using the control populations of E16 axons as the test case, different groups of T_1 and T_2 were applied to the model and the results were compared with the base case for 10% stretch.

Results

Affine and non-affine model predictions

Experimental results from each developmental stage did not follow either of the idealized extreme cases (Fig 3-3). Neither the affine nor the non-affine model perfectly matched the experimental data. The experimental data stayed between affine and non-affine cumulative histograms for each developmental stage at each stretch ratio. Unlike the previous studies from Bain et al.; we did not see dramatically increasing affine behavior at higher stretch levels. However, experimental tortuosity distributions clearly shifted from more non-affine behavior at early developmental stages (E12, E14) to more affine at later stages (E16, E18).

Impact of T_1 and T_2 on the results of the model

Before presenting the results of the switching model, it is helpful to describe the impact of T_1 and T_2 on the results of the model. When T_1<1, axons that have tortuosities between 1 and T_2 will have transition tortuosities less than one. Since the tortuosity of an axon has a lower bound of 1 (perfectly straight), any axon with T>=1 will always exhibit non-affine behavior. A percentage of the axons $(1-T_1)/(T_2-T_1)$ will have a transition tortuosites less than 1, and will always exhibit non-affine behavior. As shown in Fig 3-4,

as T_1 decreases (below 1), more axons will permanently exhibit non-affine behavior. As T_1 increases, any axon with $1<=T_{axon}<T_1$ will demonstrate affine behavior from the onset, thus the population of axons demonstrates more affine behavior. As T_2 decreases, the transition tortuosities for axons switching from non-affine to affine will decrease (Fig3-4). In such case, axons require greater stretch levels to decrease the tortuosities of axons in the upper transition zone to approach the transition point. The opposite was observed for increasing T_2. Thus, in general, a decrease in T_1 or T_2 leads to non-affine behavior, and an increase in T_1 or T_2 leads to affine behavior.

Kinematics models of axon behavior

The affine, non-affine, and switching models were compared to the experimental data for all embryonic stages (see Fig 3-5 and Fig 3-6 for representative results from E12 and E18, respectively). The tortuosity data from multiple samples was pooled by developmental stage and stretch level. Pooled control data for each developmental stage was used as input data into the kinematic models to predict tortuosity changes for these idealized extreme descriptions of microkinematic behavior. In comparison, for all developmental stages, the switching model greatly improved the predictive capacity of the model.

Chick embryo spinal cord axons exhibited a mixture of affine and non-affine behavior when exposed to stretch. The values of T_1 and T_2 that define the transition behavior for group of axons were determined for each developmental stage by minimizing the net difference between experimental and predicted histograms across all stretch levels. Because the switching model involved randomly assigning a transition

tortuosity to each axon from a uniform distribution, the model was executed 50 times for each developmental stage. In each run, the values of T_1 and T_2 were optimized by regressing the predicted tortuosity distributions against the experimental data across all stretch levels. Average regression coefficients were: 0.84+/-0.005 for E12; 0.95+/-0.003 for E14; 0.93+/-0.007 for E16; and 0.86+/- 0.01 for E18. The values of T_1 and T_2 were shown in Fig 3-7 for E12-E18 spinal cords. For all stages, $T_1<1$ and $T_2>1$, indicating a fraction of the axons exhibited pure non-affine deformation at each development stage. This percentage significantly decreased (ANOVA, $P<0.001$) with development as follows: 65.0% +/- 1.9% for E12; 60.7% +/- 2.0% for E14; 39.7% +/- 4.5% for E16; and 29.4% +/- 1.5% for E18.

The values of T_1 increased significantly (ANOVA followed by pairwise comparisons with Scheffe's post hoc test, $P<0.001$) from E12 to E18, with the steepest increase between E14-E16 (Fig 3-7), indicating increasing affine behavior during development. Unlike T_1, the values of T_2 retained relatively stable. Though statistically significant differences were observed among all stages (ANOVA, $P<0.01$), pairwise post hoc tests (Scheffe's test) revealed no discernable trends for T_2 with development. For the chick embryo spinal cord, the values of T_1 have more impact on the model than T_2. The values of T_1 may correlate to the percentage of myelinated axons. Another set of simulations was run where T_2 was fixed at the average value across all development stages (1.087) and only T_1 was determined through non-linear regression (Fig 3-7). The values and trend for T_1 from the 1-parameter fit were statistically indistinguishable from T_1 values from the 2-parameter fit (ANOVA, $P=0.37$). The percentage of axons that

exhibit solely non-affine behavior predicted from the values of T_1 and T_2 were shown in Fig 3-8.

One final set of simulations was performed to evaluate the potential influence of physical strain imparted on the spinal cord during growth as the basis for the transition from predominantly non-affine to predominantly affine kinematics during development. It was assumed that the change in length from E12-E18 could be modeled, as an extreme, as an incrementally applied stretch with the length at E12 serving as the gauge length. The kinematic models were executed for three stretch levels representing the incremental growth from E12 to E14 (λ=1.20), E12 to E18 (λ=1.41), and E12 to E18 (λ=1.55), and the results were compared to E14, E16, and E18 control distributions, respectively. Similar simulations were executed for growth/stretch from E14-16, E14-E18, and E16-E18. As shown in Fig 3-9, both non-affine and affine models grossly under-predicted the tortuosity that was measured in the unstretched controls. (The switching model naturally falls between the affine and non-affine models.)

Discussion

In this chapter, we compared the changes in axonal tortuosity that resulted from stretching of macroscopic tissue to mathematical predictions of ideal affine and non-affine behavior. It was concluded that neither affine nor non-affine model could describe the experimental results perfectly. Unlike previous studies by Bain et al. (Bain, Shreiber et al. 2003), which demonstrated that axon mechanics in the guinea pig optic nerve shifted from non-affine behavior at low stretch level to affine behavior at high stretch levels; we did not see very great transition in chick embryo spinal cord. We observed that

experimental tortuosity distribution clearly shifted from more non-affine behavior at early developmental stages (E12, E14) to more affine at later stages (E16, E18). This trend was quantified by employing the 'switching' model proposed by Bain et al., where each axon is presumed to exhibit non-affine behavior and straighten directly with stretch until its tortuosity decreases to a transition tortuosity (prescribed at random from a uniform distribution), after which it demonstrates affine behavior. The 'switching' model also predicts the experimental data at different stretch levels more accurately compared to non-affine or affine model.

A very modest shift from non-affine behavior to affine behavior with increasing stretch levels was observed in the developing chick embryo spinal cord. It was proposed that coupling to the glial matrix might contribute to the difference between chick embryo spinal cord and guinea pig optic nerve. Axons in adult guinea pig optic nerve were fully myelinated. When axons are stretched to higher levels, the surrounding cells and matrix may provide mechanical stability and force axons to deform dependently, which results in more affine behavior. However, axons in chick embryo spinal cord are not fully myelinated, especially at early development stages. Therefore, non-affine, uncoupled behavior was prevalent at all stretch levels. The transition from non-affine to affine with increasing stretch levels for same development stage was not observed. As expected, affine, coupled behavior increasingly prevailed in later development which demonstrates more myelinated axons. The other reason may be the different components of optic nerve and spinal cord. Chick embryo spinal cord consists of not only white matter, but also gray matter, whereas optic nerve is purely white matter. As discussed in Chapter 2, we do not

expect gray matter to significantly influence the white matter mechanics. The effect of gray matter should be very minimal to axonal mechanics.

The trend of transition from more non-affine mechanics at early development stage to more affine mechanics at later development stage was quantified by employing the 'switching' model. The details and equations of the model were summarized in methods. Generally, each axon is presumed to exhibit non-affine behavior and straighten directly with stretch until its tortuosity decreases to a transition tortuosity, after which it demonstrates affine behavior. The transition tortuosity was prescribed at random from a uniform distribution. The bounds of the uniform distribution that described the transition tortuosity for each developmental stage were optimized by a non-linear regression scheme. The lower bound (T_1) showed progressive, significant increases from 0.84 at E12 to 0.96 at E18. The upper bound (T_2) was significantly different with T1 for all development stages. However, no trends in the values of the upper bound with development were discerned. For all stages, significant percentages of each uniform distribution were below a transition tortuosity of 1. The actual tortuosity of axons in reality will never go below 1. Thus, the percentage of axons with tortuosity between 1 and T_1 has a transition tortuosity that will never be reached. These axons can never switch from non-affine to affine behavior; they are predicted to demonstrate purely non-affine behavior. This percentage of axons decreased during the development period being studied significantly from 64% at E12 to 30% at E18 (Fig 3-8). The decrease in the percentage of axons that deform in solely a non-affine manner demonstrates the switch from uncoupled to coupled behavior with development again. Unlike the lower bound, values of T_2 did not show sensitivity to development and they fall in the axon tortuosity

range estimated for chick embryo spinal cord at all development stages. The upper bound from the optic nerve (T_2=1.08) was close to the values of T_2 for chick embryo spinal cord. And T_1 value for the optic nerve was very slightly greater than T_1 for E18 spinal cord (T1=0.96). The observation agreed nicely with the trend of increasing T_1 with development showed in our current study since the adult guinea optic nerve is fully myelinated.

Many changes occur in chick embryo spinal cord during the development period studied. An increase in length of the spinal cord- almost 55% in 6 days –was observed as well as the size of chick embryos. The growing skeleton during development may place mechanical force on spinal cord tissue and results in the increase. Thus tensile stretch may be applied to spinal cord tissue and transfer to axons. In Chapter 2, the initial tortuosity showed very modest though significant decreases with development. We proposed that stretch due to growth of spinal cord contributes to the decrease. However, axons at later development stage maintain a significant degree of undulation and non-injured even though the spinal cord grows dramatically and the increase is beyond the threshold for axon morphology injury. The degree to which the axons population straightened as a result of growth-induced tissue stretch was far less than that predicted by any of the kinematics models. The predicted stretch ratio for E12-E14, E14-E16, and E16-E18 with the 'switching' model depending on the decrease of tortuosity results as 1.004, 1.0065, and 1.0032 respectively. These values are very minimal compared to the percent increase in growth (20%, 17%, and 10%), respectively. Thus, the tissue stretch during growth contributes minimally to the overall mechanical behavior. This

observation also implied an inherent mechanism to preserve axon tortuosity during growth as describer in Chapter 2.

Increases in affine behavior of axonal kinematics with chick embryo spinal cords suggested that strain transfer from differently developed tissue to axons is variable. This change might be caused by the mature statement of cellular compositions surrounding the axons. In Chapter 1, we have characterized the development of myelination and observed rapid process from E12-E18, indicating an increase in axon-oligodendrocytes coupling. Other glial cells might also differentiate to connect axons in the studied period. We are interested in the role of some glial cells in axonal kinematics and will study the effect in Chapter 4.

In summary, axon kinematics in chick embryo spinal cord follow neither non-affine nor affine behavior at all stages. The 'switching' model can predict the experimental results more accurate compared to non-affine or affine model. With growth, axons mechanics showed more affine behavior. The trends match reasonably well with the time course of myelination. A sharpest increase in T_1 was observed between E14 and E16 where myelination proceeds rapidly. We believe there are a lot factors that affect the parameters of the 'switching' mode such as axon tortuosity and degree of axon coupling. These parameters may change in different animals and different nervous system areas. Understanding the correlation between the parameters and cell components, in concert with this model, we may can better identify the in vivo mechanical force transfer and ultimately determine threshold for in vivo injury at microscopic level.

Figures of Results

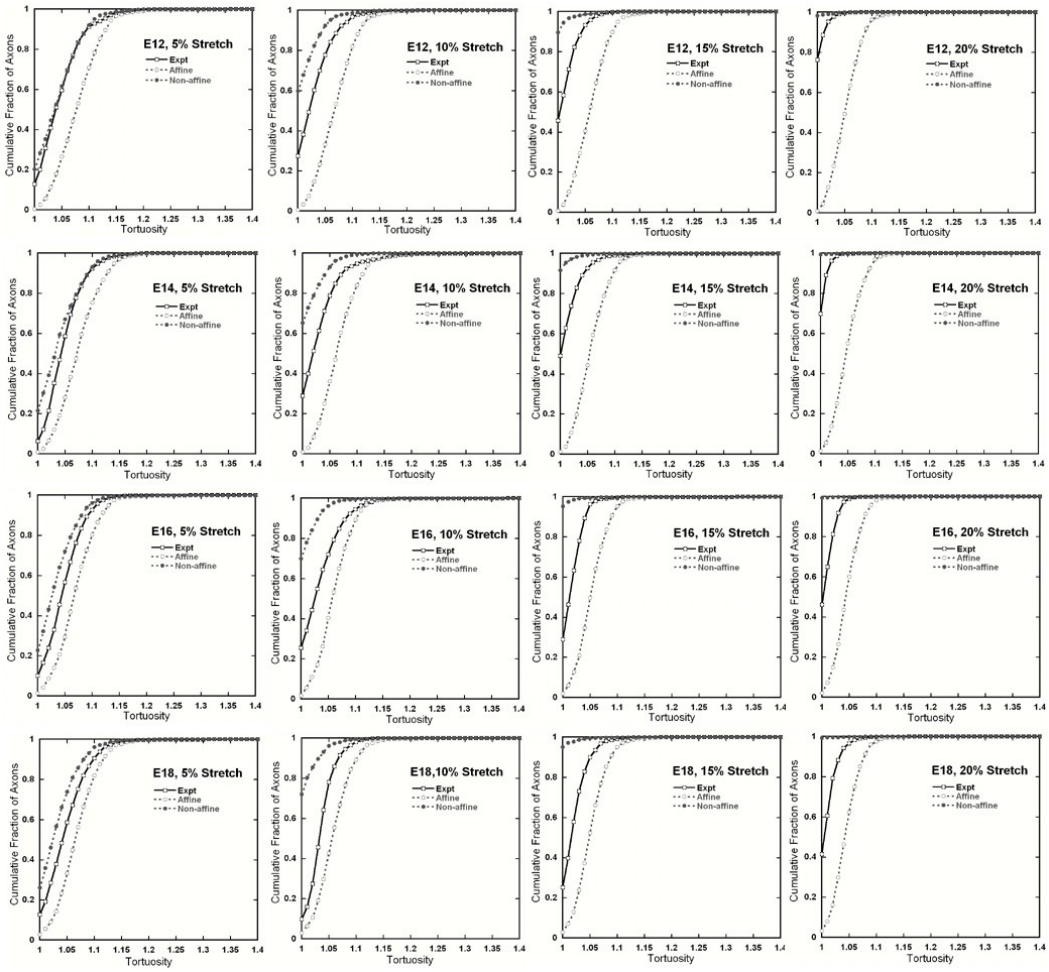

Figure 3-3: Comparison of E12-E18 experimental results to affine, non-affine models. At lower stretch level (5%), the trend in early developmental stages (E12, E14) was better predicted by the non-affine model compared to later developmental stages (E16, E18). At higher stretch levels (10%, 15%, 20%), neither the affine nor non-affine model suitably matched the experimental data describing tortuosity changes for all developmental stages.

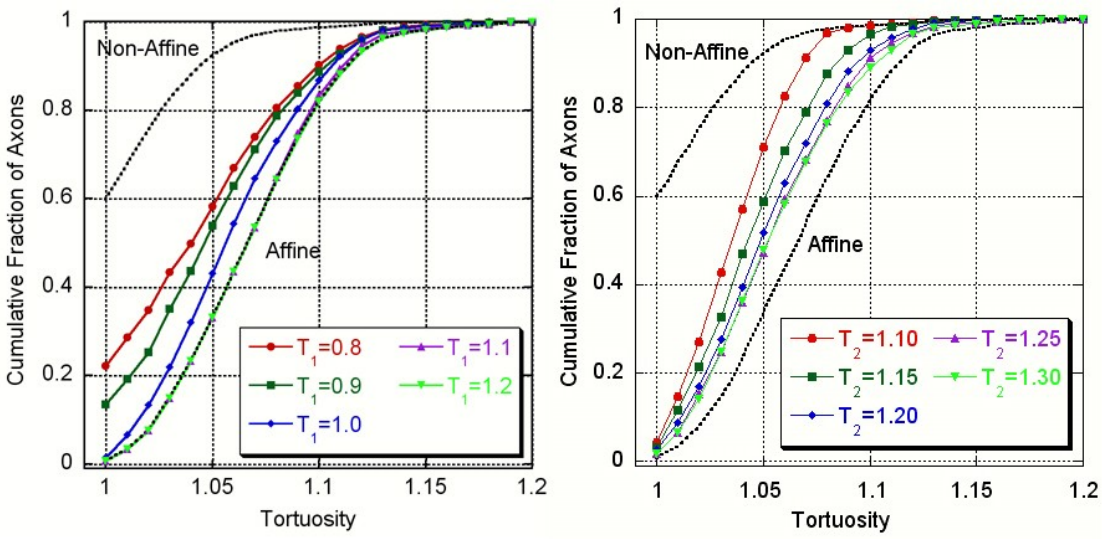

Figure 3-4: Effects of T1 and T2 on the 'switching model' predictions. (A)Effects of changing T1 on predicted tortuosity distributions of E16 control axons exposed to 10% stretch. T1, which represents the lower bound of the uniform distribution that defines the switching parameters, was varied from 0.8 to 1.2, while holding T2 constant at 1.4. T1 influences the left-hand side of the tortuosity distribution. Increasing T1 shifts the behavior from non-affine to affine. (B) Effects of changing T2 on predicted tortuosity distributions of E16 control axons exposed to 10% stretch. T2, which represents the upper bound of the uniform distribution that defines the switching parameters, was varied from 1.1 to 1.3, while holding T1 constant at 1.0. T2 influences the right-hand side of the tortuosity distribution. Increasing T2 shifts the behavior from non-affine to affine.

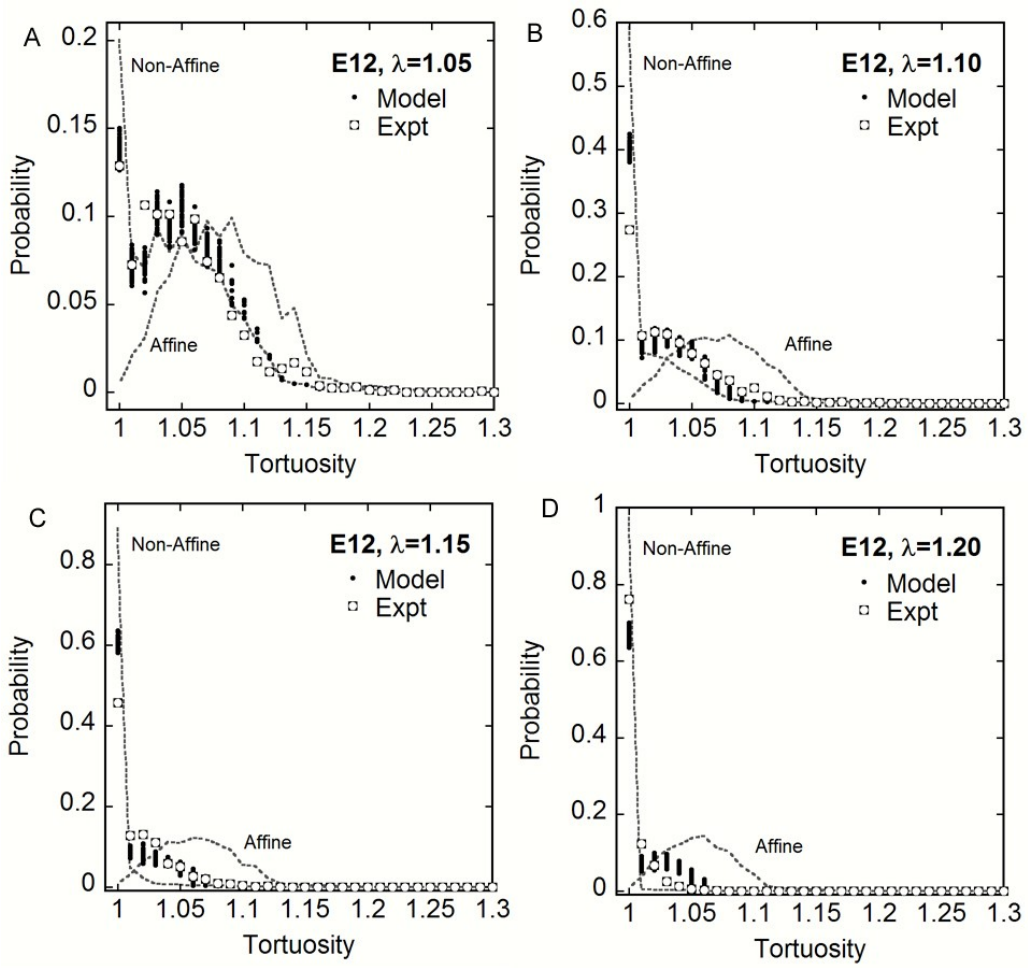

Figure 3-5: Comparison of E12 results to affine, non-affine, and switching kinematic models. Neither the affine nor non-affine model (dashed lines) suitably matched the experimental data (open squares) describing tortuosity changes with tissue level-stretch (A – 5%, B –10%, C – 15%, D – 20%), though the general trend was better predicted by the non-affine model. The experimental data across all stretch levels was used as the objective function to optimize the switching model. The non-linear regression was executed 50 times (black squares). The optimized switching model provided a much improved prediction of tortuosity (average R2 = 0.94 +/- 0.0015 for the 50 simulations).

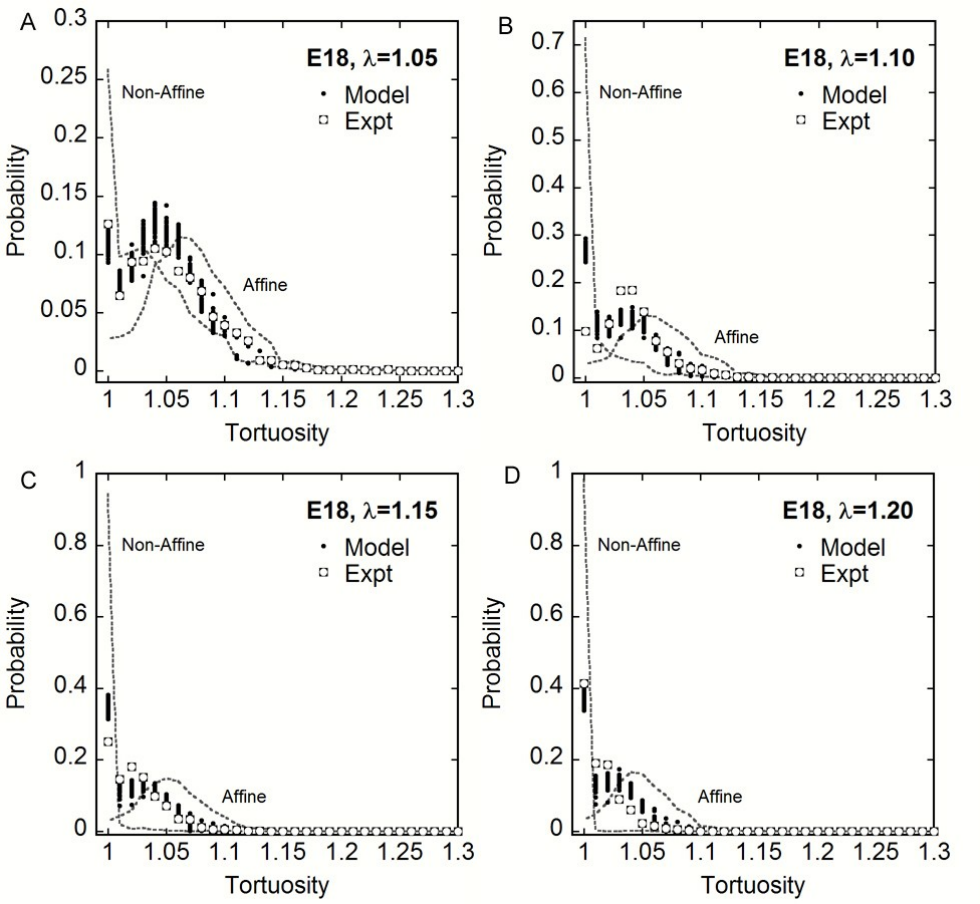

Figure 3-6: Comparison of E18 results to affine, non-affine, and switching kinematic models. Neither the affine nor non-affine model (dashed lines) suitably matched the experimental data (open squares) describing tortuosity changes with tissue level-stretch (A – 5%, B –10%, C – 15%, D – 20%), though the shift from non-affine to affine kinematics with stretch was more obvious than for E12. The experimental data across all stretch levels was used as the objective function to optimize the switching model. The non-linear regression was executed 50 times (black squares). The optimized switching model provided a much improved prediction of tortuosity (average R2 = 0.86 +/- 0.01 for the 50 simulations).

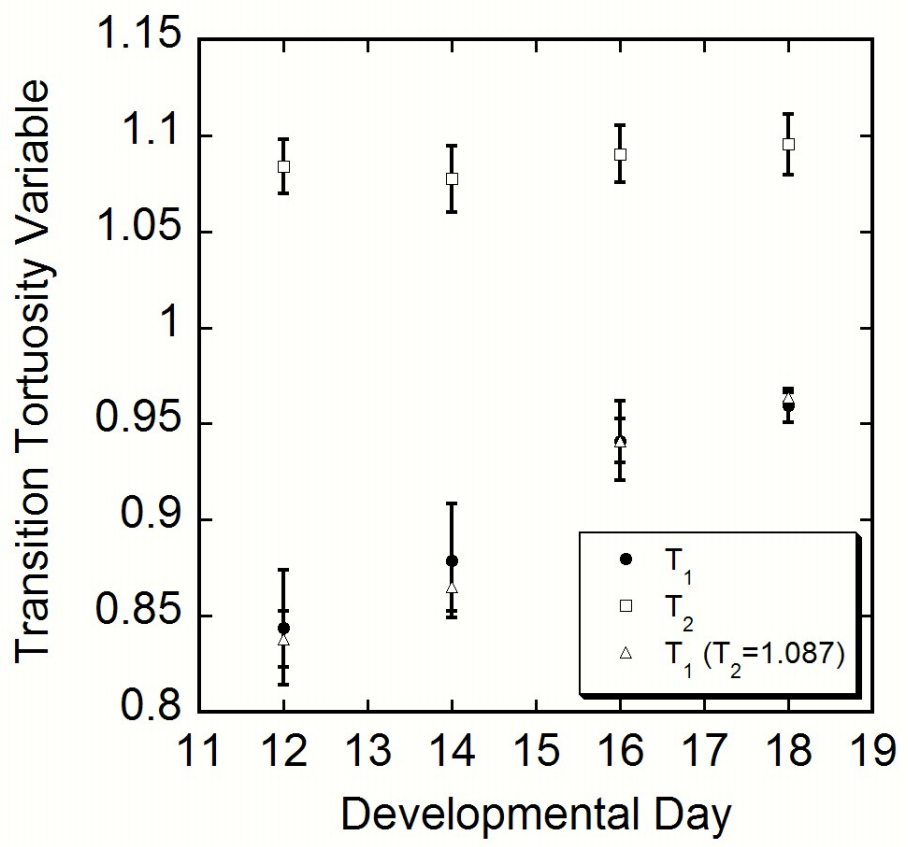

Figure 3-7: Upper and lower bounds of the uniform distribution defining the best-fit switching models for all developmental stages (average +/- standard deviation of the 50 simulations per stage). For all stages, T1 < 1 and T2 > 1, indicating that a percentage of the axons [(1- T1)/(T2- T1)*100] demonstrate solely non-affine kinematics. Though statistical differences were detected among T2 values (open squares), (ANOVA, P<0.01), no consistent trend was observed with developmental stage. Conversely, T1 (closed circles) increased with developmental stage, and showed the greatest increase between E14 and E16. A second set of simulations were run to find the values of T1 while holding T2 fixed across developmental stages at the average value from the 2-parameter fits (T2 = 1.087). T1 values from the 1-parameter fit (open triangles) were not significantly different than T1 values from the 2-parameter fit (P = 0.37).

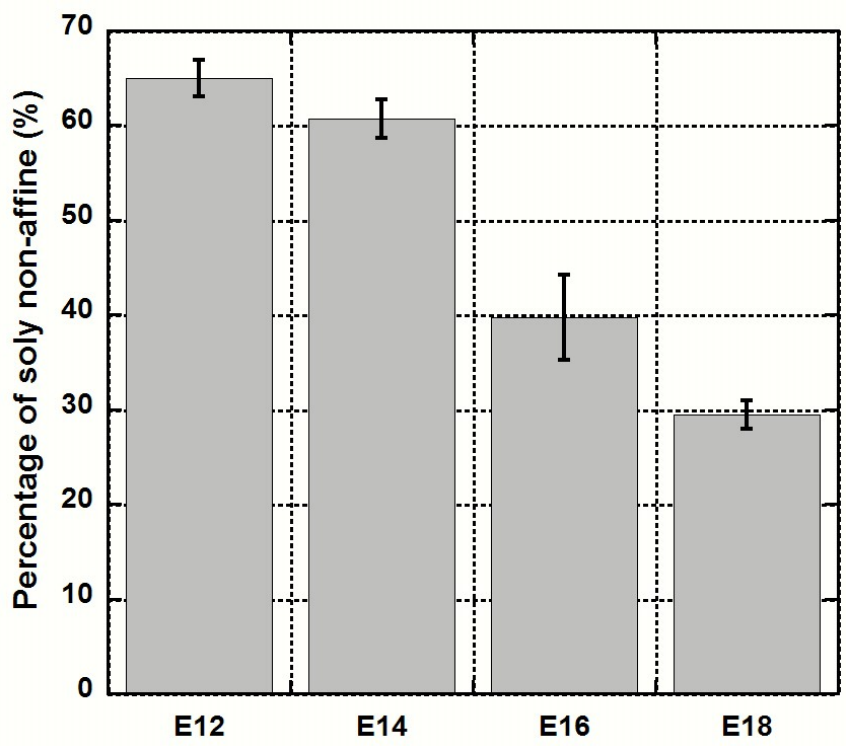

Figure 3-8: Percentage of axons that exhibit solely non-affine kinematics was predicted by the 'switching model'. The value of the percentage was determined by the values of T_1 and T_2 as $(1-T_1)/(T_2-T_1)$. This percentage significantly decreased (ANOVA, $P<0.001$) with development as follows: 65.0% +/- 1.9% for E12; 60.7% +/- 2.0% for E14; 39.7% +/- 4.5% for E16; and 29.4% +/- 1.5% for E18.

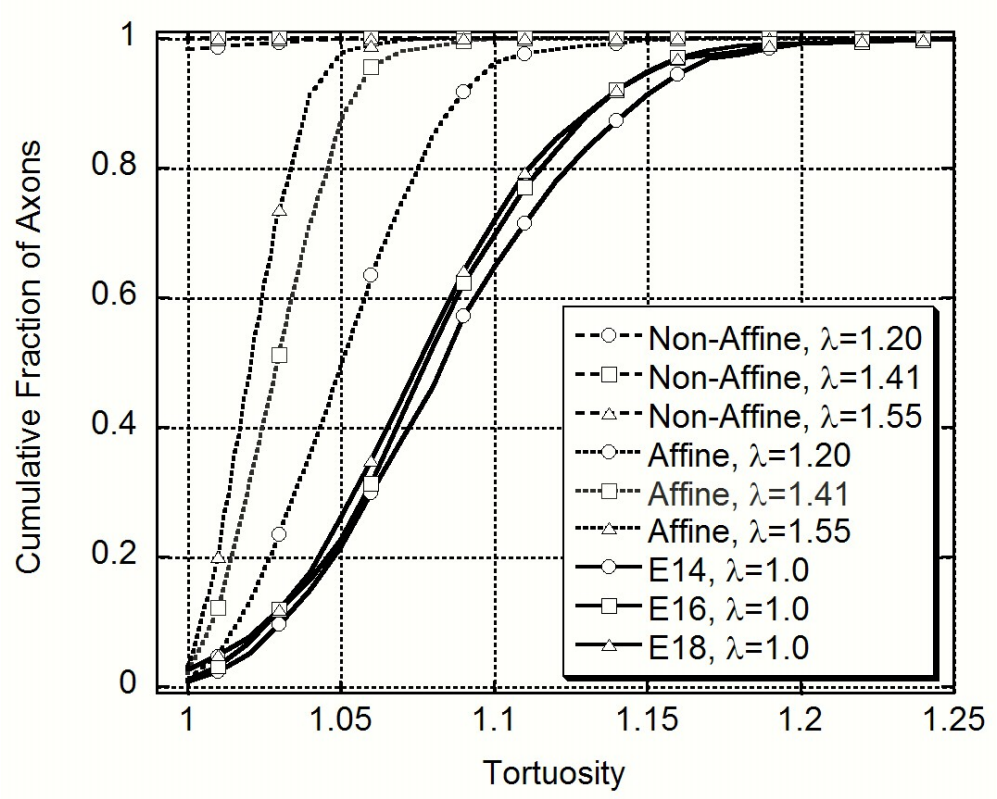

Figure 3-9: Predicted tortuosity cumulative distributions when applying incremental stretch to E12 control axons to simulate growth-induced stretch of the spinal cord. The percentage increases in length from E12-E14, E12-E16, and E12-E18 were used as the applied stretch in the kinematic models, and the results were compared to unstretched distributions from E14, E16, and E18, respectively. All three kinematic models grossly over-estimated the degree of straightening that would be produced by growth of the spinal cord. (The switching model falls naturally between the non-affine and affine models and is not shown). Similar results were observed following simulation of growth from E14-E16, E14-E18, and E16-E18.

Reference

Bain, A. C., D. I. Shreiber, et al. (2003). "Modeling of microstructural kinematics during simple elongation of central nervous system tissue." J Biomech Eng 125(6): 798-804.

Belkoff, S. M. and R. C. Haut (1992). "Microstructurally based model analysis of gamma-irradiated tendon allografts." J Orthop Res 10(3): 461-4.

Billiar, K. L. and M. S. Sacks (1997). "A method to quantify the fiber kinematics of planar tissues under biaxial stretch." J Biomech 30(7): 753-6.

Decraemer, W. F., M. A. Maes, et al. (1980). "An elastic stress-strain relation for soft biological tissues based on a structural model." J Biomech 13(6): 463-8.

Hurschler, C., B. Loitz-Ramage, et al. (1997). "A structurally based stress-stretch relationship for tendon and ligament." J Biomech Eng 119(4): 392-9.

Kastelic, J., I. Palley, et al. (1980). "A structural mechanical model for tendon crimping." J Biomech 13(10): 887-93.

Kwan, M. K. and S. L. Woo (1989). "A structural model to describe the nonlinear stress-strain behavior for parallel-fibered collagenous tissues." J Biomech Eng 111(4): 361-3.

Lanir, Y. (1979). "A structural theory for the homogeneous biaxial stress-strain relationships in flat collagenous tissues." J Biomech 12(6): 423-36.

MacKenna, D. A., S. M. Vaplon, et al. (1997). "Microstructural model of perimysial collagen fibers for resting myocardial mechanics during ventricular filling." Am J Physiol 273(3 Pt 2): H1576-86.

Markenscoff, X. and I. V. Yannas (1979). "On the stress-strain relation for skin." J Biomech 12(2): 127-9.

Rigby, B., Hirai, Nishio, Spikes, John and Eyring, Henry (1959). "The mechanical properties of rat tail tendon." The Journal of General Physiology 43: 265-283.

Chapter 4: Examining axons kinematics in demyelinated spinal cords

Abstract

The effect of axonal coupling with glia on axonal kinematics was identified by comparing the kinematic behavior between myelinated axons and demyelinated axons. Chick embryo spinal cords were demyelinated using two different protocols: toxic induction (EB), which causes cell death, and immunological methods (GalC), which interferes with the myelination process. Saline and pure rabbit IgG were used as controls for EB and GalC respectively. All chick embryos were incubated until day 18 (E18), at which time the spinal cord was harvested. Myelination-suppression for the spinal cord was confirmed by myelin basic protein immunoreactivity and quantified using osmium tetroxide staining. The spinal cords injected with EB or GalC showed prominent demyelination. Glia were identified with GFAP and GalC immunohistochemistry for astrocytes and oligodendrocytes respectively. A substantial loss of astrocytes was observed following EB injection but not GalC injection, which is consistent with their respective processes of demyelination. A dramatic lack of GalC immunoreactivity was observed following EB injection and a slight decrease in GalC immunoreactivity was observed following GalC injection. The kinematic behavior of axons was characterized by quantifying changes in axon tortuosity at 5% or 15% quasistatic stretch. The average tortuosity of axons in spinal cords injected with EB decreased significantly for not only stretched spinal cords, but also for unstretched ones. The percentage of axons that demonstrated non-affine kinematic behavior increased compared to controls. The average

initial tortuosity of axons from spinal cords injected with GalC antibody was similar to control condition. Noticeable differences were observed in stretched spinal cord following GalC injection compared to control condition. The percentage of axons that exhibit purely non-affine, uncoupled behavior in spinal cord following GalC injection increased slightly compared to control spinal cord. The results demonstrated that glia contributes to the transition from non-affine to affine kinematic behavior of axons during stretch. A difference in axonal kinematics was observed between spinal cords injected with EB and injected with GalC. Spinal cords injected with EB showed more non-affine behavior compared to spinal cords demyelinated by GalC. The different axonal kinematics between the two demyelination protocols might be caused by the different resulting tissue components. The results suggested that glial cells such as astrocytes and oligodendrocytes might play an important role in axonal kinematics.

Introduction

In the central nervous system, axons are connected to glia via physical contact with oligodendrocytes and astrocytes. The interconnection between oligodendrocytes and axons occurs via the process of myelination. Myelin is the highly differentiated membrane structure produced by oligodendrocytes (Bunge, Bunge et al. 1961; Peters 1990). One oligodendrocyte can wrap up to 60 axons. Thus, myelination can represent the degree of axon-oligodendrocytes coupling. As described in Chapter 2, axonal kinematics showed a transition from non-affine behavior at early development stage (E12, E14) to affine behavior at later development stage (E16, E18) in chick embryo spinal cord. The transition correlates positively to the increase in myelination with

growth of the chick embryo spinal cords. The connection between the oligodendrocytes and axons may affect the transition behavior of axonal deformation during stretch. However, in addition to the increased myelination, many other factors might affect the increase in affine deformation during growth. Parameters such as the size of the spinal cords, including the diameter and the length, the number of axons, and the development of other glial cells may augment the transformation to affine behavior. In this thesis, we were interested in the effect of glia and myelination on axonal kinematics and examined how axonal kinematics behaved in the demyelinated spinal cord.

Disruption of myelination has been studied previously. Myelination can be suppressed by different ways such as X-ray irradiation (Blakemore 1978); toxin induction (Blakemore 1978; Graca and Blakemore 1986; Harry, Goodrum et al. 1989); virus infection (Herndon, Price et al. 1977; Clifford-Jones, Landon et al. 1980); nerve compression (Bunge, Bunge et al. 1961; Clifford-Jones, Landon et al. 1980); and immunological means (Keirstead, Hasan et al. 1992; Keirstead, Pataky et al. 1997). These methods disrupt myelination by different mechanisms and result in different modes of cell damage. We chose to use two different methods to demyelinate axons in the spinal cord in our research: 1) chemically, by exposure to the toxic reagent ethidium bromide (EB), and 2) immunologically, by exposing CNS myelin to serum complement and GalC antibody.

Ethidium bromide has been reported to induce demyelinaton after injection into the brainstem or spinal cord of the rat (Levine and Reynolds 1999). Within 22 h after EB injection, there is a 21% decrease in the number of oligodendrocyte precursor cells. At 6 days after EB injection, there are few, if any, oligodendrocytes that survive. EB appears

not only to suppress myelin, but also damages astrocytes. Given the high degree of toxicity and inflammation due to EB, it seems likely that neurons would also suffer. (Levine and Reynolds 1999). Another aspect of EB injection is that remyelination begins at about 12-15 days after injection and continues over an extended period of time. We injected EB into the developing chick spinal cord at E14 and incubated the injected embryo until E18. Myelin basic protein (MBP) immunohistochemistry was used to assess the degree of myelination for chick embryo spinal cord at E18. A decrease in MBP immunoreactivity was observed, suggesting a decrease in the degree of myelination.

Galactocerebroside (GalC) is the major oligodendrocyte sphingolipid and is highly conserved across species (Ranscht, Clapshaw et al. 1982). GalC is present on the oligodendrocyte surface and myeline membranes (Ranscht, Clapshaw et al. 1982). Antisera against GalC have been shown to demyelinate CNS tissue in vitro (Dyer and Benjamins 1990), as well as demyelinating the optic nerve (Sergott, Brown et al. 1984) and spinal cord in vivo (Mastaglia, Carroll et al. 1989). H.S.Keirstead and his colleagues found that a single injection of serum complement proteins plus GalC or O4 antibodies into the thoracic spinal cord of an E9-E12 chicken embryo result in a delay of the onset of spinal cord myelination until E17 (Keirstead, Dyer et al. 1995; Keirstead, Pataky et al. 1997). They found a lack of MBP immunoreactivity throughout the spinal cord, except for the most rostral 1-4 cervical segments. This developmental myelin-suppression does not disturb either the astrocytic or neuronal development. Previous studies suggest that the oligodendrocyte cell bodies survive the demyelination procedure and are a likely origin of subsequent myelin. In our study, we injected GalC antibody into the developing chick spinal cord at E12 and isolated the cord at E18. While the majority of myelination

was suppressed, there was still some MBP immunoreactivity observed in the white matter. Astrocyte development was assessed using glial fibrillary acidic protein (GFAP) immunohistochemistry. GFAP is an intermediate filament protein that is highly specific for cells of astrocytes. A decrease in GFAP express was observed in spinal cords injected with EB while none of the other operations altered astrocyte development. Thus, different cellular compositions resulted from the two different protocols.

After injection, the chick embryos were incubated until E18 and the spinal cord was dissected and stretched to two levels, 5% and 15%. The kinematical behavior of myelinated and demyelinated axons was characterized and compared. All procedures were the same as described in Chapter 3. A substantial difference was observed in spinal cord injected with EB. However, demyelinating the spinal cords with GalC antibody did not make the kinematics as 'non-affine' as spinal cords that were demyelinated with EB. Considering the different mechanism and effects between GalC antibody and EB, we could conclude that the different cell components, especially those that connect axons such as oligodendrocyte and astrocytes, contribute to the different mechanical behavior of axons.

Methods

Developmental myelin -suppression

Fresh fertile eggs were incubated at 38°C and injections were performed at the appropriate day. Cervical-thoracic spinal cord injections were performed in chick embryos using a microsyringe (Hamilton). Different reagent were injected: 1) an IgG rabbit anti-GalC antibody (Chemicon international inc., Temecula, California #AB142) at

a dilution of 1:25 with 20% serum complement in 0.1M PBS (PH7.4) injected into E12 embryos, 2) 3 μg/ml EB 0.01% EB (Sigma) injected into E14 embryos. Two reagents were used as a control to GalC antibody and EB respectively: 1) pure rabbit IgG (Jackson ImmunoResearch Laboratories) at a 1:25 dilution with serum complement in 0.1M PBS (PH 7.4), or 2) 0.1% saline solution injected to E14 embryos. These injections are briefly summarized in table 4-1. Each intraspinal injection was performed with 2-3μl of solution; each animal received a total volume of 4-6ul, injected directly into the cervical and thoracic spinal cord twice at different positions. Injected embryos were placed back into the incubator for further development. At E18, the spinal cords were excised for mechanical property testing.

Antigen Injected	Day of Injecton	Amount of Injection	Day of Dissection	Stretch Levels
GalC Anitbody	E12	4/6 microliter	E18	5, 15%
Pure rabbit IgG	E12	4/6 microliter	E18	5, 15%
Ethidium Bromide	E14	4/6 microliter	E18	5, 15%
Saline	E14	4/6 microliter	E18	5, 15%

Table 4-1: Reagents used for demyelination. GalC was used to delay the myelination, while EB was used to cause oligodendrocyte death or delay the myelination. All of the injected embryos were dissected at E18 and excised spinal cords were then stretched and tested..

Chick embryo spinal cord measurement, isolation, and stretching

Injected embryos were incubated until day 18 post-fertilization (E18) and the full spinal column with spinal cord intact was excised. The ventral surface of the spinal cord was exposed. The gauge length of a segment of the spinal cord beginning at the first nerve root after the cervical enlargement and extending rostrally for 11 segments was measured. Each measurement was repeated 3 times to obtain the average *in situ* length. After the final measurement, the dorsal half of the vertebrate was removed to allow free stretch of the spinal cord, and the length of spinal cord was re-measured. Each

measurement was again repeated 3 times after full dissection for the average *in vitro* length.

Spinal cords were immediately transferred to a custom-built device that enabled reproducible, quasistatic stretch of tissue in a buffered saline bath. The ends of the spinal cords were clamped, the gauge length between the clamps was measured with digital calipers and recorded, and the spinal cord was restored to the original *in situ* length. The spinal cord was stretched to a stretch ratio (λ) of 1 (unstretched control), 1.05, or 1.15, where λ is defined as:

$$\lambda = \frac{Final\ Spinal\ Cord\ Length}{Initial\ Spinal\ Cord\ Length} \quad \text{Equation 4-1}$$

Three spinal cords were tested for each operation at each level of stretch. Following stretch, the saline was replaced with 4% paraformaldehyde to fix the spinal cord in its elongated state. Spinal cords were fixed in their stretched state for 30 minutes, removed from the device, and re-measured to ensure that the stretched length remained the same. Spinal cords were post-fixed in 4% paraformaldehyde overnight and then incubated in a 20% sucrose-saline solution overnight at *4°C* for cryoprotection in preparation for immunohistochemical labeling of axons.

Immunohistochemistry

Frozen horizontal sections (10μm) were cut on a cryostat (Thermo Electron, Pittsburgh, PA) and placed on pre-treated glass microslides (Fisher Scientific, Hampton, NH). Sections were rinsed in buffered solution (1% bovine serum albumin (BSA – Sigma, St. Louis, MO), 0.5% TritonX-100 (Sigma) in phosphate buffered saline (PBS -

Sigma)) for 5 minutes, then incubated in a 10% solution of goat serum (Atlanta Biologicals, Lawrenceville, GA) for 1 hour. Sections were then incubated overnight in a 1:1000 dilution of mouse α-neurofilament-200 (Sigma), 1:100 dilution of mouse anti-pig GFAP (Sigma Immunochemicals, #G-3893), or 1:10 rabbit anti-GalC antibody (Chemicon international inc., Temecula, California #AB142). The next day, sections were washed with buffer four times for five minutes apiece, and then incubated in a 1:400 dilution of Alexa 488 goat anti-mouse secondary antibody (488nm/515nm excitation/emission, Molecular Probes, Eugene, OR) or 1:100 goat anti-rabbit immunoglobulin (Caltag, South San Francisco; #L42018). Sections were again rinsed (4 x 5minutes), and slides were coverslipped (Vectashield mounting medium for fluorescence, Vector Labs, Burlingame, CA).

Separate, unstretched spinal cords were harvested similarly and sectioned coronally (10μm) for immunohistochemical labeling of oligodendrocytes and myelin. Alternate sections were double labeled with a 1:400 dilution of rabbit anti-myelin basic protein (MBP) (Accurate Chemical Scientific, Westbury, NY), as well as the 1:1000 dilution of mouse α-NF-200, followed by incubation in 1:100 goat anti-rabbit immunoglobulin (Caltag, South San Francisco; #L42001) to visualize the MBP and 1:100 goat anti-mouse Alexa 546 (Molecular Probes) to visualize the neurofilaments.

Microscopy and image analysis

Composite images of spinal cord sections from C4/5 – T4/T5 were generated with Olympus Microsuite software controlling an Olympus IX81 inverted epifluorescent microscope (Olympus, Melville, NY) and a Hamamatsu ORCA 285 digital camera

(Hamamatsu City, Japan). Individual axonal segments in the lateral funiculus that spanned at least several periods of undulation were identified at random. Two measurements were made for each axonal segment with the Microsuite software. The actual pathlength was found by tracing the segment with the cursor. The end-to-end length was then identified from the coordinates of the beginning and end of the traced line. Each segment was considered an independent sample. These two measurements were made for several hundred randomly located axons for each spinal cord, and the results tabulated in a database. The tortuosity of each axon was then calculated as:

$$T = \frac{actual\ length}{end\text{ - }to\text{ - }end\ length} = \frac{L_A}{L_E} \quad \text{. . . . . .} \quad \text{Equation 4-2}$$

Myelination quantification

Frozen cross sections (5 μm) were cut on a cryostat (Thermo Electron, Pittsburgh, PA) and placed on pre-treated glass microslides (Fisher Scientific, Hampton, NH). Slides were treated in 2% osmium tetroxide (Electron Microscopy Sciences) for 30 minutes and washed in 95%, 70%, and 50% alcohol for 3 minutes to dehydrate. Slides were mounted with xylene (Sigma) and coverslipped. Images were taken with a light microscope at 40X magnification. The myelin sheath appeared black under the light microscope. Five areas were taken randomly from each slice in white matter and five slices were taken for each spinal cord. The distance between each slice was 30-40 microns. Three spinal cords were imaged for each experimental condition. The number of myelin sheaths was measured by touch count from the Microsuite software for each area. The average number of myelin sheaths was recorded for each slice, each spinal cord, and each condition.

Kinematics model

The results from the experiments were compared to the affine and non-affine mathematical model to determine the kinematic behavioral trends. Tortuosity distributions of axons from unstretched spinal cords were compared to identify the effects of injected reagents on axonal tortuosity distribution. The 'switching' model was employed to evaluate the values of the lower bound (T_1) and upper bound (T_2) for each operation. The values of T_1 and T_2 define the transition behavior for the group of axons. These values were estimated for each instance by minimizing the net difference between experimental and predicted histograms across both stretch levels using a Levenberg-Marquart multi-parameter, non-linear regression scheme. Since the 'switching model' involves the random assignment of a particular transition tortuosity to a given axon, the optimization was executed 50 times for each injection, from which the mean transition values and standard deviations were determined.

Results

Growth of chick embryo spinal cords

Chick embryos survived exposure to all experimental reagents. After injection, chick embryos continued development until E18 and were ready for dissection. Growth of chick embryo spinal cords was affected by both EB and GalC. The length of spinal cord decreased compared to control embryos that did not receive any operation. Spinal cord length in embryos injected with EB decreased 2.9% and spinal cords injected with GalC antibody decreased 4.5% in length (Fig 4-1). Saline or pure rabbit IgG did not affect the growth of the spinal cords. The length of spinal cords injected with saline or

pure rabbit IgG was similar to unoperated chick embryos. The results showed that the injection operation did not affect the growth of the spinal cord

Myelination characterization

The progress of myelination was assessed using immunolabeling of myelin basic protein (α-MBP). Spinal cords injected with different reagents showed different MBP immunoreactivity as shown in Fig 4-2. Spinal cords injected with saline or pure rabbit IgG showed similar MBP immunoreactivity compared to unoperated chick embryos. MBP immunolabeling was prominent in white matter, suggesting that majority of axons were myelinated. Thus, saline or pure rabbit IgG did not affect the progression of myelination in the spinal cord. Spinal cords injected with EB or GalC antibody showed a dramatic decrease in MBP immunoreactivity spanning the cervical-thoracic spinal cord. Thus, both EB and GalC antibody disrupted myelination in developing embryo spinal cords. In both instances, some myelinated axons were visible throughout the spinal cord white matter.

Following osmium tetroxide staining, the myelin sheath appeared as a black annulus of different sizes under light microscopy as shown in Fig 4-3 for all conditions. Distribution of myelin sheaths was non-uniform for each area or each region. In order to minimize the error caused by the non-uniform distribution, we picked 5 regions and 5 areas for each region to quantify the myelination for each spinal cord. For each condition, 3 spinal cords were assessed. No significant difference was observed among three spinal cords for each condition (Table 4-2). Spinal cords injected with demyelinating reagents showed different numbers of myelin sheaths as compared to controls: 64.42 +/- 0.71 for

unoperated spinal cords; 63.77 +/- 0.49 for spinal cords injected with saline; 63.38 +/- 0.75 for spinal cords injected with pure rabbit IgG; 30.45 +/- 0.48 for spinal cords injected with EB; and 34.18 +/- 0.99 for spinal cords injected with GalC antibody. The distribution of myelin sheaths did not appear to be changed as a result of injection of saline or pure rabbit IgG as compared to unoperated embryos. As assessed by osmium tetroxide staining, the average number of myelin sheaths decreased in spinal cords injected with EB or GalC. There was a small but noticeable difference in average myelin sheath number between spinal cords injected with EB and GalC antibody. The result of myelin quantification again confirmed the disruption of myelination by both myelin-suppression protocols.

Glia characterization

Oligodendrocyte and astrocyte development was assessed with immunolabeling of GalC antibody and GFAP respectively. The immunoreactivity for GalC was similarly for spinal cord non-operated (Fig 4-4A), following saline injection (Fig 4-4B), and following IgG injection (Fig 4-4D). Similar immunoreactivity was also observed in spinal cord following GalC injection (Fig 4-4E) compared to controls, indicating that oligodendrocyte cell bodies survived the immunological protocol. A decrease in GalC expression was observed in spinal cord following EB injection (Fig 4-4C) compared to all other injections, suggesting that oligodendrocyte cell bodies were disrupted by EB. The mature state of the spinal cord astrocyte population did not appear to be disturbed by injection of saline, pure rabbit IgG, or GalC antibody. Immunohistochemical assessments of E18 spinal cord operated with saline (Fig 4-5B), pure rabbit IgG (Fig 4-5D), or GalC

antibody (Fig 4-5E) showed very similar astrocyte immunoreactivity compared to unoperated control spinal cords (Fig 4-5A) at E18. Additionally, individual astrocytes in all instances did not appear to express different levels of GFAP. However, astrocyte development appeared to be disturbed following EB injection (Fig 4-5C), as assessed by GFAP immunohistochemistry. The distribution of astrocytes within the spinal cord in tissue injected with EB was different compared to all other conditions. At 4 days after injection of EB, the affected spinal cord showed much lower express of GFAP. The remaining GFAP-immunoreactivity most likely reflected the phagocytosis of astrocytic debris.

Tortuosity characterization of axons in spinal cords

Digital imaging following immunolabeling of neurofilaments with α-NF200 revealed many continuously-labeled axons that were easily viewed with epifluorescence microscopy at both stretch levels (Fig 4-6 for unoperated spinal cord, Fig 4-7 for saline operation, Fig 4-8 for EB operation, Fig 4-9 for IgG operation, and Fig 4-10 for GalC operation). For all chick embryos, axons in the unstretched spinal cord were visibly undulated and the tortuosity followed a Gamma distribution. The average tortuosity of axons in spinal cords injected with saline, pure rabbit IgG, or GalC antibody was similar to unoperated embryos. However, the 'perfectly straight' axons (tortuosity equals 1) showed noticeable different distribution between injected spinal cords and unoperated spinal cords. In operated spinal cords, a smaller population of 'perfectly straight' axons was observed. The percentage of 'perfectly straight' axons was as follows: 3.5% for unoperated spinal cords; 0.5% for spinal cords injected with saline; 1.4% for spinal cords

injected with IgG; 0.5% for spinal cords injected with EB; and 0.2% for spinal cords injected with GalC. Axons in spinal cord injected with EB showed a lower initial average tortuosity than with the other conditions.

Axons became less tortuous and straightened following stretch of the spinal cords for all instances as shown in Fig 4-6 to Fig 4-10. Spinal cords injected with different reagents showed different degree of straightness. Spinal cords injected with saline or pure rabbit IgG showed similar trend to the unoperated embryos at both stretch levels. For spinal cords injected with GalC antibody, the average tortuosity decreased slightly but noticeably at both stretch levels. The ability of axons to maintain a tortuous morphology slightly decreased in spinal cords following GalC injection compared to control embryos. Decreased average tortuosity was also observed in spinal cords following EB injection at both stretch levels. However, no conclusion could be made since the initial tortuosity of axons was different.

Axonal kinematics

Similarly to the unoperated embryonic spinal cords, the axon tortuosity distribution in experimental spinal cords did not follow either ideal kinematic behavior. Neither the affine nor the non-affine model perfectly predicted the experimental results. The experimental data stayed between affine and non-affine cumulative histograms for each injected spinal cord at each stretch ratio as shown in Fig 4-11.

The ‘switching’ model was executed 50 times for each injection operation because of the randomly assigned transition tortuosity to each axon from a uniform distribution, as described in Chapter 3. In each run, the values of T_1 and T_2 were optimized by

minimizing the net difference between tortuosity distributions against the experimental data across both stretch levels. As shown in Fig 4-12, the value of T_1 was similar for each condition while the value of T_2 was significantly different (ANOVA, $P<0.001$). $T_1<1$ and $T_2>1$ for all instances, suggesting a fraction of the axons exhibited purely non-affine deformation. This percentage significantly increased (ANOVA, $P<0.001$) in spinal cords injected with EB or GalC as follows (Fig 4-13): 25.9% +/- 3.7% for unoperated spinal cord; 25.5% +/- 3.5% for spinal cord injected with saline; 26.2% +/- 4.0% for spinal cord injected with IgG; 31.1%+/-3.7% for spinal cord injected with EB; and 28.0% +/- 7.0% for spinal cord injected with GalC antibody. The values of T_2 decreased in spinal cords with myelin-suppression compared to control embryos. However, the decrease was greater in spinal cords injected with EB compared to spinal cords injected with GalC antibody (Fig 4-13). The results suggest that EB and GalC antibody did affect the axonal kinematic response, with EB having the most substantial effect.

Discussion

In this Chapter, we investigated the mechanical behavior of axons in myelinated and demyelinated spinal cords. We have characterized axonal mechanical behavior in the developing chick embryo spinal cord and observed an increase in affine deformation in more developed embryos. The reason why axons in chick embryo spinal cords showed different kinematics at different developmental stages is not clear. Previous research has demonstrated that myelination develops rapidly in chick embryos during development. Axons are connected to oligodendrocytes via myelination and this coupling may provide mechanical integrity. Thus, we have identified the effect of the coupling between axons

and oligodendrocytes on axon kinematics in our research by characterizing axonal mechanical behavior in the demyelinated spinal cord. Disruption of compact CNS myelination was performed with injection of EB or GalC antibody into developing chick embryos. EB and GalC antibody were chosen due to the different mechanisms by which each reagent acts to demyelinate the spinal cord, which might result in damage to different tissue components. EB not only suppresses myelination, but also causes damage to other cells including astrocytes, neurons, and macrophages. GalC delays the myelination until E17 without causing any cell death and it does not alter normal neuronal development. We expected to see not only different kinematic behavior between myelinated and demyelinated spinal cords, but also differences between spinal cords injected with EB and GalC antibody. We characterized the myelination via immunostaining in injected spinal cords and also quantified the myelination degree with osmium tetroxide staining. We also characterized GalC and GFAP immunoreactivity in injected spinal cords to elucidate the effect of EB or GalC antibody on astrocyte development.

EB was injected into chick embryos at E14 and GalC antibody was injected at E12. Saline was used as a control to EB and pure rabbit IgG was used as a control to GalC antibody. We first characterized the change in spinal cord length of injected embryos by measuring the cord length between 11 nerve roots. No significant change in spinal cord length was observed in embryos injected with saline or pure rabbit IgG as compared to unoperated age-matched embryos, suggesting that the injection operation did not affect the chick development. In chick embryos injected with EB or GalC, the decrease in spinal cord length was substantial. Spinal cords injected with EB decreased 2.9% and spinal

cords injected with GalC antibody decreased 4.5% in length compared to unoperated embryos (Fig 4-1). It is not clear why the length decreased. It is possible that the two reagents resulted in different cell populations in the spinal cord tissue and thus produced a difference in tissue volume.

Myelination suppression in the spinal cord was characterized using MBP immunohistochemistry. MBP is produced only in myelinating oligodendrocyte cells. Demyelination was confirmed in spinal cords injected with EB or GalC antibody. Saline or pure rabbit IgG were ineffective in eliciting developmental myelination-suppression. In spinal cords injected with EB or GalC antibody, a decrease in MBP immunoreactivity was observed throughout the spinal cord and the majority of axons were demyelinated. We did not assess the temporal MBP immunoreactivity reaction in spinal cords injected with different reagents in our research. However, previous research has demonstrated that neither EB nor GalC antibody alter the myelination permanently (Keirstead, Pataky et al. 1997; Levine and Reynolds 1999). Besides the different MBP expression, we also observed differential GFAP immunoreactivity in spinal cords injected with EB compared to all other conditions. Spinal cords injected with saline, pure rabbit IgG, or GalC showed similar GFAP expression compared with unoperated embryos, suggesting that astrocyte development was not disturbed in these conditions. GalC immunoreactivity was slightly decreased in spinal cords following GalC injection compared to controls, indicating that oligodendrocyte cell bodies survived the immunological protocol while the maturation of oligodendrocyte cells was delayed as observed in previous research (Keirstead, Pataky et al. 1997). However, a decrease of GFAP expression and GalC immunoreactivity were observed in spinal cords following EB injection, suggesting a different astrocyte

population and disrupted oligodendrocyte cells. Thus, these two different myelin-suppression protocols result in different cellular compositions in chick embryo spinal cord white matter.

In order to quantify the myelin sheath in spinal cords injected with different antigens, we stained spinal cords with osmium tetroxide, which binds at double bonds of unsaturated lipids and imparts a dense brownish or black color under light microscopy. The myelin sheath is stained because of the abundance of lipids in the membranes wrapping around the axon. Three spinal cords were sectioned for each condition and five slices were measured for each spinal cord to minimize the error due to possibly different myelin sheath distributions at different spinal cord regions. For each slice, five areas were randomly picked for measurement in order to minimize the error due to the non-uniform size of myelin sheaths as well as the non-uniform distribution of myelin sheath across the white matter. There was a 30-40 micron gap between each slice. The concentration of myelin sheaths in spinal cords injected with saline or pure rabbit IgG appeared relatively equivalent to unoperated, age-matched control embryos. The concentration decreased in spinal cords injected with EB or GalC antibody. Myelin sheath number decreased 52% in spinal cords injected with EB and 46% in spinal cord injected with GalC antibody. The results again confirmed the myelination-suppression by EB or GalC injection. The axon-glia coupling decreased using these two protocols.

The tortuosity distribution of axons in chick embryos injected with different reagents was characterized to identify whether any reagents affect the developmental axon geometry. Statistical analysis of axonal tortuosity in unstretched spinal cords (0%) for unoperated condition, saline injection, and pure rabbit IgG injection did not reveal

significant changes in tortuosity distributions (K-W test, $p=0.720$) . However, we observed more 'perfectly straight' axons in unoperated spinal cords compared to all other operated embryos. It is unclear why there is a discrepancy in the distribution of tortuosities. It might be caused by tissue response to injection. The individual treatments are therefore best compared against their respective controls (saline for EB and IgG for GalC). Tortuosity distributions in unstretched spinal cords following pure rabbit IgG injection and GalC injection were not significantly different (K-S test, $p=0.037$). However, significant difference in unstretched spinal cords was observed for saline injection and EB injection (K-S test, $p<0.001$). Initial tortuosity, which is the tortuosity at 0% stretch, decreased for spinal cord following EB injection. The initial tortuosity was 1.078 for spinal cord following EB injection while it was 1.083 for unoperated spinal cord, and 1.085 for spinal cord following saline injection respectively. The decrease in axon tortuosity might be caused by a lack of myelination as well as astrocytes and oligodendrocytes. Thus, some connective cells such as oligodendrocytes and astrocytes might contribute to maintaining axon tortuosity during chick embryo growth.

We observed noticeable differences in the kinematical response of axons in the demyelinated spinal cord. For both myelinated and myelination-suppressed spinal cords, axons exposed to controlled stretch did not follow purely non-affine or affine mechanics at either stretch level (Fig 4-11). Axons in spinal cords injected with saline or pure rabbit IgG showed similar kinematics as unoperated embryos. The similarity was also confirmed by employing the 'switching model' (Bain, Shreiber et al. 2003). The values of T_1 and T_2 were similar and the percentage of axons that behaved purely non-affine was similar as well for unoperated spinal cords and spinal cords injected with saline or pure

rabbit IgG. Thus, axonal kinematics in chick embryo spinal cords did not show any sensitivity to saline or pure rabbit IgG injection. Compare to saline injection, EB injection did change the axon tortuosity distribution in both unstretched and stretched spinal cords. The initial tortuosity with EB injection was lower than the saline control in unstretched spinal cords, as discussed previously. Axons' tortuosity decreased with increasing stretch in spinal cord following EB injection as well. Considering the lower initial tortuosity, we can not conclude that spinal cords injected with EB undergo a more non-affine deformation. The trend was quantified by employing 'switching model'. Similar to the control spinal cords, the value of T_1 was less than 1 for spinal cords injected with EB. Thus, there was a population of axons behaving purely non-affine. The percentage of axons behaving solely non-affine mechanics predicted by 'switching model' increased from 25.5% in spinal cords injected with saline to 31.1% in spinal cords injected with EB. T_1 did not show sensitivity to EB injection compared to control, while the upper bound, T_2, decreased from 1.131 in spinal cords injected with saline to 1.108 in spinal cords injected with EB. The result demonstrated that axons in spinal cords injected with EB exhibit increasingly non-affine kinematics during stretch. In contrast to EB injection, no dramatic difference was observed between the pure rabbit IgG control and GalC antibody condition. The average tortuosity in stretched spinal cords injected with GalC antibody showed a slight decrease compared to control. A shift to the left in axonal tortuosity distribution was observed at both stretch levels, suggesting a decrease in the population of highly tortuous axons. The decrease was very slight but significant, and it happened at both stretch levels. Considering the similar initial tortuosity distribution, there might be an increase in non-affine, uncoupled behavior in spinal cords injected with

GalC antibody compared to control. The trend was confirmed by employing the 'switching model' as well. The upper bound (T_2) showed a significant decrease from 1.136 in spinal cords injected with pure rabbit IgG to 1.122 in spinal cords injected with GalC antibody while the lower bound was qualitatively similar. The percentage of axons exhibiting solely non-affine behavior predicted by the 'switching model' increased from 26.2% in spinal cords injected with pure rabbit IgG to 28.0% in spinal cords injected with GalC antibody. The increase was much lower than the EB injected condition. Thus, axonal kinematics did not show the same sensitivity to GalC as EB injection. This difference might be caused from the different cellular composition that resulted from EB treatment as compared to GalC antibody treatment. However, compared to the decrease in myelination (52% and 46% for EB and GalC antibody injection, respectively), the increase in percentage of solely non-affine kinematics was proportionally much lower.

Previous research has demonstrated that GalC antibody does not alter neuronal or astrocyte development. Demyelinated axons with GalC antibody showed a very slight increase in non-affine kinematics. Thus, coupling between axons and oligodendrocytes did cause axons to switch from non-affine to affine mechanics. However, the effect was not as important as we predicted. Considering the differential GFAP and GalC expression in spinal cords following EB injection, astrocytes, oligodendrocytes, or them together may play an important role in axonal kinematics. Moreover, EB injection might possibly damage other cell types such as microglial. These cells, alone or together with other spinal tissue, may contribute to axonal mechanics. The results indicated that the effect of coupling between axons and oligodendrocytes alone on the axonal kinematics is not principle. The effects of the coupling to multiple glial cells on the transition from non-

affine to affine are important. Thus, the mechanical response of axons highly depends on the nature of the coupling between axons and glial matrix. The nature of the coupling varies for developmental stage and nervous location. Therefore, the threshold for individual axons is different for age and region. To understand the threshold will help predicting axon mechanical behaviors. The information can also be used for prevention strategies. To understand the role of any single cell line and multiple cell lines is important to study the threshold for age and regions.

In addition to the change in percentage of axons exhibiting purely non-affine kinematical behavior in demyelinated axons, we also found several interesting observations. First, the values of T_1 and T_2 were different for unoperated spinal cords when two stretch levels were applied to the 'switching model' compared to a previous study when four stretch levels were applied. It might be caused by different axonal kinematics at different stretch ratios. Second, the values of T_2 showed sensitivity to demyelination of axons while the T_1 value was qualitatively similar for each operation. In previous research, we have demonstrated that the values of T_1 increased greatly with development from E12-E18 while T_2 showed insensitivity. Thus, the lower and upper bounds might be affected by different contributors. Lengthening of the spinal cord, increasing cell numbers, or growing increased axonal coupling all possibly affect the value of the lower bound. The growth might not affect the upper bound. Cells that connect axons as well as initial axon tortuosity might contribute to the values of upper bound. Thus, axons in different neuronal areas or at different developmental stages might result in a different threshold for either morphological injury or functional injury. Identification of the roles of different cell components in axonal kinematic behavior is

important to understand how strain is transmitted from tissue to axons. We believe that a better understanding of these possible contributors helps predict axonal kinematics by defining unique parameters for different neuronal areas depending on their microstructure and cellular components.

In summary, the axonal mechanical response to tissue strain is a complicated phenomenon. The number of cells, the population of cells, the cellular microstructure, and the connection between cells all possibly affect axonal kinematics. Any change in these factors could change the axonal kinematic response through different mechanisms. Coupling between glial cells and axons appears to contribute to the affine kinematic behavior of axons. The results were not as substantial as expected, especially when compared to the trends observed in Chapter 2. Demyelinating the spinal cords did not make the kinematics as 'non-affine' as spinal cords that were relatively unmyelinated (E12) or partially myelinated (E14). However, the change in initial tortuosity after injecting with demyelinating agents and the difference in growth make the observed changes difficult to interpret, particularly at the micro-scale. In the next chapter, we examine how EB or GalC exposure affects that bulk, macroscopic, mechanical properties of the spinal cord, which offers another means of examining the effects of glia on tissue mechanics.

Figures and Tables of Results

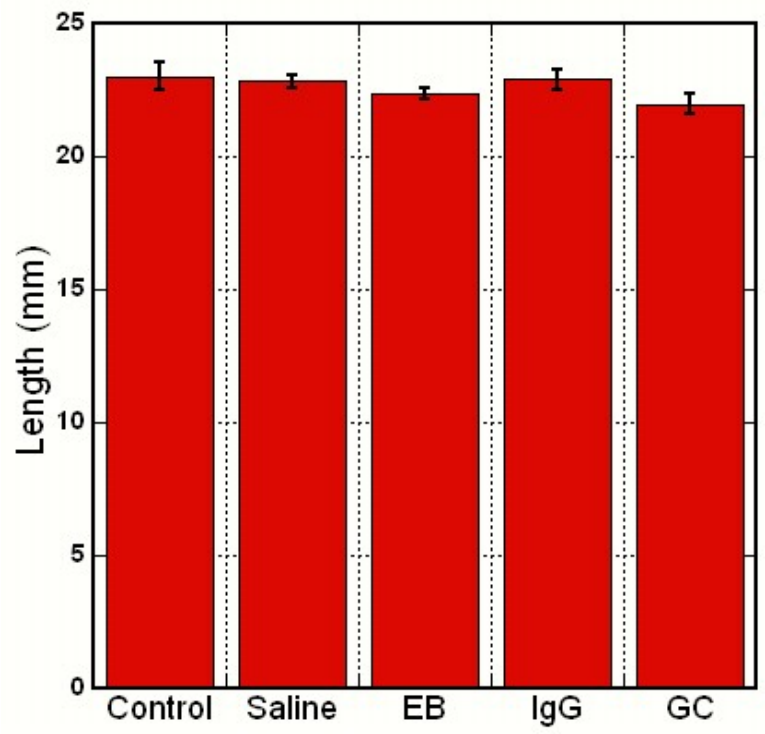

Figure 4-1: Chick embryo spinal cord length between the 3rd to 13th nerve roots in ovo at E18. Saline or pure rabbit IgG did not affect the growth of the spinal cords compared to unoperated spinal cords. Spinal cord length in embryos injected with EB decreased 2.9% and spinal cords injected with GalC antibody decreased 4.5% in length.

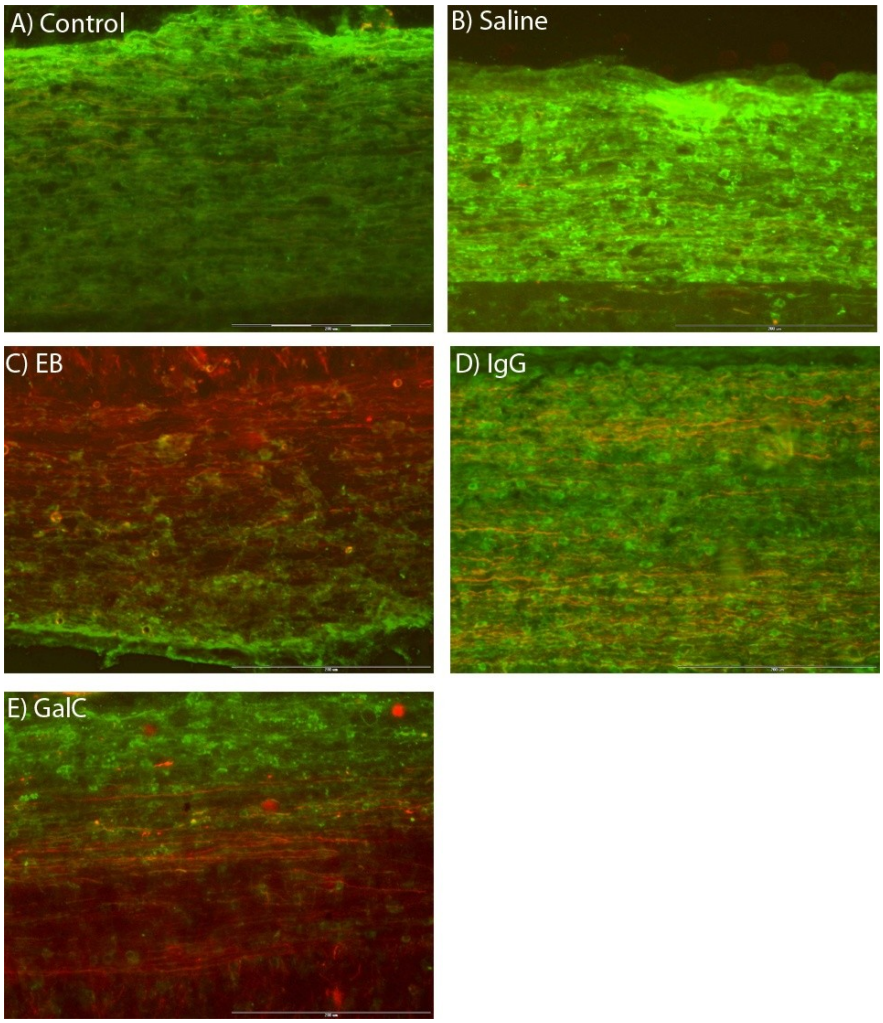

Figure 4-2: Progression of myelination in the chick embryo spinal cord at E18. Coronal sections were taken following immunohistochemical double-labeling of the chick embryo spinal cord were double-labeled immunohistochemically for neurofilament proteins (NF-200 - red) and myelin basic protein (MBP-green). Myelin is pronounced throughout the white matter for unoperated spinal cords (A), spinal cords injected with saline (B), and spinal cords injected with pure rabbit IgG (D). Less myelin was observed in spinal cords following EB injection (C) and GalC injection (E) compared to controls. Majority of axons were demyelinated following EB injection and GalC injection (Scale bars = 200μm).

.

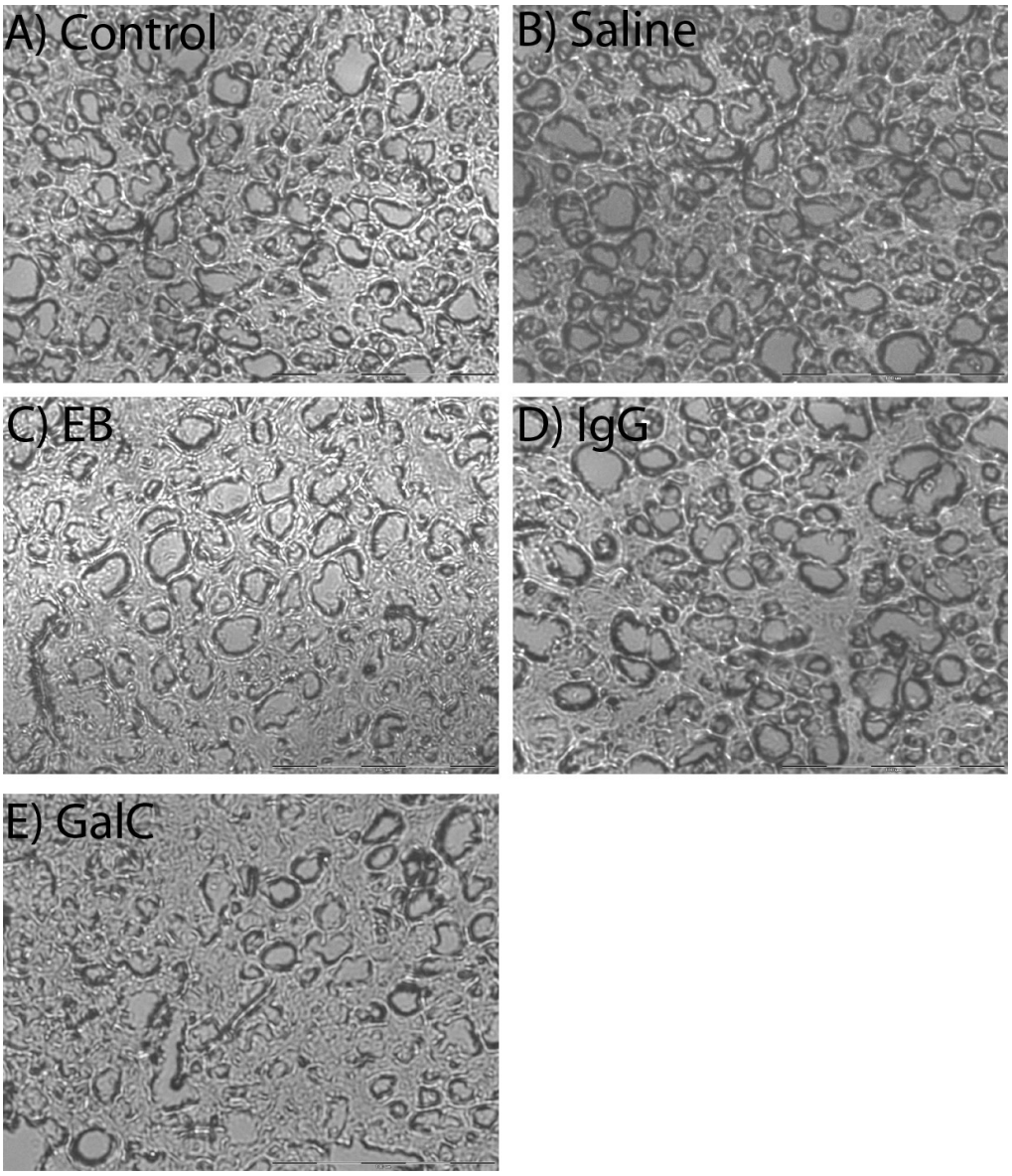

Figure 4-3; Patterns of osmium tetroxide staining in white matters for transverse spinal cord sections following different injections. The myeline sheath appeared like a black donut under light microscopy. The number and distribution of myelin sheath were similar for unoperated spinal cords (A), spinal cords injected with saline (B), and spinal cords injected with pure rabbit IgG (D). Dramatic decrease in numbers of myelin sheath was observed for spinal cords following EB (C) and GalC (E) (Scale bars = 100μm).

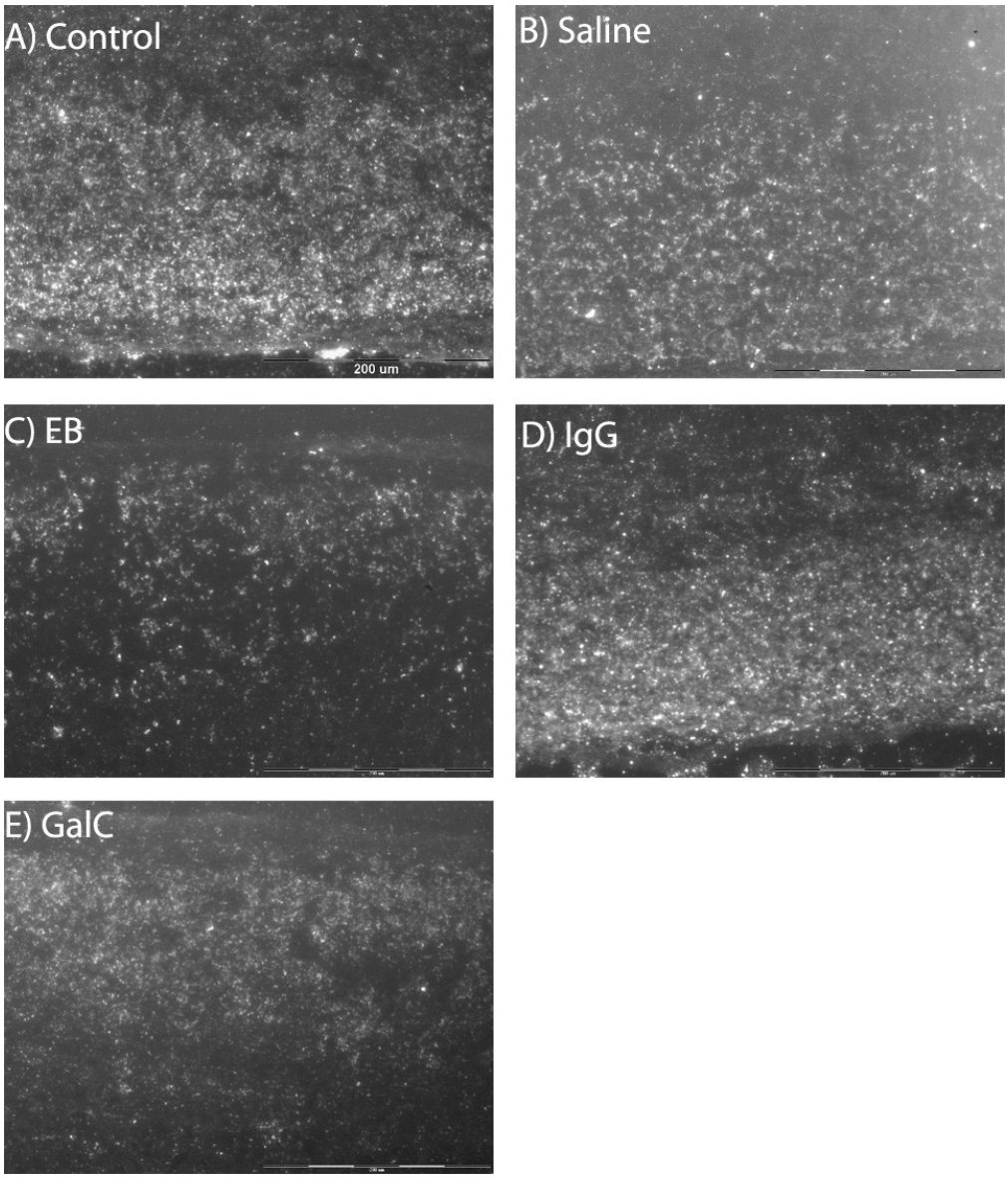

Figure 4-4 : Patterns of GalC immunoreactivity in white matters for spinal cords following different injections. Unoperated spinal cords (A), spinal cords following saline (B) and pure rabbit IgG (D) injection showed abundant GalC immunoreactivity throughout the white matter. Following EB injection (C), spinal cords showed dramatic lack of GalC immunoreactivity, suggesting that oligodendrocyte cell bodies were disrupted by EB. Noticeable however not significant decrease in GalC immunoreacitity was observed in spinal cords following GalC injection (E), suggesting that oligodendrocyte cell bodies survived the immunological protocol (Scale bars = 200μm).

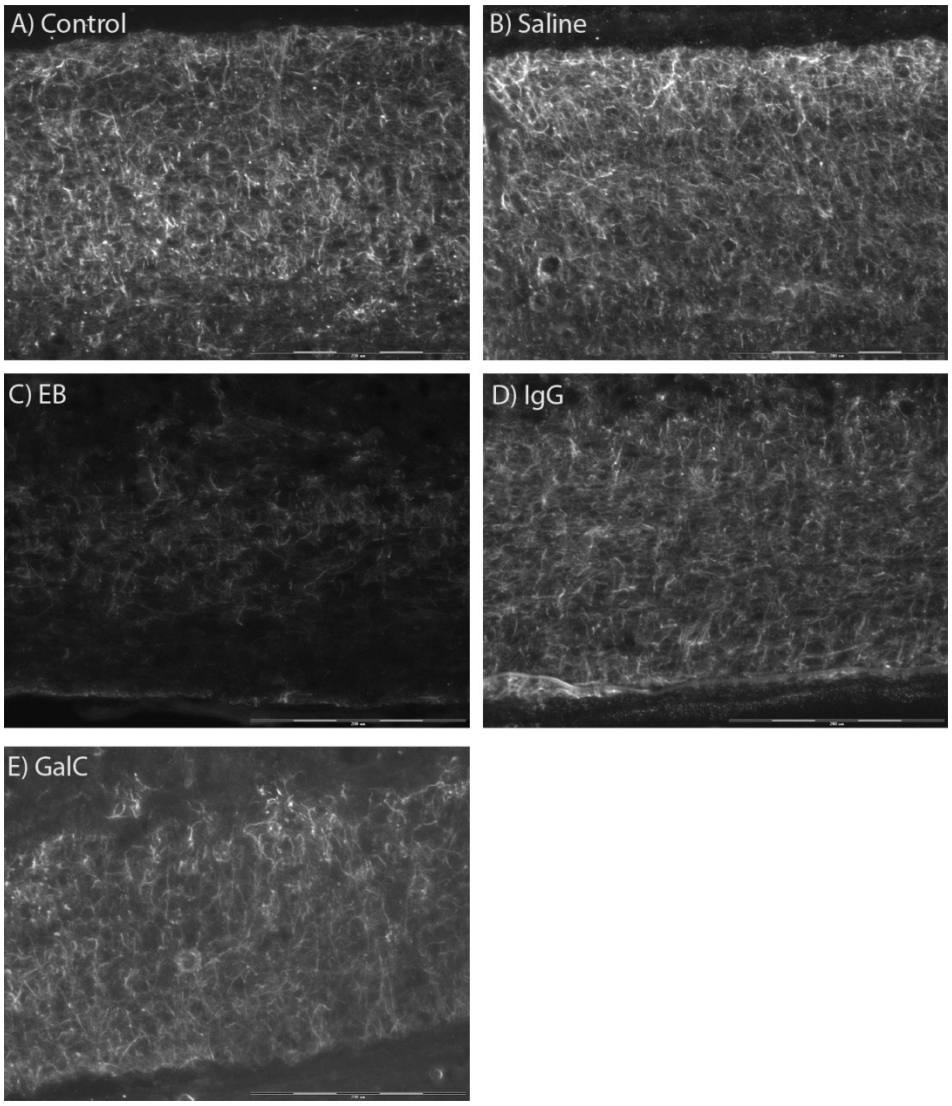

Figure 4-5: Patterns of GFAP immunoreactivity in white matters for spinal cords following different injections. Unoperated spinal cords (A), spinal cords following saline (B), pure rabbit IgG (D), and GalC (E)injections showed prominent GFAP immunoreactivity throughout the white matter, indicating that astrocytes development was similar for all these conditions. Following EB injection (C), spinal cords showed dramatic decrease in GFAP immunoreactivity, suggesting that astrocytes development was disrupted by EB (Scale bars = 200μm).

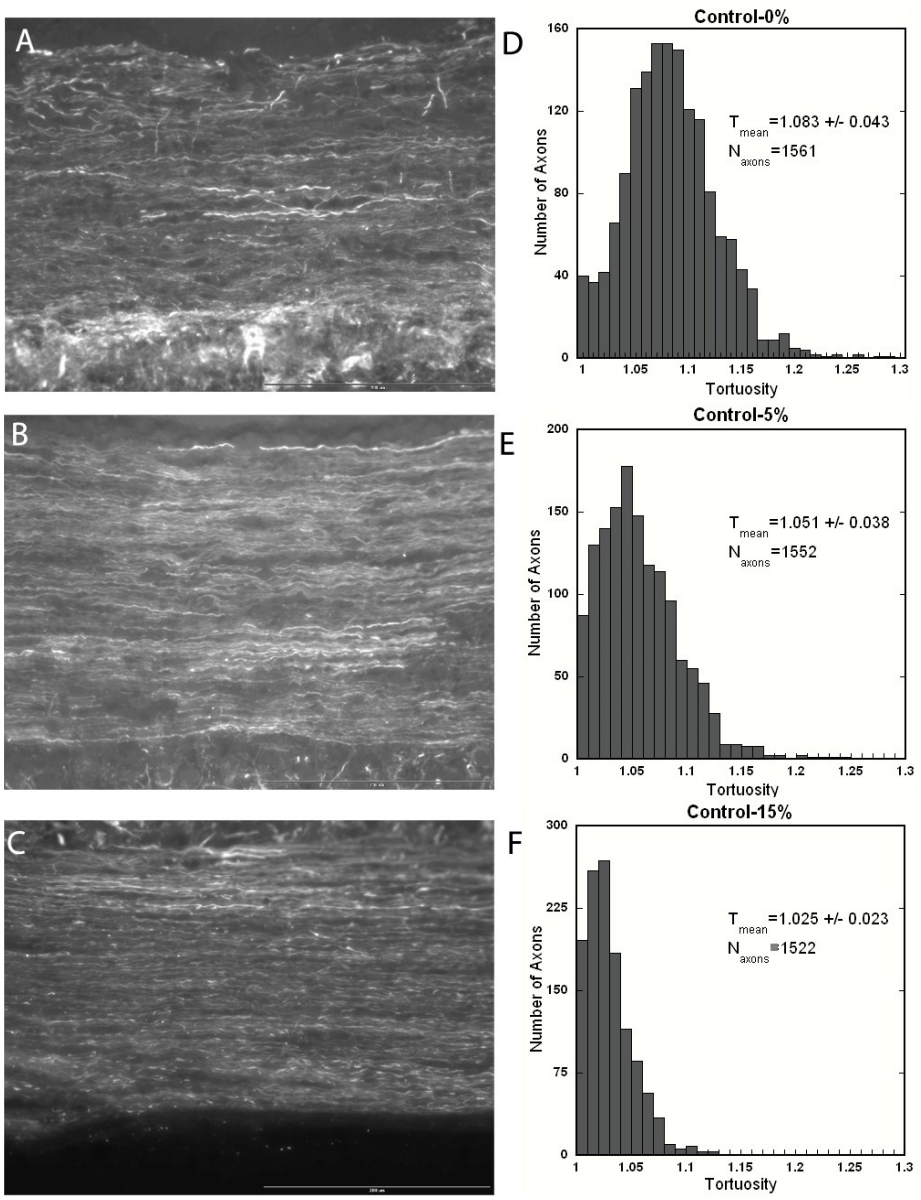

Figure 4-6: Immunohistochemistry and tortuosity characterization for unoperated spinal cords at E18. Coronal sections were collected and immunhistochemically stained for neurofilament proteins. The tortuosity distribution for axons in the sections was determined by tracing several hundred axons from each spinal cord. (A) Many axially- oriented, wavy axons were observed in unstretched spinal cords. The distribution of axonal tortuosity followed a normal distribution. As stretch increased (B = 5%, C = 15%) axons became progressively straighter, and some of axons had tortuosity equal or near one. (Scale bars = 200μm.)

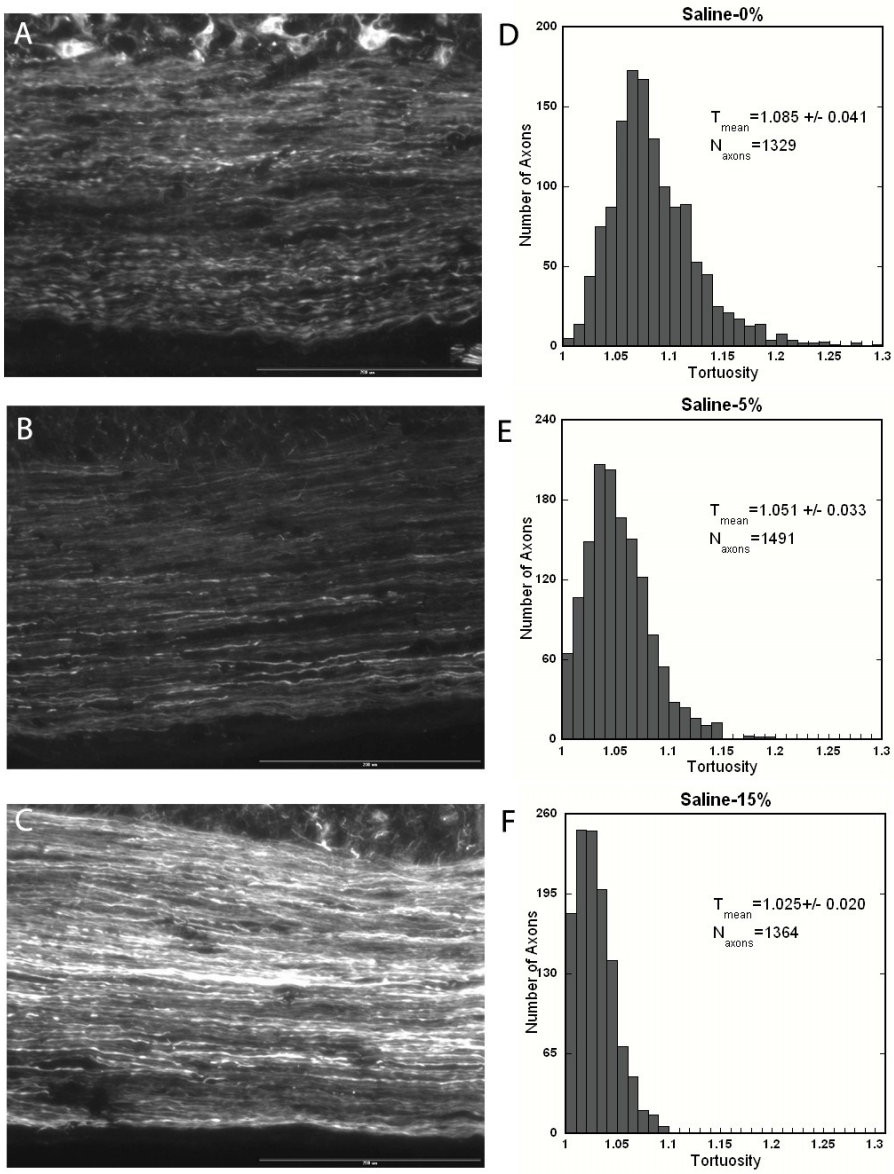

Figure 4-7: Immunohistochemistry and tortuosity characterization for spinal cords at E18 following saline injection. Coronal sections were collected and immunhistochemically stained for neurofilament proteins. The tortuosity distribution for axons in the sections was determined by tracing several hundred axons from each spinal cord. (A) Many axially- oriented, wavy axons were observed in unstretched spinal cords. The distribution of axonal tortuosity followed a normal distribution. Smaller populations of axons with lower tortuosity (T< 1.03) were observed compared to unoperated spinal cords. As stretch increased (B = 5%, C = 15%) axons became progressively straighter, and some of axons had tortuosity equal or near one. (Scale bars = 200μm.)

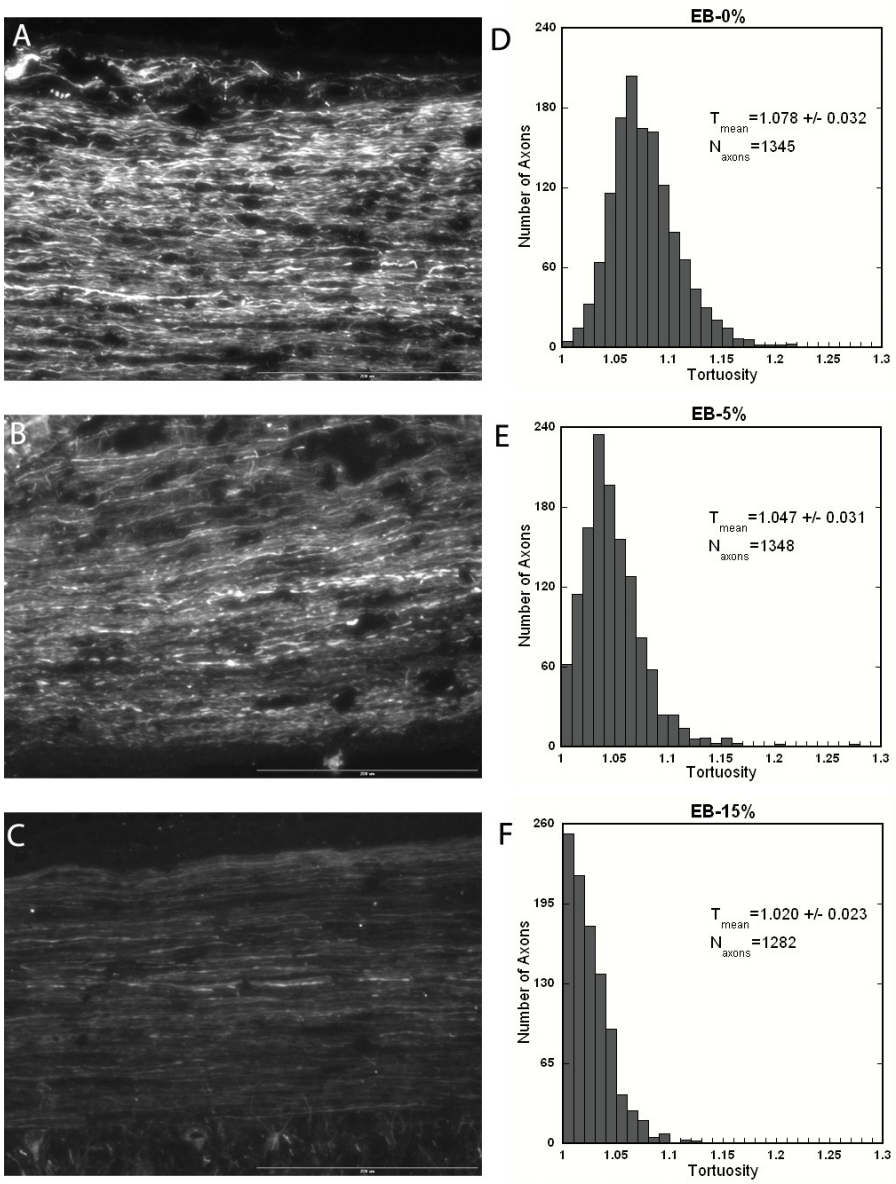

Figure 4-8: Immunohistochemistry and tortuosity characterization for spinal cords at E18 following EB injection. (A) Many axially- oriented, wavy axons were observed in unstretched spinal cords. The distribution of axonal tortuosity followed a normal distribution. Smaller populations of axons with lower tortuosity (T< 1.03) were observed compared to unoperated spinal cords. The distribution was similar to spinal cords following saline injection. The average tortuosity was lower compared to control. As stretch increased (B = 5%, C = 15%) axons became progressively straighter, and a significant number of axons had tortuosity equal or near one. Higher populations of axons with tortuosity of 1 were observed at 15% stretch compared to spinal cords following saline injection (Scale bars = 200μm.)

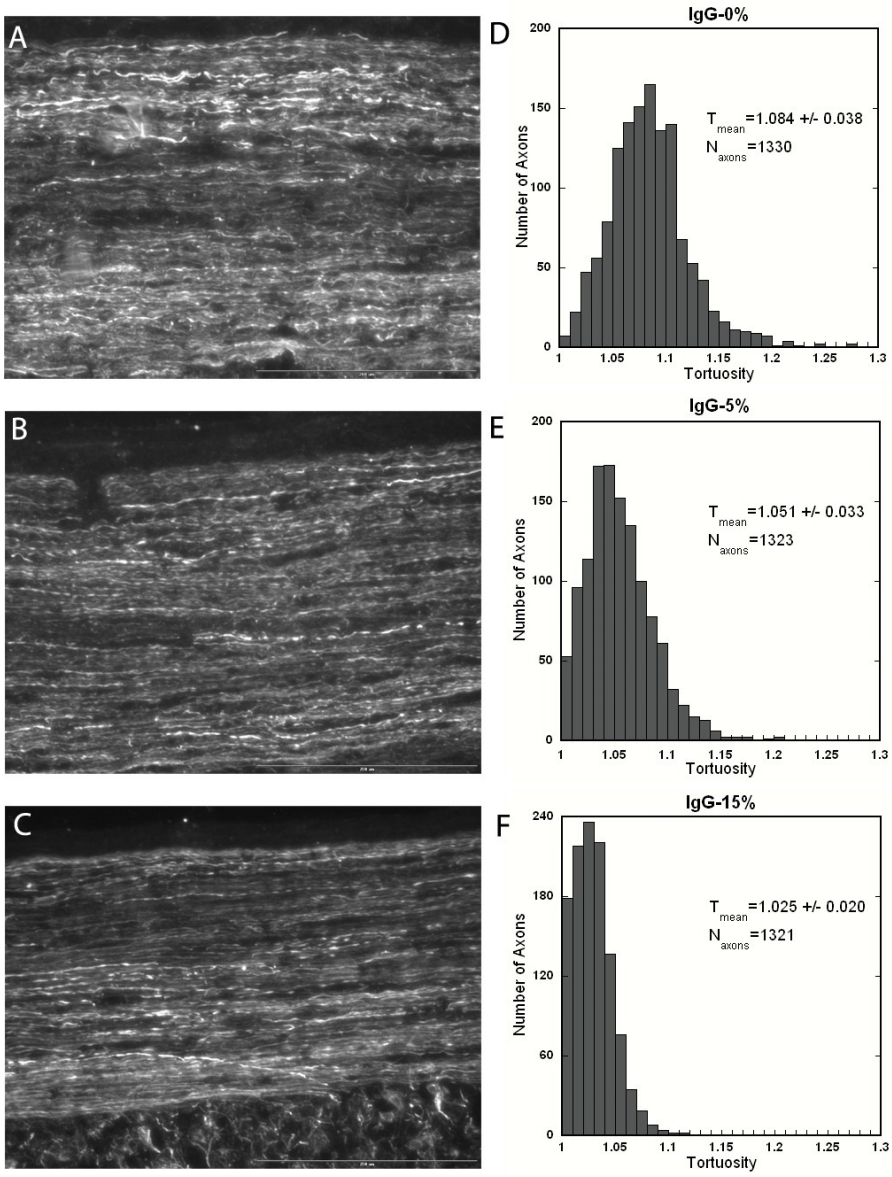

Figure 4-9: Immunohistochemistry and tortuosity characterization for spinal cords at E18 following pure rabbit IgG injection. (A) Many axially- oriented, wavy axons were observed in unstretched spinal cords. The distribution of axonal tortuosity followed a normal distribution. Smaller populations of axons with lower tortuosity (T< 1.03) were observed compared to unoperated spinal cords. As stretch increased (B = 5%, C = 15%) axons became progressively straighter, and some of axons had tortuosity equal or near one. (Scale bars = 200µm.)

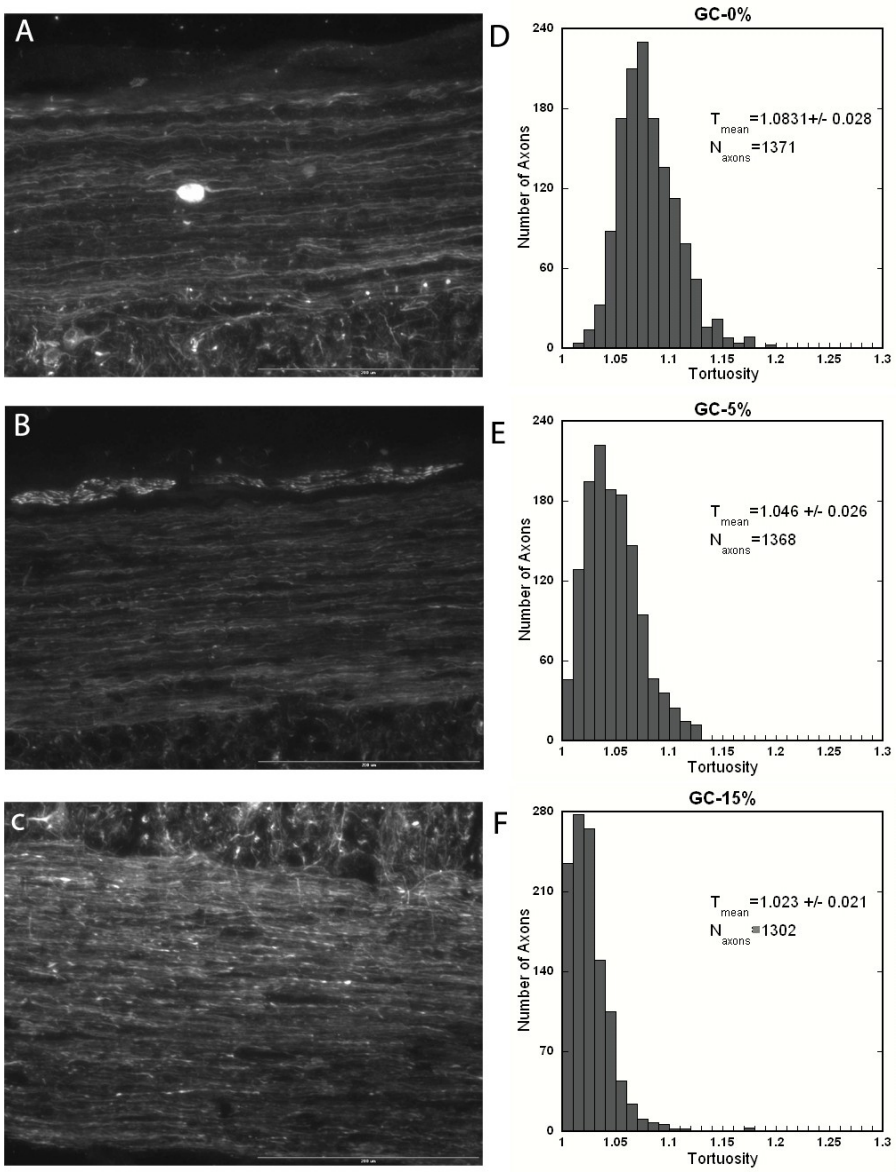

Figure 4-10: Immunohistochemistry and tortuosity characterization for spinal cords at E18 following GalC injection. (A) Many axially- oriented, wavy axons were observed in unstretched spinal cords. The distribution of axonal tortuosity followed a normal distribution. Smaller populations of axons with lower tortuosity (T< 1.03) were observed compared to unoperated spinal cords. The distribution was similar to spinal cords following IgG injection. As stretch increased (B = 5%, C = 15%) axons became progressively straighter, and a significant number of axons had tortuosity equal or near one. (Scale bars = 200μm.)

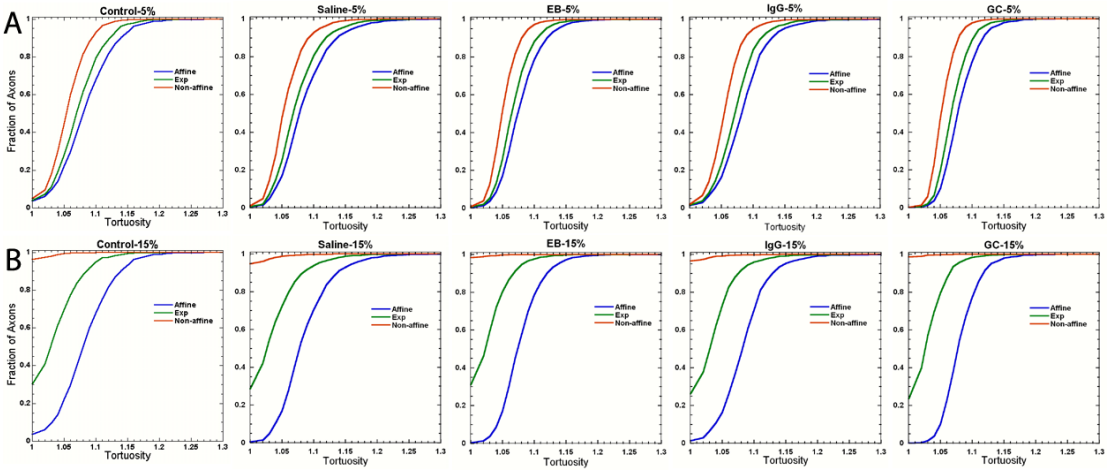

Figure 4-11: Comparison of experimental results to affine, non-affine models. At both lower stretch level (A) and higher stretch level (B), axonal kinematics did not follow any of the ideal deformation manner for all conditions.

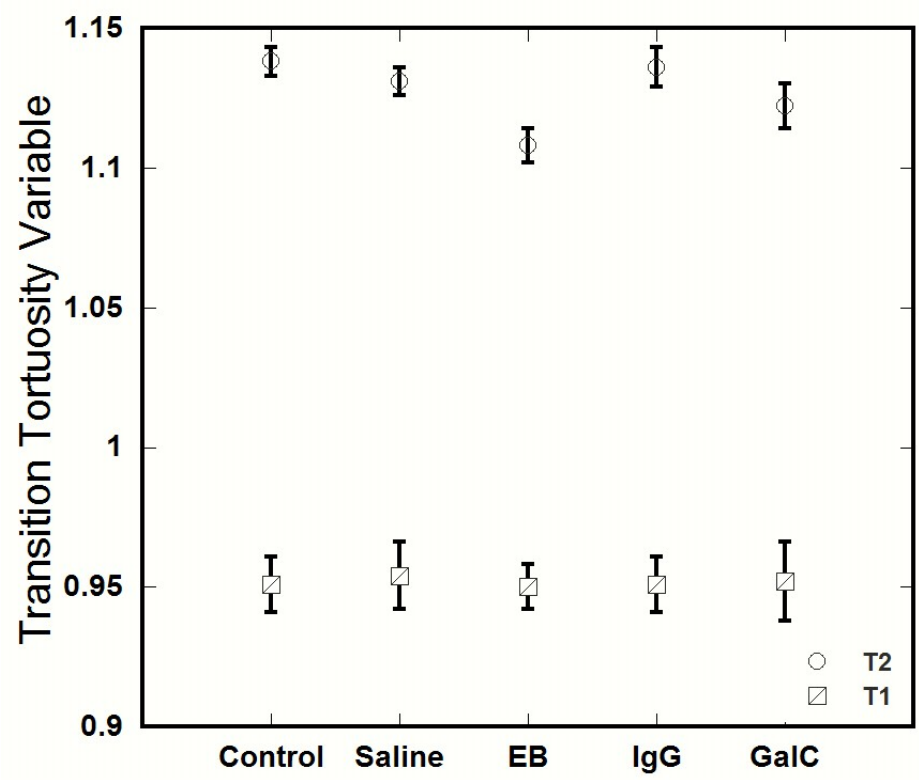

Figure 4-12: Upper and lower bounds of the uniform distribution defining the best-fit switching models for all conditions (average +/- standard deviation of the 50 simulations per stage). For all conditions, $T_1 < 1$ and $T_2 > 1$, indicating that a percentage of the axons $[(1- T_1)/(T_2- T_1)*100]$ demonstrate solely non-affine kinematics. No significant difference was observed for T_1 (square) value among all conditions. T_2 (circle) decreased in demyelinated spinal cords compared to controls and the greatest decrease was observed in spinal cords following EB injection.

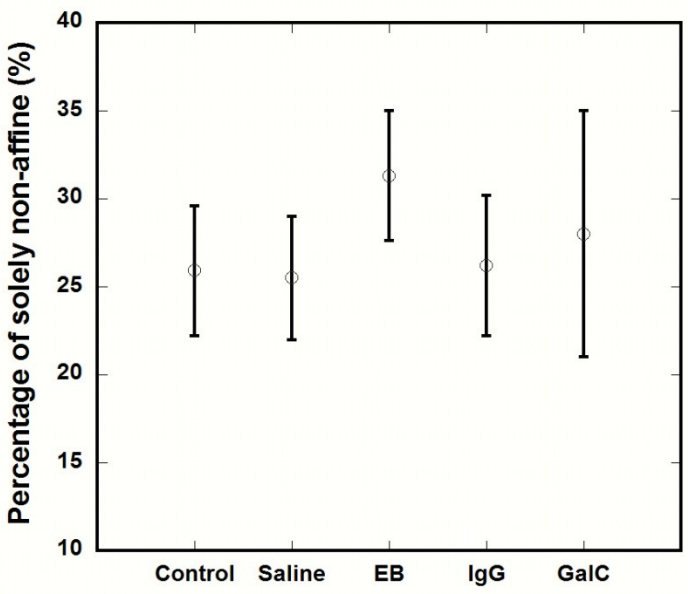

Figure 4-13: Percentage of axons that exhibit solely non-affine kinematics (average +/- standard deviation) was predicted by the 'switching model'. The value of the percentage was determined by the values of T_1 and T_2 as $(1-T_1)/(T_2-T_1)$. This percentage significantly increased for spinal cords following EB injection and spinal cords following GalC injection compared to controls (Anova, $P<0.001$).

Injection	SC1		SC2		SC3		Total	
	Ave.	Std Error	Ave.	Std Error	Ave.	Std Error	Ave.	Std Error
None	63	1.30	65.12	1.65	65.16	1.92	64.42	0.71
Saline	64.76	1.26	63.16	0.75	63.4	0.44	63.77	0.49
EB	30.12	3.39	31.4	3.16	29.84	4.32	30.45	0.48
IgG	64.52	0.49	63.68	1.16	61.96	1.36	63.38	0.75
GalC	35.9	1.87	32.44	2.89	34.2	2.77	34.18	0.99

Table 4-2: Statistics of myelin sheath numbers for each condition.

Antigen Injected	Stretch Level	Mean Tortuosity	Std. Deviation	Total Number of axons
None	0%	1.083	0.043	1561
	5%	1.051	0.038	1552
	15%	1.025	0.023	1522
Saline	0%	1.085	0.041	1329
	5%	1.051	0.033	1591
	15%	1.025	0.020	1364
EB	0%	1.078	0.032	1345
	5%	1.047	0.031	1348
	15%	1.020	0.023	1282
Pure Rabbit IgG	0%	1.084	0.038	1330
	5%	1.051	0.033	1323
	15%	1.025	0.02	1321
GalC antibody	0%	1.083	0.028	1371
	5%	1.046	0.026	911
	15%	1.023	0.021	1302

Table 4-3: Summary statistics for tortuosity measurements

Reference

Bain, A. C., D. I. Shreiber, et al. (2003). "Modeling of microstructural kinematics during simple elongation of central nervous system tissue." J Biomech Eng 125(6): 798-804.

Blakemore, W. F. (1978). "Observations on remyelination in the rabbit spinal cord following demyelination induced by lysolecithin." Neuropathol Appl Neurobiol 4(1): 47-59.

Bunge, M. B., R. P. Bunge, et al. (1961). "Ultrastructural study of remyelination in an experimental lesion in adult cat spinal cord." J Biophys Biochem Cytol 10: 67-94.

Clifford-Jones, R. E., D. N. Landon, et al. (1980). "Remyelination during optic nerve compression." Trans Ophthalmol Soc U K 100(Pt 2): 274-5.

Dyer, C. A. and J. A. Benjamins (1990). "Glycolipids and transmembrane signaling: antibodies to galactocerebroside cause an influx of calcium in oligodendrocytes." J Cell Biol 111(2): 625-33.

Graca, D. L. and W. F. Blakemore (1986). "Delayed remyelination in rat spinal cord following ethidium bromide injection." Neuropathol Appl Neurobiol 12(6): 593-605.

Harry, G. J., J. F. Goodrum, et al. (1989). "Tellurium-induced neuropathy: metabolic alterations associated with demyelination and remyelination in rat sciatic nerve." J Neurochem 52(3): 938-45.

Herndon, R. M., D. L. Price, et al. (1977). "Regeneration of oligodendroglia during recovery from demyelinating disease." Science 195(4279): 693-4.

Keirstead, H. S., J. K. Dyer, et al. (1995). "Axonal regeneration and physiological activity following transection and immunological disruption of myelin within the hatchling chick spinal cord." J Neurosci 15(10): 6963-74.

Keirstead, H. S., S. J. Hasan, et al. (1992). "Suppression of the onset of myelination extends the permissive period for the functional repair of embryonic spinal cord." Proc Natl Acad Sci U S A 89(24): 11664-8.

Keirstead, H. S., D. M. Pataky, et al. (1997). "In vivo immunological suppression of spinal cord myelin development." Brain Res Bull 44(6): 727-34.

Levine, J. M. and R. Reynolds (1999). "Activation and proliferation of endogenous oligodendrocyte precursor cells during ethidium bromide-induced demyelination." Exp Neurol 160(2): 333-47.

Mastaglia, F. L., W. M. Carroll, et al. (1989). "Spinal cord lesions induced by antigalactocerebroside serum." Clin Exp Neurol 26: 33-44.

Peters, a., Palay, S.L., Webster, D. (1990). the fine structures of the nervous system. Saunders, Philadephia.

Ranscht, B., P. A. Clapshaw, et al. (1982). "Development of oligodendrocytes and Schwann cells studied with a monoclonal antibody against galactocerebroside." Proc Natl Acad Sci U S A 79(8): 2709-13.

Sergott, R. C., M. J. Brown, et al. (1984). "Antigalactocerebroside serum demyelinates optic nerve in vivo." J Neurol Sci 64(3): 297-303.

Chapter 5: Identification of material properties of myelinated and demyelinated spinal cords

Abstract

Chick embryo spinal cords were demyelinated by EB and GalC. Saline and pure rabbit IgG were used as a control respectively. Spinal cords following EB injection resulted in disruption of myelination and glial cells while spinal cords following GalC injection resulted in only lack of myelination at E18. Spinal cords at E18 were stretched at low strain rate with an Enduratec uniaxial testing machine. Load and displacement were recorded with Wintest software and data was analyzed in Excel file. The stress-strain data was fit to an Ogden, non-linear constitutive equation. Shear modulus and increase of stiffness as a result of strain were determined from the Ogden model curve fit. The results demonstrated that disruption of myelination alone resulted in lower ultimate stress and lower shear modulus, not the strain at ultimate stress. Disruption of both myelination and glial cells resulted in not only lower ultimate stress and lower shear modulus, but also lower strain at ultimate stress. Our studies demonstrated that myelination and glia contribute to the mechanical response of tissue. Tissue is stronger when myelinated than demyelinated and with glial cells than without glial cells.

Introduction

In our previous research, we observed that tissue of different cell components cause different modes of kinematic transfer of mechanical loads from the spinal cord to axons

at the microscopic level. These changes in cellular components may affect the mechanical properties of the spinal cord itself. It is suggested from previous research that different tissue compositions and mechanical properties can affect the resulting deformation and thus the injury patterns (Prange and Margulies 2002). Developing an appropriate relationship between the mechanical load and the mechanical response of tissues is important to understanding injury at the tissue and axonal levels. In this chapter, we examine how glia influence the macroscopic mechanical properties of the spinal cord by selectively altering the glial matrix during chick embryo development.

Previous research demonstrated that brain is inhomogeneous and its properties are age- and region- dependent (Prange and Margulies 2002). A link between tissue material properties and white matter injury has been suggested from different biomechanical studies of diffuse axonal injury (Lee 1987; Margulies, Thibault et al. 1990; Meaney, Smith et al. 1995; Zhou 1995; Miller and Meaney 1998). Regional, directional, and age-dependent properties of brain have been identified (Prange and Margulies 2002). However, the material properties of spinal cords have received relatively less attention compared to brain, and little is known about the influence of different cellular components on the material properties of either brain or spinal cord tissue. We observed from our previous research that introduction of EB or αGalC to chick embryonic spinal cords during development results in different degree of glia and myelination loss. Astrocytes, oligodendrocytes, and myelination are all disrupted following EB injection while GalC injection only affected the myelination. We also observed that these changes in the cellular environment affected axon kinematics at the microscopic level. These

results suggested that disrupting glia may also affect the macroscopic, bulk, mechanical properties of the spinal cord.

Material properties of adult spinal cord have been studied in rats (Fiford and Bilston 2005), and human (Bilston and Thibault 1996) at different strain rates. In our research, we characterized the stress-strain response in uniaxial tension at a very low strain rate for day 18 post-fertilization (E18) spinal cords. The stress-strain data was fit to an Ogden, non-linear constitutive equation (Ogden 1984), which has been identified as an effective model for CNS tissue undergoing large deformation (Miller and Chinzei 2002; Prange and Margulies 2002). We observed that the effective shear modulus decreased when spinal cord was demyelinated.

Methods

Suppression of developmental myelin

Spinal cords were demyelinated as described in detail in Chapter 4. The methods will be briefly reviewed. Fresh fertile eggs were incubated at 38°C and injections were performed at the appropriate day. Cervical-thoracic spinal cord injections were performed in chick embryos using a microsyringe (Hamilton). Two reagents were used to demyelinate spinal cords: rabbit anti-GalC antibody and EB. Pure rabbit IgG and saline were used as control respectively. Each intraspinal injection was performed with 2-3μl of solution; each animal received a total volume of 4-6ul, injected directly into the cervical and thoracic spinal cord twice at different positions. Injected embryos were placed back into the incubator for further development. At E18, the spinal cords were excised for mechanical property testing.

Spinal cord preparation and measurement

Eggs were incubated until E18 and the full spinal column with spinal cord intact was excised. Before spinal cord isolation, the length of dissected spinal column was measured as an in situ length with a digital caliper. Then the dorsal side of column was removed under a dissection microscope, leaving the other half still attached to the spinal cord. The width and height of spinal cord was measured with digital calipers in order to calculate the cross area as an ellipse for each spinal cord. The whole spinal cord was then removed very carefully from the column and stored in PBS buffer. The length of removed spinal cord was measured as the in vitro length. The percentage of shrinkage (λ_s) due to dissection was calculated as the in vitro length ($L_{in\ vitro}$) divided by in situ length ($L_{in\ situ}$). Twelve millimeters of spinal cord was used for testing. A segment of the spinal cord beginning at the first thoracic enlargement and extending rostrally for 12 mm was measured and marked with two pieces of glitter, which remained adhered to the tissue throughout testing. Three more pieces of glitter were also placed along the 12 mm spinal cord for assessment strain uniformity.

Uniaxial Testing

An Enduratec uniaxial testing machine (ELF 3200, Electroforce systems group of Bose Corporation, Eden Prairie, Minnesota) with a 0.5N load cell (Meaurement Specialities, Hampton, VA) was used for testing the chick embryo spinal cord. The machine was placed horizontally as shown in Fig 5-1. Two polyethylene plates were placed with a 10 millimeters distance apart in the Enduratec machine with one bolted onto the cantilever of the load cell and the other gripped by the crosshead. The prepared

spinal cord was laid onto the plastic plates. The marked site of the spinal cord which defined 12 mm length was placed precisely at the edge of the plastic edge as shown in Fig 5-2. This procedure ensured that the spinal cord was not stretched before the test since the distance between two plates was less than the spinal cord length. Either end of spinal cord was fixed to the plastic plates using a cyanoacrylate (Elmers Produts, INC, Columbus, OH) and left for dry 30 seconds while hydration of spinal cord was maintained using an ultrasonic humidifier. A digital camera (Samsung Digimax 4500) was fixed on top of the tested spinal cord to take pictures every 0.5mm of displacement to assess strain uniformity. The Enduratec machine was controlled by Wintest software and the time elapsed, displacement and load were recorded. Each sample was stretched once uniaxially at 0.012mm/sec which is equivalent to a $0.001s^{-1}$ strain rate. No preconditioning was applied to the tissue, as preliminary studies indicate that the tissue was too delicate. The data was fit to a 1-term Ogden hyperelastic strain energy function, which is described in details in a later paragraph.

Strain distribution quantification

The initial and final lengths between two ends of the stretched spinal cord segment, defined as the distance between marker 1 and marker 5 (Fig 5-3), were measured to calculate the overall stretch ratio λ_{15}. Markers 2, 3, and 4 separated each spinal cord into 4 individual segments. The stretch ratio for each individual segment ($\lambda_{12,}$ $\lambda_{23,}$ $\lambda_{34,}$ λ_{45}) was measured and normalized to the overall stretch ratio. The closer this normalized value was to one, the more the stretch was uniformly distributed.

Experimental analysis

The database recorded from the mechanical test was transferred to an Excel file. The initial length of the spinal cord was defined as the length before spinal cord was removed from the spinal column. As such, the in vitro 12 mm length was divided by the 'shrink ratio' (λ_s) to restore to the in situ length (L_i =12/ λ_s) for each individual spinal cord. The shrink ratio for each individual spinal cord was recorded during the specimen preparation. The stretch ratio (λ), therefore, started at 1 when the segment of spinal cord reached its in situ length.. Load was assumed to be zero when the spinal cord reached the in situ length. Load recorded at the in situ length was defined as N_i. Net load (N_n) at any time applied to spinal cord after λ reached 1 was calculated as recorded load minus N_i. (N_n = recorded load – N_i)..

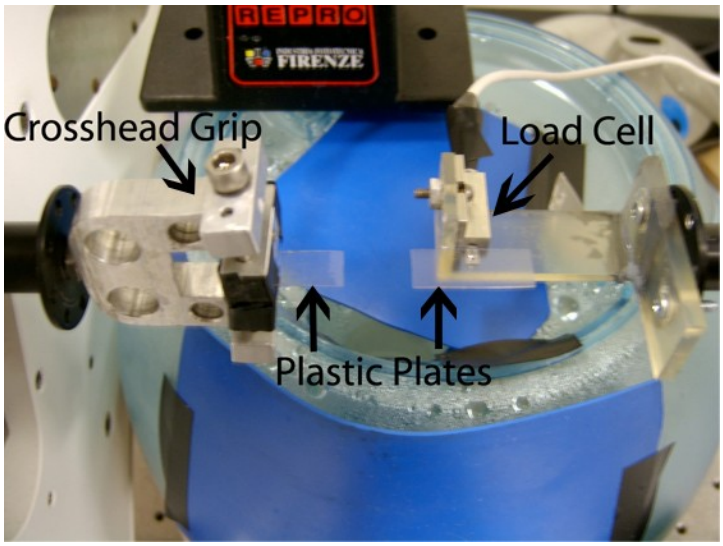

Figure 5-1: The Enduratec ELF 3200 was used to test the mechanical properties of spinal cords for each condition. Two plastic plates were stabilized with one bolted onto the cantilever of the load cell and the other gripped by the crosshead. A humidifier was placed under two plastic plates to maintain hydration.

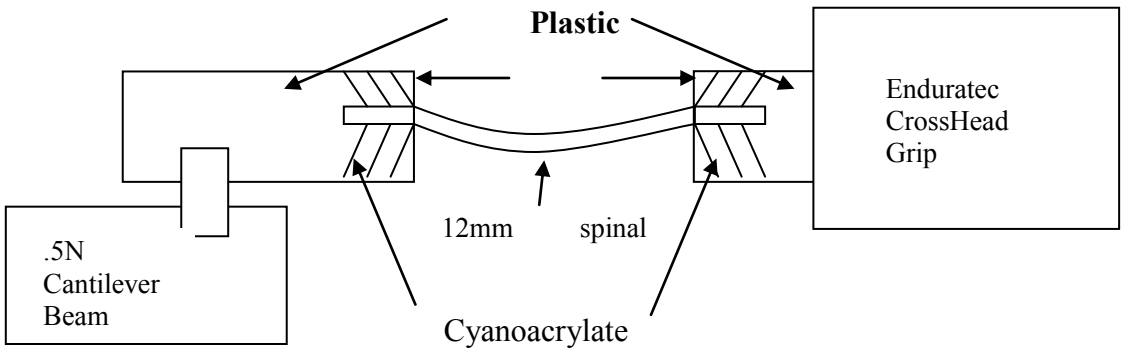

Figure 5-2: Schematic of the spinal cord preparation on Enduratec ELF 3200 before stretching. Two ends of the spinal cord, which were 12mm apart were glued to plastic plates that were separated by 10mm to provide 2mm of slack.

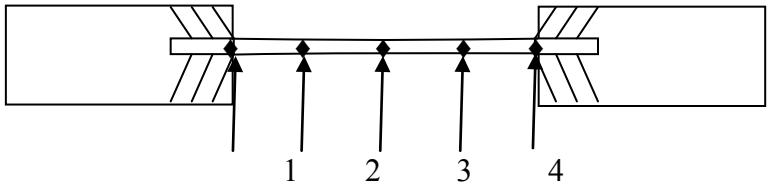

Figure 5-3: Schematic of the spinal cord demonstrating the four segments. Five glitter pieces were placed on spinal cord and divided spinal cord to four segments. The displacement between each consecutive pieces of glitter was measured to calculate the strain uniformity.

Ogden model

Spinal cord material properties were characterized using a first-order Ogden hyperelastic model. The function of Ogden hyperelastic material model in terms of stretch ratios was as:

$$W = \sum_{i=1}^{N} \frac{2G_i}{\alpha_i^2}\left(\lambda_1^{\alpha_i} + \lambda_2^{\alpha_i} + \lambda_3^{\alpha_i} - 3\right). \quad \text{Equation 5-1}$$

Parameters G and α are material properties, and $\lambda_{1\text{-}3}$ are the principal stretch ratios. The parameter G corresponds to the shear modulus of the tissue, and α is a measure of the increase in material stiffness as a result of loading. In simple tension for an incompressible material, the law is given by:

$$\sigma = \sum_{i=1}^{N} \frac{2G_i}{\alpha_i}\left(\lambda_1^{\alpha_i - 1} - \lambda_1^{-0.5\alpha_i - 1}\right). \quad \text{Equation 5-2}$$

σ here is the nominal stress. A first-order Ogden hyperelastic model, where N = 1, was suitable to fit all data. The model was fit to the experimental data to determine values of G and α for individual spinal cords (KaleidaGraph).

Results

Strain distribution

For each condition, 5-6 spinal cords were tested within which 3 spinal cords were measured to assess the strain uniformity. The stretch ratio of each segment varied within a spinal cord. As shown in table 5-1, this variation was not consistent among different nerves. The average value of each normalized stretch ratio was quantitatively similar for each condition. Thus, the stain distribution did not show sensitivity to neither location of the spinal cord nor treatment to the spinal cord.

Stress–stretch behavior

Stress vs. stretch was plotted for each condition as shown in Fig 5-4. We first compared the plot among saline injection, IgG injection and unoperated embryonic spinal cord (Fig 5-4A). The plot for these conditions showed overlapping, suggesting very similar behavior among these conditions. We next compared the plot between saline injection and EB injection (Fig 5-4B) and between IgG injection and GalC injection (Fig 5-4C). A difference was observed between myelinated and demyelinated spinal cords (Fig 5-4). Plots for demyelinated spinal cords (EB and GalC injection) showed a dramatic decrease in stress for same stretch ratio compared to myelinated ones (Saline and IgG injection). We last compared the plot between EB and GalC injection (Fig 5-4D). These two conditions demonstrated dramatic overlapping, suggesting similar behavior between these two conditions.

For each condition, spinal cords demonstrated variable ultimate stress and strain at ultimate stress. The average value and standard deviation of ultimate stress and strain for each condition was analyzed as shown in Table 5-3. Significant differences between myelinated and demyelinated spinal cords were observed. Higher ultimate stress was observed for all myelinated spinal cords – saline injected, IgG injected and unoperated embryonic spinal cords. Strain at ultimate stress was higher for spinal cords following GalC injection than following EB injection. Thus, myelinated spinal cords were stronger and more resilient compared to demyelinated spinal cords.

Ogden model

The values of parameters for each treatment are summarized in Table 5-2. The coefficient of determination (R) was > 98% for each fit, indicating that Ogden model was

an appropriate material model to represent the spinal cord tissue. The values of G, which represents the shear modulus, were significantly different between myelinated spinal cords and demyelinated spinal cords as follows: 32.51 +/- 8.73 for unoperated spinal cord, 38.97 +/-13.09 for saline injection, 20.83 +/- 4.95 for EB injection, 35.68 +/- 7.84 for IgG injection, and 21.26 +/- 6.77 for GalC injection (ANOVA, followed by Schefe's Post hoc test, $P<0.05$). The values decreased significantly for spinal cord injected with EB and GalC compared to respective control spinal cords. No significant difference was observed between EB injection and GalC injection. The values of α were as follows: 8.73 +/- 0.72 for unoperated spinal cord, 7.40 +/- 2.28 for saline injection, 6.97 +/- 1.95 for EB injection, 7.50 +/- 1.02 for IgG injection, and 8.03 +/- 1.34 for GalC injection. No significant differences were observed for the value of α between demyelinated spinal cords and respective controls.

Discussion

In this chapter, we characterized the material properties for myelinated and demyelinated spinal cords and discussed the analysis of Ogden model of tissue deformation behavior. We injected different reagents into chick embryonic spinal cords as described in Chapter 4. EB causes disruption of myelination and glial cells including astrocytes and oligodendrocytes. GalC delays the myelination process without causing any obvious cell damage. Spinal cords at the same developmental stage (E18) were stretched at low strain rates in vitro and the non-linear relationship of stress-strain was observed for all conditions. We thus fit the experimental data to an Ogden model and observed a decrease in the effective shear modulus for demyelinated spinal cords.

For each treatment, each sample showed a unique ultimate stress and different strain at ultimate stress. The stress-strain relationship also showed slight differences for each spinal cord. Many factors could cause these differences, such as the developmental status including the spinal cord length and cross area, the shrinkage because of the isolation, the stabilization of the two ends by the glue, the moisture of the spinal cord, and human operation. The development of the spinal cord during this period is very rapid, and even several hours of difference in the development time may introduce significant changes. To minimize the error due to the individual spinal cord difference, we tested 5-6 spinal cords for each condition

A difference of mechanical properties were observed between myelinated and demyelinated spinal cords. In spinal cords following GalC injection, which resulted only delay of myelination development, lower ultimate stress and lower shear modulus was observed. The results indicated that spinal cords were stronger and more resilient when myelinated than demyelinated. Myelination is suggested to hold axons together and contributes to the material properties of the spinal cords and provides support to the resistance of spinal cords during the tensile stretch. For spinal cords following EB injection, not only lower ultimate stress, lower shear modulus, but also lower strain at ultimate stress was observed compared to myelinated spinal cords. The results demonstrated that spinal cords are stronger with glial cells than without glial cells. Herein, tissue with different compositions has different mechanical properties. It suggested that the properties of white matter can be very inhomogeneous because of degree of myelination and glia development, and perhaps the nature of myelinaion. Our

results confirmed the conclusion from previous research that the properties of white matter are age- and region-dependent.

In summary, material properties of myelinated spinal cords and demyelinated spinal cords are different. Myelinated spinal cords are stronger and more resilient. Tissue with different cellular compositions has different material properties. The effects of different cellular compositions on tissue material properties are different. The material properties of tissue in turn affect the cellular kinematic response to tissue strian. Thus, the different axonal kinematics studied in Chapter 4 might be also affected by the different material properties of the spinal cord tissue. Future researchers could study how the macroscopic material properties affect the microscopic kinematics.

Figures and Tables of Results

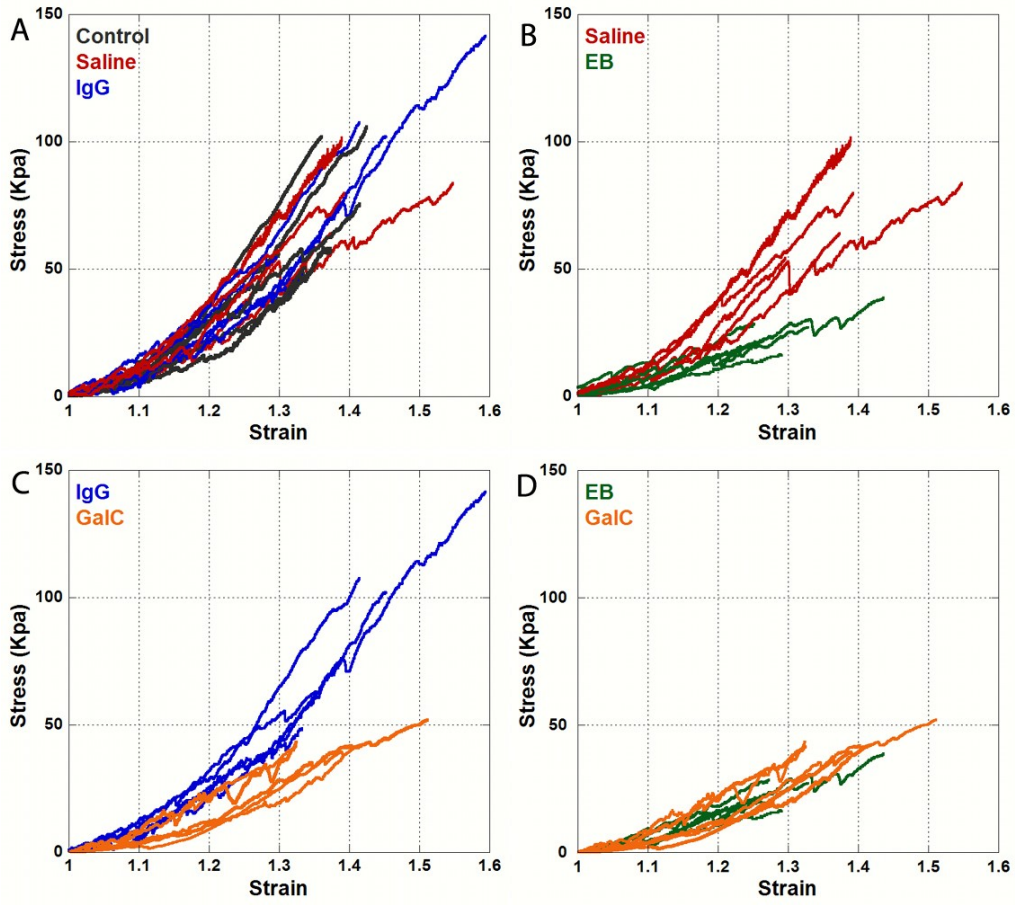

Figure 5-4: Comparisons of stress-strain relationship for all conditions. Non-operation, IgG injection, and saline injection showed similar stress-strain relationship (A). EB injection showed significant difference compared to saline injection at both ultimate stress and strain at ultimate stress (B). GalC injection showed significant stress-strain relationship compared to IgG injection (C). GalC injection and EB injection showed similar stress-strain relationship while the strain at ultimate stress was higher for GalC injection.

	$\lambda_{12}/\lambda_{15}$		$\lambda_{23}/\lambda_{15}$		$\lambda_{34}/\lambda_{15}$		$\lambda_{45}/\lambda_{15}$	
	Ave.	Stdev	Ave.	Stdev	Ave.	Stdev	Ave.	Stdev
Control	0.999	0.035	0.989	0.036	1.015	0.039	0.989	0.028
Saline	1.011	0.023	0.982	0.034	0.987	0.036	1.010	0.032
EB	1.014	0.053	1.004	0.037	1.002	0.058	0.987	0.028
IgG	1.009	0.034	1.010	0.028	1.005	0.042	0.986	0.023
GalC	0.996	0.053	1.013	0.056	0.980	0.030	1.014	0.069

Table 5-1: Strain distribution along the spinal cord for all conditions. The average value of each normalized stretch ratio was quantitatively similar for each condition.

	Ultimate Strain	stdev	Ultimate Stress(Kpa)	stdev	G(Kpa)	stdev	α	stdev
Control	1.38	0.06	80.05	23.36	32.51	8.73	8.73	0.72
Saline	1.40	0.09	76.68	18.32	38.97	13.09	7.40	2.28
EB	1.29	0.09	23.53	9.04	20.83	4.95	6.97	1.95
IGG	1.43	0.10	92.53	37.11	35.68	7.84	7.50	1.02
GC	1.42	0.07	53.06	22.52	21.26	6.77	8.03	1.34

Table 5-2: Experimental results and Ogden model analysis for all treatments.

Reference

Bilston, L. E. and L. E. Thibault (1996). "The mechanical properties of the human cervical spinal cord in vitro." Ann Biomed Eng 24(1): 67-74.

Edward L. Mazuchowski , L. E. T. (2003). Biomechanical properties of the human spinal cord and pia matter. Summer Bioengineering Conference, Sonesta Beach Resort in Key Biscayne, Florida.

Fiford, R. J. and L. E. Bilston (2005). "The mechanical properties of rat spinal cord in vitro." J Biomech 38(7): 1509-15.

Lee, M., Melvin, J., and Ueno, K., (1987). Finite Element Analysis of Traumatic Subdural Hematoma. Proc of 31st Stapp Car Crash Conference.

Margulies, S. S., L. E. Thibault, et al. (1990). "Physical model simulations of brain injury in the primate." J Biomech 23(8): 823-36.

Meaney, D. F., D. H. Smith, et al. (1995). "Biomechanical analysis of experimental diffuse axonal injury." J Neurotrauma 12(4): 689-94.

Miller, K. and K. Chinzei (2002). "Mechanical properties of brain tissue in tension." J Biomech 35(4): 483-90.

Miller, R., Margulies, S., Leoni, M., Nonaka, M., Chen, X., Smith, D., and and D. Meaney (1998). Finite Element Modeling Approaches for Predicting Injuryin an Experimental Model of Severe Diffuse Axonal Injury. Proc. of 42ndStapp Car Crash Conference.

Ogden, R. W. (1984). Non-Linear Elastic Deformations. Ellis Horwood.

Prange, M. T. and S. S. Margulies (2002). "Regional, directional, and age-dependent properties of the brain undergoing large deformation." J Biomech Eng 124(2): 244-52.

Zhou, C., Khalil, T., and King, A., (1995). A New Model Comparing Impact Responses of the Homogeneous and Inhomogeneous Human Brain. Proc. Of 39th Stapp Car Crash Conference.

Chapter 6: Thesis discussion

The goal of this research was to understand how glia can contribute to the mechanical properties of central nervous system tissue. Previous research demonstrated that axons deform independently (non-affine) at low stretch level and exhibit increasingly interdependent behavior (affine) at high stretch levels (Bain, Shreiber et al. 2003). However, the mechanism of the transition from non-affine to affine is unclear. It was proposed that coupling to the glial matrix, primarily via oligodendrocytes but also via astrocytes, would contribute to the transition from predominantly non-affine to affine behavior. We therefore characterized the kinematic response of axons to controlled stretch in the developing chick embryo spinal cord during a period of rapid establishment of interconnections via the glial matrix. We also disrupted the glial cells during the embryo development and characterized the axonal kinematic behavior with/without glia for the same developmental stage. In this thesis, we studied the strain transfer from tissue-level to axons using a chick embryo spinal cord model and investigated the effects of the glial matrix on the transfer behavior. In addition, we also characterized material properties of the spinal cord with and without axonal interconnectivity via glia and believed that the macroscopic mechanical properties affect the axonal mechanical response. These studies are important to the successful completion of our final goal, which is to investigate the thresholds for individual axons injury in different nervous area. Each individual investigation is not only critical to our understanding of the axonal kinematics, but also provides a valuable tool for future research in axonal injury.The foundation of the current analysis was the characterization of axonal tortuosity distributions at variable stretch ratios for spinal cords at different stages. Our existing

model, the chick embryo spinal cord stretch model, was an ideal model because it allowed the characterization of reproducible axonal tortuosity distributions at controlled stretch ratios in a system with rapidly growing glial cells at different developmental stages. Moreover, the glia-disruption of developing chick embryo spinal cords was well studied, and thus we were able to study the role of axonal coupling to glia on axonal mechanical behavior. Additionally, the chick model offers significant cost advantages compared to equivalent studies in rodent models.

Axonal kinematics showed increasing affine behavior with development

Based on myelin development in chick embryo spinal cords (Macklin and Weill 1985; Anderson, Bjartmar et al. 2000), we examined axon behavior at 4 stages: E12, E14, E16, and E18;and at 4 stretch levels: 5%, 10%, 15%, and 20%. By quantifying the tortuosity distribution of randomly selected axons at each stretch ratio for each developmental stages, we were able to determine the effect of growth on axonal mechanical behavior. The results suggested that the tortuosity distribution was highly dependent on the developmental stage.

As expected, non-affine, uncoupled behavior was more prevalent at earlier developmental stage, and affine, coupled behavior was more prevalent at later developmental stage. No purely non-affine or affine behavior was observed for any stage. The trend was verified quantitatively by employing the ‘switching model’, where each axon is able to transition from non-affine behavior to affine behavior after its tortuosity decreases to a transition tortuosity following stretch of tissue. The lower bound (T1) showed progressive increases with development, though no trends in the value of the

upper bound (T2) were discerned with development. The values of T1 and T2 predicted the percentage of axons that perform solely non-affine behavior. This percentage decreased progressively with development, again indicating more coupled axonal kinematics with development.

Several changes occur during the development period, such as the lengthening of spinal cord, formation of new axon tracts, maturation of glial cells, and vasculogenesis. Any change was possibly responsible for the increased coupling behavior. Regardless of the mechanism of increased coupling following growth, the results we observed can help in defining the tolerances for brain and spinal cord injury. The initial tortuosity and the axonal kinematic behavior combine to determine how strain is transferred from tissue-level to axons which ultimately produce injury. For instance, if the tortuosity of the axons is taken into account, and purely non-affine behavior is assumed, the axon-level threshold decreases compared to tissue-level threshold since a tortuous axon will not experience stretch until it is completely straightened. If the axons were able to 'switch' from non-affine to affine kinematics, the actual axon-level threshold lies between the non-affine prediction and the tissue-level prediction. The observed variations in mechanical behavior and tortuosity distribution for each developmental stage would cause different axons to reach a single axon-level injury threshold value at different tissue-level strain, and might provide different patterns of axonal pathology. The results also provide an explanation for the previous observation that axonal injury severity increases with the level of macroscopic stretch. Any spatial and/or temporal variations during development would affect the injury response. For instance, the degree of tortuosity could decrease with development, as observed in this thesis. Human spinal cord and brain continue to

develop after birth. Hence, the tolerance of human spinal cord to mechanical load could highly depend on the development. Brain tissue demonstrates different regional properties and compositions. Thus, the tolerance of brain tissue could vary significantly for different regions. Information of axonal kinematics is important to understanding the tolerance of tissue since it contribute to the tissue-level mechanical behavior. Any axonal kinematics model of white matter mechanics requires consideration of the axonal tortuosity and the dynamics of kinematic coupling. We did not attempt to measure the axonal tortuosity in three-dimensions (3D). We sectioned the spinal cords longitudinally and only measured the pathlength and end-to-end length in coronal plane. Preliminary confocal imaging of axons in chick embryo spinal cords indicates that axons are tortuous in both coronal and sagittal planes, and we believe that measurements in this two-dimension (2D) plane underestimate the actual axonal tortuosity. However, it was not possible to distinguish and measure the actual 3D pathlength for hundreds of axons with current techniques. An attempt to quantitatively evaluate the axonal tortuosity in 3D in future will provide more precise assessment of axonal kinematics behavior. Future researchers might develop valid techniques to trace single axons in the whole tissue and characterize the axonal construct in 3D. Previous research has demonstrated that axonal injury did not show sensitivity to the size of axons (Jafari, Maxwell et al. 1997; Jafari, Nielson et al. 1998; Shi, Asano et al. 2000). We thus believe that axon diameter is not critical to our experimental analysis. Previous studies have demonstrated that the microstructure failure was mostly dependent on the applied tissue strain, not the strain rate (Adams, Graham et al. 1982; Gennarelli, Thibault et al. 1989). We thus did not attempt to apply different strain rate to spinal cords for our experiments.

In addition to the axonal kinematics changes during development, we also observed that the initial tortuosity decreased significantly with development. The decrease in average initial tortuosity is possibly due to the tension applied to elongate spinal cords during the growth. For humans, the difference possibly presents between children and adults since spinal cords of children are still elongating during the growth. The initial tortuosity of chick embryo spinal cords is also different with the value characterized for adult guinea pig optic nerve which is 1.13 from previous study (Bain, Shreiber et al. 2003). The difference might be due to the variance of species or tissue locations. The initial tortuosity of axons is important to determine the actual strain transferred from tissue to axons since tortuous axon will not experience stretch until it become straight – wavier axons, if deforming in a non-affine manner, have more slack available before experiencing strain than straight axons. Our results indicated that the initial tortuosity might be variable dependent on developmental stages, age, and location of the nervous tissue, and therefore the transfer behavior might depend on these factors.

Axonal kinematics showed more affine behavior with glia vs. without glia

The results of the developing chick embryo model demonstrated that axonal kinematics showed increasing affine behavior with development. The mechanism of the increased coupling is unclear. Interconnections of axons via oligodendrocytes and astrocytes are being rapidly established during the studied period. Therefore, we proposed that the glial matrix is most likely the source of increased coupling behavior. With disrupting glia by two different protocols, we were able to examine the axonal

kinematics for spinal cords with different compositions at same developmental stage (E18).

The effects of glia on axonal kinematics was quantified by employing the 'switching model' to the experimental results across all stretch levels and determined the values of the parameters for each condition. We observed higher value of T2 when with glia vs. without glia. However, the value of T1 was relatively stable and did not show sensitivity to glia or myelination. The values of T1 and T2 showed different trend with those for developing spinal cords from E12-E18. With development from E12-E18, the value of T2 was relatively stable while T1 increased significantly. We proposed that the values of T1 and T2 could be determined by different factors. The growth of tissue might affect the lower bound while glia populations might affect higher bound. With knowledge concerning the effects of these factors, the 'switching model' can be a potential significant tool to predict axonal tortuosity distribution dependent on the tissue strain and tissue conditions. Our studies demonstrated that the values of each parameter are affected by developmental stage, degree of myelination and glia maturation. Future studies can examine other factors and correlate these factors to the model quantitatively. If the tolerance of axonal injury is known, the model can predict the axonal injury and thus provides more information for therapies. Depending on the microstructure of cells, there is significant potential to further develop the 'switching model' to examine kinematics of other cell types including oligodendrocytes, astrocytes and collagens.

With employing the 'switching model', we observed more solely non-affine behavior when without glia vs. with glia. Although the difference was not as great as expected, particularly considering the large changes seen with development in Chapter 2.

The microkinematic characterization is complicated by the change in initial tortuosity following demyelination, particularly in spinal cords injected with EB. The decrease in initial tortuosity after demyelinating with EB may be the result of losing the slack in axons because the behavior become more non-affine, and we are then unable to detect that change following stretch. We fell that the bulk properties measured in Chapter 5 provide a clearer picture of the influence of glia on tissue mechanics, though we cannot definitively state the mechanism of the influence. Thus, we can say that the axonal coupling to glia is partly responsible for change in axonal kinematics. Glia couple axons and act to maintain axon's geometry during increasing stretch ratios. Oligodendrocytes and astrocytes may physically connect many axons and act as a cellular crosslinks. Without glia, axons behave more independently and would experience more strain from macroscopic level. The observation also provides a potential explanation for the increased affine manner during chicken embryo growth. The composition of the population of myelinating oligodendrocytes varies throughout the spinal cord development, and may affect the nature of axonal coupling. The maturation of glial cells and their connection to axons define the nature of axonal coupling and may determine when the axon is able to 'switch' from non-affine to affine kinematics. For instance, myelination of the human spinal cord is incomplete at birth and continues to at least 3 years of age, and maturation of white matter tracts can continue well into adolescence. Thus, the axonal kinematics behaves differently during human development. The human white matter tolerance to stretch could vary significantly during development.

Despite that the glia process during development, the nature of axon-glia coupling is highly dependent on the glial cells. It is possible that axons within specific regions are

more vulnerable due to the types of oligodendrocytes. In CNS, oligodendrocyte morphology is related to axon diameter. Generally, axons with small diameters are myelinated by type I and II oligodendrocytes, and axons with large diameter are myelinated by type III and IV oligodendrocytes. The ratio of oligodendrocyts and axons is dependent on the types, such as type I and II myelinate many axons while type III and IV myelinate a few (and may only myelinate one) axons. Thus, the types of myelinating oligodendrocytes may affect the nature of axon-axon mechanical coupling. Areas of predominantly small diameter axons or large diameter axons, or areas with a mixture of large and small diameter axons, may demonstrate variable axonal kinematics. Moreover, areas with a mixture of large and small diameter axons, such as the ventral funiculus, are generally myelinated earlier during development while areas with predominantly small diameter axons, such as corticospinal tract are myelinated later. Thus, the nature of axonal coupling is highly dependent on the developmental stage and tissue location, and so dose the vulnerability of axons. The population of axons that are especially at risk may be influenced by any spatial or temporal variations. Our studies provide potential direction to identify populations of axons that are more vulnerable. In addition, our observations also provide more accurate in vivo information for FEM, which can be used to develop injury prevention strategies such as vehicle manufacturing. Regardless, our studies provide insights into potential contributors to transition of axonal kinematics from non-affine to affine.

Our studies also provide a potential tool to study axon-level tolerance. If periaxonal cell-cell coupling contributes to affine kinematics, then the injury to these cells would change with development and areas as well. For instance, the alteration in axonal

coupling may cause the mature and immature white matter to reveal different ionic dynamics, such as calcium influx due to the mechanical trauma, and subsequent stress and strain distribution during trauma. Thus, tolerance of individual axons varies during development and varies within specific white matter regions. Knowledge of the axon-level tolerance is important to studying the underlying mechanisms of injury during or post-trauma. However, the tolerance of individual axons has not been studied in vivo because of the limitation of current techniques. With the knowledge concerning the correlation between tissue-level strain and axonal kinematics, and knowledge concerning the tissue-level thresholds for axonal injuries, tolerance of individual axons is possible to be determined. The developing spinal cords exhibited variable axonal kinematics, thus provide a potential tool to study the temporal correlation between tissue strain and axonal mechanical behavior. Tissue-level tolerance for axonal morphological and functional injuries has been studied in guinea pig optic nerves in vivo and spinal cords in situ (Bain and Meaney 2000; Shi and Pryor 2002). Axonal morphological injury can be characterized using immunostaining methods, such as neurofilament and amyloid precursor protein (APP) immuno-reacitvity. Axonal functional injury can be assessed by measuring the electrophysiological impairment such as the membrane potential, and latency shift. Combined with our studies, information gathered from these previous studies might provide the tolerance of individual axons in vivo. In this thesis, we did not investigate the relationship between tissue strain and axonal function and morphology injury for the chick embryo spinal cords. We believe that future studies to analyze the relationship by quantify the percentage of axons exhibiting functional or morphological

injury at different tissue strain could be incorporated to the axonal tortuosity distribution presented in our current studies and therefore determine axonal injury thresholds.

Material properties of spinal cord change after removing glia

We finally investigated the material properties of spinal cords with different injections. Different cellular compositions result in different material properties. We were interested if the demyelinated spinal cords will show different material properties compared to myelinated ones. The results demonstrated that spinal cords were stronger when myelinated vs. demyelianted, as well as with glial cells vs. without glial cells. Though glia were first characterized as the 'glue' that holds CNS tissue together or a scaffold for which neurons and axons can grow, recent research has indicated that the glial cells and the glial matrix are much more compliant than their neuronal and axonal counterparts (Arbogast and Margulies 1998; Lu, Franze et al. 2006), and calls into question the role of glia as in providing mechanical support. Our study is the first to characterize the role of the glial network on bulk mechanics in tension. We found that the two demyelinating protocols generated statistically indistinguishable decreases in the stiffness of the spinal cord in uniaxial tension. The failure properties decreased significantly for the GalC treatment and even further for EB treatment. The results demonstrate that axon-axon coupling via astrocytes and oligodendrocytes is an important component that dictates the overall tissue response to tensile loading. The glia likely force the axons to act as a composite to increase overall stiffness and strength. Moreover, regions with different degrees of axon coupling – via myelinating oligodendrocytes

and/or astroglia, will respond differently to mechanical force and may be more or less prone to injury.

In summary, our results suggested that axonal kinematics is complex. The relationship of tissue strain and axonal strain depends on the growth, initial tortuosity, and cellular compositions of the tissue. The interconnection via glia likely force axons to switch from non-affine to affine behavior during stretch. Thus, axons in different nervous area such as spinal cord, brain, or peripheral nervous system may have unique thresholds for axonal injuries. Incorporating axon level information into biomechanical models of brain and spinal cord injury require the accurate characterizing of axonal kinematics of age and location. Future studies could determine the specific relationship between microstructure changes and tissue strains for a given situation, and thus the unique thresholds for axonal injury at different tissue conditions. The information can provide more accurate cellular properties and can be applied to FEM and thus helps developing prevention strategies for injuries.

Future studies

Current results demonstrated that axonal kinematics highly depend on the age and location of nerves. We have identified the axonal kinematics following development in chick embryo spinal cord. Future studies can characterize the axonal kinematics for different nervous area such as brain in animals at different ages. We believe that the information can be incorporated into tissue-level biomechanics models and make the models more accurate. We have studied the effects of axonal coupling with glia on the axonal kinematics and found out that the glia contribute to the transition from non-affine

to affine behavior. We propose that the types of the glial cells, such as oligodendrocytes, define the nature of the coupling, and therefore affect the axonal mechanical response. Future studies can characterize the axonal kinematics for tissue area with different types of oligodendrocytes, such as ventral funiculus or corticospinal tract, to identify the effects of the nature of coupling on the axonal kinematics. Our studies also provide a direction for in vitro studies for future studies. Future studies can co-culture neurons with different glial cells and characterize the axonal kinematics with different cellular compositions. We didn't correlate the axonal kinematics to axonal injury in this thesis. We believe that future studies on the correlation can help define the axon-level threshold for injury and can be used for the FEM model to better predict the injury patterns.

Reference

Adams, J. H., D. I. Graham, et al. (1982). "Diffuse axonal injury due to nonmissile head injury in humans: an analysis of 45 cases." Ann Neurol **12**(6): 557-63.

Anderson, E. S., C. Bjartmar, et al. (2000). "Developing chicken oligodendrocytes express the type IV oligodendrocyte marker T4-O in situ, but not in vitro." Neurosci Lett **284**(1-2): 21-4.

Anderson, E. S., C. Bjartmar, et al. (1999). "Molecular heterogeneity of oligodendrocytes in chicken white matter." Glia **27**(1): 15-21.

Arbogast, K. B. and S. S. Margulies (1998). "Material characterization of the brainstem from oscillatory shear tests." J Biomech **31**(9): 801-7.

Bain, A. C. and D. F. Meaney (2000). "Tissue-level thresholds for axonal damage in an experimental model of central nervous system white matter injury." J Biomech Eng **122**(6): 615-22.

Bain, A. C., D. I. Shreiber, et al. (2003). "Modeling of microstructural kinematics during simple elongation of central nervous system tissue." J Biomech Eng **125**(6): 798-804.

Del Rio Hortega, P. (1924). "La glie a radiations peu nombreuses et la cellule deSchwann sont elles homologables." C.R. Soc. Biol. **91**: 818-820.

Fanarraga, M. L., I. R. Griffiths, et al. (1998). "Oligodendrocytes are not inherently programmed to myelinate a specific size of axon." J Comp Neurol **399**(1): 94-100.

Gennarelli, T. A., L. E. Thibault, et al. (1989). "Axonal injury in the optic nerve: a model simulating diffuse axonal injury in the brain." J Neurosurg **71**(2): 244-53.

Jafari, S. S., W. L. Maxwell, et al. (1997). "Axonal cytoskeletal changes after non-disruptive axonal injury." J Neurocytol **26**(4): 207-21.

Jafari, S. S., M. Nielson, et al. (1998). "Axonal cytoskeletal changes after nondisruptive axonal injury. II. Intermediate sized axons." J Neurotrauma **15**(11): 955-66.

Lu, Y. B., K. Franze, et al. (2006). "Viscoelastic properties of individual glial cells and neurons in the CNS." Proc Natl Acad Sci U S A **103**(47): 17759-64.

Macklin, W. B. and C. L. Weill (1985). "Appearance of myelin proteins during development in the chick central nervous system." Dev Neurosci **7**(3): 170-8.

Shi, R., T. Asano, et al. (2000). "Control of membrane sealing in injured mammalian spinal cord axons." J Neurophysiol **84**(4): 1763-9.

Shi, R. and J. D. Pryor (2002). "Pathological changes of isolated spinal cord axons in response to mechanical stretch." Neuroscience **110**(4): 765-77.

VITA

Hailng Hao

1977 Born July 07 in JiaXiang, Shandong Province, China.

1995-99 Attended Zhejiang University, China; majored in Biology.

1999 B.S., Zhejiang University.

1999-2001 Research Assistant, State Key Laboratory of Plant Physiology and Biochemistry, China.

2001-07 Graduate work in Biomedical Engineering, Rutgers University, NewBrunswick, New Jersey.

2006-07 Teaching Assistant, Department of Biomedical Engineering.

2007 Article: "Axon Kinematics Change during Growth and Development," The Journal of Biomechanical Engineering, August 2007, vol. 129, p: 511-522.

2007 Ph.D. in Biomedical Engineering